THREE- AND FOUR-DIMENSIONAL COMPUTED TOMOGRAPHIC ANGIOGRAPHY AND VENOGRAPHY FOR IMAGING OF THE MICROVASCULAR ANATOMY OF PERFORATOR FLAPS

by

Mr Mark V Schaverien

MBChB, MRCS, MSc(Hons)

This being a thesis submitted for the degree of Medical Doctorate

to the Faculty of Medicine of the University of Edinburgh

Department of Plastic Surgery

University of Texas Southwestern Medical Center

Dallas, Texas

2009

ACKNOWLEDGEMENTS

Over the last year I have had the great privilege of working alongside a remarkably talented and productive group of colleagues, all of whom have contributed to the work contained within this thesis. Their participation in the work described in this thesis is gratefully acknowledged.

I wish to express my warm and sincere gratitude to all those who made this work possible, in particular my supervisor, Dr Pete Hoskins, Reader in Medical Physics at the Medical University of Edinburgh, for his patient help with producing this thesis. I remain indebted to Dr Michel Saint-Cyr, Assistant Professor in the Department of Plastic Surgery at the University of Texas Southwestern Medical Center, my research supervisor at UT Southwestern. His relentless energy, dynamism, direction and ideas have formed the backbone of this thesis. Dr Gary Arbique, Assistant Professor in the Department of Radiology, has been chiefly responsible for enabling the CT angiography techniques outlined in this study to be carried out, and this study would not have been possible without his help. Thank-you also to Dr Spencer Brown, Assistant Professor, who oversaw all of the projects contained in this thesis and ensured that they received adequate funding. I remain very grateful to Dr Rod Rohrich, Professor and Chairman of the Department of Plastic Surgery at UT Southwestern, for allowing me to spend a year at his centre. Many thanks also to Holly Smith, Chief Medical Photographer for the Department of Plastic Surgery at UT Southwestern, who has patiently helped with the editing of all of the figures used in this thesis and the publications arising from it, as well as to Alexandra Hernandez, whose beautiful illustrations are pivotal to explaining many of the concepts in this thesis and the publications arising from it, and which have been

included in this thesis with her permission. Above all, thank-you to all of the staff at the Willed Body Program at UT Southwestern, without whom this study would not have been possible.

The projects presented in this thesis were financially supported by the Department of Plastic Surgery at UT Southwestern.

AUTHOR'S DECLARATION

I declare that all the work presented in this thesis was carried out by myself, except as described in the acknowledgements. The work described in this thesis has not been submitted for any previous degree.

Mark Schaverien

November 2009

LIST OF CONTENTS

LIST OF FIGURES

1.5ml of contrast. The large-diameter linking vessels can clearly be seen spanning between the adjacent angiotomes at the level of the suprafascial plexus, with branches to the subdermal plexus (it is important to note that the linking vessel complex is morphologically distinct from a perforator complex). (Right) Both the anterolateral thigh B and C perforators have been injected with 1.5ml of contrast. The lateral view shows the dense communicating branches between adjacent perforators of the same angiotome (vascular territory of the descending branch of the lateral circumflex femoral artery) through subdermal, subcutaneous, and suprafascial plexuses. This further supports the angiosome theory. SFA, superficial femoral artery. 102

Figure 3.7 Polar plot of the arterial vascular territories of the descending branch of the lateral circumflex femoral artery by means of injection of the anterolateral thigh B perforator (corrected for left thigh). The black line represents the mean. Note that the territories are axial with respect to the axiality of the limb. 103

Figure 3.8 Type I perforator complex with illustration. Note that the branches of the perforator course obliquely through the adipose layer to reach the subdermal plexus, without a component at the suprafascial layer. 104

Figure 3.9 Type II perforator complex with illustration. Branches of the perforator course obliquely through the adipose layer to the subdermal plexus, and there are also branches that course out horizontally to form a suprafascial plexus. 105

Figure 3.10 Type III perforator complex with illustration. The perforator divides into several branches at the suprafascial level, coursing horizontally for variable distances before coursing vertically to the subdermal plexus. 106

Figure 3.11 Anteroposterior views of a type II perforator complex with progressive flap thinning and injection of 1.5 ml of contrast. A 5-cm radius about the perforator has been preserved (wire circle) and thinning has been performed at 30 degrees to the horizontal followed by 90 degrees to the horizontal, with washout of the contrast between successive stages. Note how the vascular territory is reduced by any angle of thinning because of the interruption of filling at the level of the suprafascial plexus and the linking vessels. Thinning should therefore be avoided if a large flap is planned. 107

Figure 3.12 Lateral views of a type II perforator complex, with progressive flap thinning and injection of 1.5 ml of contrast. Note how the vascular territory is reduced by any angle of thinning because of the interruption of filling at the level of the suprafascial plexus and the linking vessels. 108

Figure 3.13 Anteroposterior views of dynamic filling of the venous system after cannulation of the vena comitans of the B perforator, with images acquired at 1-ml filling increments. The image on the right is a static study performed after injection with a barium sulphate/gelatin mixture. Note that drainage in the superficial venous system occurs medially toward the long saphenous vein. Note also that the superficial venous

perforator from the descending branch of the thoracodorsal artery, with images acquired at 1-ml filling increments. The final image has been acquired following injection with a barium sulphate/gelatin mixture. The superficial venous system was arranged in a polygonal configuration at the level of the subdermal plexus, and flow into the deep venous system can be seen to occur through the venae comitantes of adjacent perforators within the same angiotome. Note that drainage in the superficial venous system occurred both superolaterally and inferomedially/medially toward the vertebral venous plexus, coursing progressively deeper within the flap as the veins approached the midline. 121

Figure 4.2 Lateral dynamic computed tomographic angiograms of the most proximal perforator from the descending branch of the thoracodorsal artery at 0.5-ml filling increments. Note that the linking vessels are found within the flap at the level of the subdermal plexus, enabling thinning to be performed safely. 122

Figure 4.3 Three-dimensional static image after cannulation of the most proximal perforator from the descending branch and injection with a barium sulphate/gelatin mixture, with illustration. Note the filling of the adjacent dorsal intercostal artery perforators by means of recurrent flow through the subdermal plexus, with an absence of a suprafascial plexus. This enables the flap to be thinned without disrupting its vascular supply. 123

Figure 4.4 Type I perforator complex with illustration. Note that the branches of the perforator course obliquely through the adipose layer to reach the subdermal plexus, without a component at the suprafascial layer. 125

Figure 4.5 Type II perforator complex with illustration. The perforator divides into several branches at the suprafascial level, coursing horizontally for variable distances before coursing obliquely to the subdermal plexus. The maximal length of the horizontal component was measured at 4.1 cm, and this would therefore be the recommended radius to preserve during flap thinning unless the branches are visualized directly. 126

Figure 4.6 Left: Polar plot of the arterial vascular territories about the most proximal perforator from the descending branch of the thoracodorsal artery. Each color represents the vascular territory for each flap about the first perforator from the descending branch, measured from the 2D images on the CT workstation. The black line represents the mean vascular territory for all of these values. Note that the territories are axial with respect to the latissimus dorsi muscle. Right: Scatterplot of the perforators from the descending (red) and transverse (blue) branches of the thoracodorsal artery with respect to the posterior axillary fold. The yellow area represents the region in which the most proximal, and largest, perforator from the descending branch was found in all specimens. This area was found within 3 cm of the lateral edge of the latissimus muscle from 6.6 to 15.4 cm caudal to the posterior axillary fold. A mean of 3.6 musculocutaneous perforators (range, 1 to 8) were found, with a mean of 2.5 (range, 1 to 7) originating from the descending branch and 1.1 (range, 0 to 3) originating from the transverse branch. The mean intramuscular length of perforators was 2.8 cm (range, 1.3 to 4.7) from the descending branch and 3.1 cm (range, 1.2 to 6) for the transverse branch. 127

!!!

from the descending and transverse branches were found to have the largest vessel diameters and thickest tunica media layers, with a proportional decrease in size with increasing distance from the bifurcation. Note also that a branch of the thoracodorsal nerve and two venae comitantes were found to accompany all perforators. 134

Figure 5.1 Lateral view of large lateral row perforator following injection with 0.2ml of contrast medium. The large diameter branches to the subdermal plexus are seen in all perforators, regardless of location, and vary from two to several. Branches at the suprafascial level by contrast are of much smaller diameter. Some perforator complexes did not have any branches at the suprafascial level. The suprafascial branches only course horizontally for a short distance before anastomosing with those of adjacent perforators, and were never seen to cross the midline. A variety of branching patterns could be seen within the subcutaneous adipose layer, although flow was seen to predominantly occur through the branches at the level of the subdermal plexus. Recurrent vessels to the adipose layer, filled via flow through the subdermal plexus, can be clearly seen. This phenomenon was first noted in the abdominal flap occurring across the midline by Moon and Taylor. 141

Figure 5.2 Anteroposterior view of static CT of flap following injection of a single medial row DIEA perforator (see white arrow) with a barium sulphate/gelatin mixture. Note the lattice of large diameter linking vessels across the midline connecting adjacent medial row perforators. The injection pattern resembles a centrally perfused ellipse with declined perfusion at the edges. This study was performed in a cadaveric flap, and thus is an underestimate of the *in vivo* vascular territory. 142

Figure 5.3 Anteroposterior and lateral views of dynamic CTA of a left medial row perforator, with images acquired at 0.5ml fill intervals. During early filling recurrent flow was seen to perfuse the adjacent medial row perforator and ipsilateral lateral row perforators, as well the contralateral medial row perforators via a lattice of large diameter vessels across the midline at the level of the subdermal plexus. Further injection was seen to perfuse the contralateral lateral row perforators, with branches extending to zone IV. Perfusion of a medial row perforator reveals a centrally perfused ellipse with declining perfusion at the edges. 143

Figure 5.4 Anteroposterior and lateral views of dynamic CTA of a left lateral row perforator. Images are acquired at 0.5ml fill intervals. Predominantly lateral filling can be seen occur at the first interval, with early filling of the ipsilateral medial row perforator via recurrent flow through the subdermal plexus. Only a few branches can be seen to cross the midline, and perfusion of contralateral perforators has not occurred. This pattern was stereotyped for lateral row perforators, irrespective of the injection volume. 145

Figure 5.5 Illustration comparing flow within the flap following cannulation and injection of a medial versus lateral row perforator (lateral view). Note that in the lateral row perforator flow predominantly occurs laterally, with perfusion not seen to extend beyond the contralateral medial row perforator after passing through the subdermal plexus twice. The medial row perforators are connected across the midline by large

diameter linking vessels, with flap perfusion up to the contralateral lateral row perforators. 146

Figure 5.6 The largest lateral row perforator was cannulated immediately following harvest (position marked by red pin) and injection of 20ml red dye was performed within one hour of flap harvest. Once the cutaneous staining pattern was evident the vessels were copiously irrigated with warmed herparinised saline until the effluent was clear. The boundary of the skin staining was marked and the flap was refrigerated at 4°C for 72 hours. Following this the same perforator was injected with methylene blue and the specimen was photographed. Dye injection immediately following harvest revealed staining of the zone contralateral to the midline, without staining of zone IV (a). Later injection of blue dye revealed that the dye did not cross the midline (b), suggesting that although cadaveric injection studies are an underestimate of that seen *ex vivo* in the fresh specimen, zone IV is not perfused by injection of a lateral row perforator. 147

Figure 5.7 Anteroposterior, lateral, and side-on views of dynamic CTA of the right superficial inferior epigastric artery. Images were acquired at 0.5ml fill intervals. Injection of the SIEA revealed that terminal branches coursed to the subdermal plexus, followed by filling of ipsilateral lateral and medial row perforators via recurrent flow through the subdermal plexus. The perfusion pattern was therefore very similar to that seen with a lateral row perforator. Perfusion contralateral to the midline was not seen in any of the injection studies. 148

Figure 5.8 *In vivo* CTA demonstrating the relationship between the DIEA paraumbilical perforators and the SIEVs. Note that *in vivo* the SIEVs are larger than the DIEVs, suggesting that they represent the dominant source of venous drainage for the abdomen. 150

Figure 5.9 Anteroposterior and lateral views of dynamic CTV of the left SIEV. Images are acquired at 1ml fill increments. The superficial and deep venous drainage systems were found to consist of the superficial and deep inferior epigastric veins, connected by the venae comitantes of the perforators of the DIEA. Injection of either the venae comitantes or the superficial epigastric veins revealed the same venous filling pattern, with filling of all of the adjacent venae comitantes. Filling of the adjacent superficial epigastric vein across the midline occurred through vessels crossing the midline at the level of the subdermal plexus, and drainage vessels from the subdermal plexus were seen to return to the SIEVs. 151

Figure 5.10 Illustrations of flap venous drainage pre- and post- flap harvest. In the normal physiological state venous drainage predominantly occurs via the SIEVs with some contribution through the venae comitantes of the DIEA. Following harvest all venous drainage is diverted into the venae comitantes of a single perforator. Absence of midline linking vessels may therefore lead to diffuse venous congestion. 152

Figure 5.11 Anteroposterior static images of the venous system following cannulation of the left SIEV (by convention) and injection of a barium sulphate/gelatin mixture. A variety of venous morphological patterns were seen: in one flap no midline crossover was seen, with a linking vein seen coursing cepahalad to the umbilicus (*left*); in another flap the linking vein was seen to course cephalad to the umbilicus to connect with the contralateral SIEV *(right)*. 153

Figure 5.12 Hart's elastin histology of cross-section of all of the DIEA perforators ≥ 0.5mm in diameter from a single flap. Note that there are no significant differences in vessel diameter or smooth muscle wall thickness for perforators from the medial or lateral row. In general the largest perforators were found in the paraumbilical region. 154

Figure 5.13 Illustration of the location of all of the perforators ≥ 0.5mm in diameter originating from the DIEA in ten flaps. All perforators were found within a 10cm radius of the umbilicus, and a mean of 5.3 perforators (range 2 to 8) perforators were found per specimen. 155

LIST OF TABLES

LIST OF ABBREVIATIONS

2D	Two-dimensional
3D	Three-Dimensional
CT	Computed Tomography
CTA	Computed Tomographic Angiography
CTV	Computed Tomographic Venography
DIEA	Deep Inferior Epigastric Artery
DIEAP	Deep Inferior Epigastric Artery Perforator
DIEV	Deep Inferior Epigastric Vein
DSA	Digital Subtraction Angiography
EBCT	Electron Beam Computed Tomography
HU	Hounsfield Units
kVp	Peak Kilovoltage
KeV	Kiloelectron Volt
LCFAP-*vl*	Anterolateral thigh perforator
MDCT	Multidetector Array Computed Tomography
MIP	Maximum Intensity Projection
SCT	Spiral Computed Tomography
SIEA	Superficial Inferior Epigastric Artery
SIEV	Superficial Inferior Epigastric Vein
σ_M	Standard Error of the Mean
TAP	Thoracodorsal Artery Perforator
TRAM	Transverse Rectus Abdominis Musculocutaneous

PUBLICATIONS AND PRESENTATIONS ARISING FROM THIS THESIS

Publications

Saint-Cyr, M., **Schaverien, M. V.**, Arbique, G., Hatef, D., Brown, S. A., and Rohrich, R. J. (2008). Three- and four-dimensional computed tomographic angiography and venography for the investigation of the vascular anatomy and perfusion of perforator flaps. *Plast. Reconstr. Surg.* 121: 772-80.

Schaverien, M. V., Saint-Cyr, M., Arbique, G., Hatef, D., Brown, S. A., and Rohrich, R. J. (2008) Three- and four-dimensional computed tomographic angiography and venography of the anterolateral thigh perforator flap. *Plast. Reconstr. Surg.* 121: 1685-96.

Schaverien, M. V., Saint-Cyr, M., Arbique, G., Brown, S. A., and Rohrich, R. J. (2008). Three- and four-dimensional arterial and venous anatomies of the thoracodorsal artery perforator flap.
Plast. Reconstr. Surg. 121: 1578-87.

Schaverien, M. V., Saint-Cyr, M., Arbique, G., Brown, S., Rohrich, R. (2008). Three- and four-dimensional CT-angiography for the study of the vascular anatomy and perfusion of the deep inferior epigastric perforator and superficial inferior epigastric artery flaps. *Plast. Reconstr. Surg.* 121: 1909-1920.

Schaverien, M. V., Saint-Cyr, M.V, and Rohrich, R. J. (2009). Perforator flaps: history, controversies, anatomy, and their use in reconstruction. CME. *Plast. Reconstr. Surg.* 123: 132e-145e.

Saint-Cyr M., **Schaverien M.**, Wong C., Nagarkar P., Arbique G., Brown S., Rohrich R. J. (2009). The extended anterolateral thigh flap: anatomical basis and clinical experience. *Plast. Reconstr. Surg.* 123: 1245-55.

Saint-Cyr M., **Schaverien M.**, Wong C., Rohrich R. J. The perforasome theory: vascular anatomy and clinical implications. . *Plast. Reconstr. Surg.* 124: 1529-44.

Presentations

Schaverien, M. V., Saint-Cyr, M., Arbique, G., Brown, S., and Rohrich, R. J. Three- and four-dimensional CT angiography for the study of the vascular anatomy and perfusion of the deep inferior epigastric perforator and superficial inferior epigastric artery flaps. American Society for Plastic Surgery annual meeting October 2007.

Schaverien, M. V., Saint-Cyr, M., Arbique, G., Brown, S., and Rohrich, R. J. Three- and four-dimensional computed tomographic angiography and venography for the investigation of the vascular anatomy and perfusion of perforator flaps. British Association of Plastic and Reconstructive Surgeons meeting June 2007.

Saint-Cyr, M., **Schaverien, M. V.**, Arbique, G., Hatef, D., Brown, S., Gao, J., and Rohrich, R. J. Four-dimensional CT-scan analysis of the anterolateral thigh flap perforator branching pattern. American Society for Reconstructive Microsurgery annual meeting. January 2007.

Saint-Cyr, M., Arbique, G., **Schaverien, M. V.**, Hatef, D., Brown, S., Gao, J., and Rohrich, R. J. Four-dimensional analysis of the vascular architecture and perfusion of the anterolateral thigh flap. American Society of Plastic Surgeons annual meeting. September 2006.

Saint-Cyr, M., **Schaverien, M. V.**, Arbique, G., Brown, S., and Rohrich, R. J. The extended anterolateral thigh flap: anatomical basis and clinical experience. American Society for Reconstructive Microsurgery annual meeting January 2009.

Saint-Cyr, M., Wong C, **Schaverien, M. V.**, Arbique G, and Rohrich, R. J. Basis of perforator flap perfusion: the perforasome theory. American Society for Reconstructive Microsurgery annual meeting January 2009.

SUMMARY

Two-dimensional (2D) contrast radiography utilising the intravascular injection of lead oxide or barium sulphate mixtures is the current gold-standard for investigating the vascular anatomy of surgical flaps. The vascular anatomies of surgical flaps, however, are three-dimensional (3D), and their evaluation is conceptually limited by evaluation in 2D. Static 3D computed tomographic (CT) angiography enables vascular anatomy to be evaluated in the coronal, axial, and sagittal plane, and dynamic four-dimensional (4D) CT angiography (CTA) allows the vascular filling of a surgical flap to be visualized over short time intervals in three dimensions. These methods are also capable of elucidating the vascular anatomy and perfusion of the integument in general.

The tissues of the body are perfused by source arteries in 3D blocks. The perforating vessels that provide blood supply to the skin may be dissected from between or through the underlying muscle, and flaps based on these vessels are termed perforator flaps. These flaps have the advantages of reduced donor site morbidity due to preservation of the underlying muscle, versatility to accurately replace the components required at the recipient site, and freedom from orientation of the pedicle. Their development has followed our understanding of the blood supply from a source artery to the skin, which has been achieved due to landmark studies by Manchot, Salmon, Cormack and Lamberty, Taylor, and others. Many articles now attest to the safety and reliability of perforator flaps. The arterial and venous anatomies of the workhorse perforator flaps, which include the anterolateral thigh (LCFAP-*vl*), the thoracodorsal artery perforator (TAP), and deep inferior epigastric artery perforator (DIEAP) flaps, remain poorly understood, and better understanding may improve the reliability of these

flaps, aid in optimal flap design with regards to the vascular anatomy, and may aid in the development of new perforator flaps.

To elucidate the 3D and 4D arterial and venous anatomies and perfusion of perforator flaps, this thesis studied the vascular anatomies of the workhorse perforator regions in fresh adult cadavers acquired through the Willed Body Program at the University of Texas Southwestern Medical Center in Dallas using novel 3D imaging techniques. These regions included the thigh, the abdomen, and the back. The techniques consisted of cannulation of the vessels at the level of perforators and their accompanying venae comitantes, followed by either injection of a lead oxide or barium sulphate and gelatin mixture, or by iodinated CT contrast medium injected using a precision pump prior to acquisition of CT images and three-dimensional volume-rendered reconstructions. CT contrast medium has a viscosity similar to that of blood and enabled better physiological modelling of perforator flap perfusion than had been achievable previously.

In conclusion this thesis studied novel techniques for acquiring both static and dynamic three-dimensional images of microvascular perforator flap anatomy using CTA and venography (CTV). The information gained has provided a better understanding of how perforator flaps and the integument in general are perfused.

Chapter 1

INTRODUCTION

1.1 Two-dimensional radiography

1.1.1 Two-dimensional projection and digital radiography

The X-ray was discovered by Professor Wilhelm Conrad Röntgen, Head of the Department of Physics of Julius-Maximillan University at Würzburg, on 8th November 1895. Whilst working with cathode rays he noticed fluorescence of a barium platinocyanide screen, and immediately started investigating the phenomenon. The first radiograph was of "Mrs Roentgen's hand", taken on 22 December 1895, and on 28th December 1895 he submitted a manuscript entitled "On a New Kind of Ray", outlining the essential features of X-rays (Röntgen, 1895). The discovery earned Röntgen the Nobel Prize for physics in 1901.

Radiographs rely on the emission of electromagnetic radiation upon a specified region in the body, which passes through less dense matter, such as air, to reach the radiographic film cassette, but is absorbed or scattered by denser materials, such as bone. Areas of film exposed to higher amounts of radiation will appear as black or grey on X-ray film, while areas exposed to less radiation will appear lighter or white. In digital radiography the X-rays strike a plate of X-ray sensors producing a digital computer image directly. This allows image postprocessing to be performed.

1.1.2 Fluoroscopy

Fluoroscopy is a special application of X-ray imaging, allowing real-time visualisation using low intensity X-ray to continuously irradiate the patient. An image intensifier system is used to detect the X-rays and display these as a real-time video images. Two radiocontrast agents are currently in clinical use. Barium sulphate may be given orally or rectally for evaluation of the gastrointestinal tract. Several iodinated compounds are also available that may be given by oral, rectal, intraarterial or intravenous routes. These contrast agents strongly absorb X-ray radiation, and in conjunction with the real-time imaging allow demonstration of dynamic processes, such as blood flow in arteries and veins.

1.1.3 Angiography

In January 1896, only a few months after the discovery of the X-ray, Haschek and Lindenthal injected Teichmann's mixture, a suspension of chalk, cinnabar (mercury) and petroleum into the blood vessels of a cadaveric hand, producing the first angiogram (Haschek and Lindenthal, 1896). The first *in vivo* angiogram was obtained by Fuch in 1899, when an abdominal aortic aneurysm was imaged. The major breakthrough in angiography was the introduction of the technique described by Seldinger in 1953, which avoided direct cannulation of the area of interest. Diagnostic angiography now includes examinations of the heart, carotids, cranial circulation, aorta, renal system, mesenteric circulation, and the peripheral vascular system.

Contrast agents have evolved to gain the maximum trade-off between patient toxicity and contrast enhancement. Early contrast agents included bismuth and oil, introduced in 1910, barium sulphate, lipiodol, strontium bromide, and sodium iodide.

The first organic iodides (Selectan) were introduced in 1929, and the first triiodinated contrast agent was introduced in 1944. Iohexol (Omnipaque), a non-ionic contrast medium, was introduced in 1982, and to date over 200 million examinations have been performed using this agent. Compared with ionic contrast media, eliminating the carboxyl decreased the neurotoxicity, eliminating ions decreased the osmotoxicity, and the addition of hydroxyl groups decreased the chemotoxicity. The iodine content is 46.6%, and Omnipaque 240, which is the most frequently used agent, has a concentration of 240mg/ml. The elimination half-life is 121.2 min, and this is independent of dose, with approximately 99% of the contrast excreted during the first 24 hours after injection.

Digital subtraction angiography (DSA) enables rapid, high definition imaging, whilst eliminating the background image. It is widely available and is involved in many therapeutic procedures.

1.1.4 Limitations of conventional two-dimensional radiography

Conventional 2D radiography is the current gold-standard for the investigation of flap vascular anatomy. Limitations include the inability to visualize low-contrast tissues and structures, limited by inefficient absorption of the X-ray screens, as well as high scatter-to-primary X-ray ratios, and limitations of superimposition and conspicuity due to the representation of 3D volume as a 2D image resulting in reduced conspicuity and subject contrast. Sufficient exposure latitude is also required to record as much of the range of X-ray intensities exiting the subject as possible, limiting receptor contrast. Although improved X-ray absorption efficiency of modern radiographic technology and

digital radiography have nearly eliminated the contrast–latitude trade-off, these limitations of radiography still exist today (Goldman, 2007) (**Figure 1.1**).

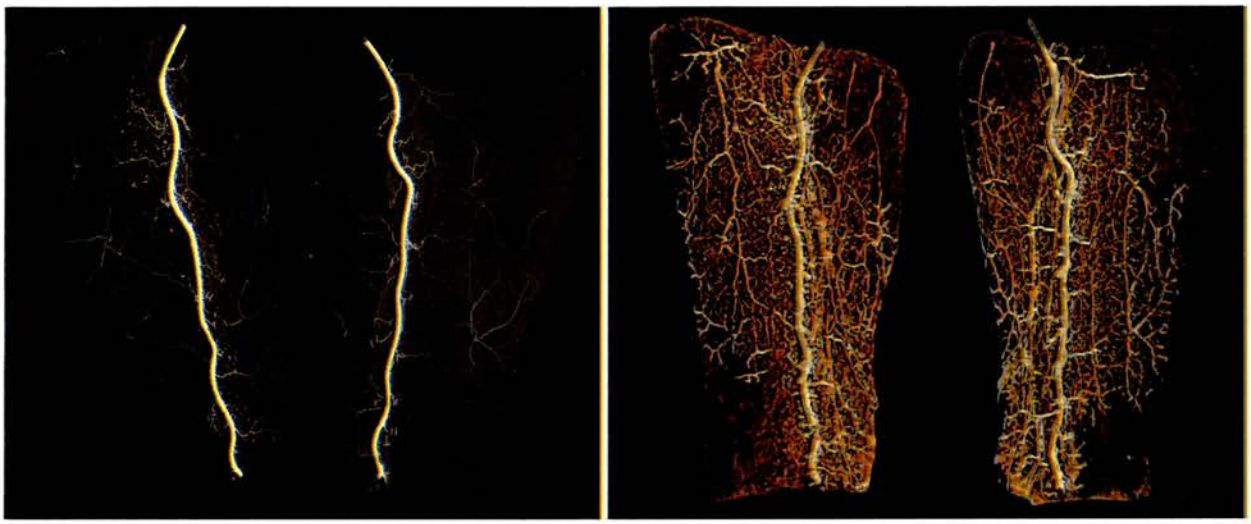

Figure 1.1 Left: Digital radiograph of a pair of radial forearm flaps following cannulation of the brachial artery and injection of a barium sulphate/gelatin mixture. Right: CT angiogram of the same flaps. Note the absence of depth perception and the inability to distinguish between plexi within the flap in the digital radiograph.

1.2 Computed tomography

1.2.1 History of computed tomography

CT imaging involves acquisition of transmitted intensity projecion data at multiple angles around the body. The data is reconsructed in the computer to produce a 2D cross-sectional image. Images are acquired in the axial plane, while coronal and sagittal images can be rendered by computer reconstruction. Radiocontrast agents allow enhanced delineation of anatomy, and

intravenous contrast can allow 3D reconstructions of arteries and veins. Although radiographs provide higher spatial resolution, CT can detect more subtle variations in attenuation of X-rays, although with higher patient exposure to ionizing radiation. Multi-detector CT (MDCT) results in much finer detail images in a shorter exam time proportional to the number of detectors.

Although the theory of image reconstruction from projections, which is central to the concept of CT, was described in 1917, and its application for medical imaging was suggested as early as 1940, the development of the first modern CT scanner was begun in 1967 by Godfrey Hounsfield, an engineer at British EMI Corp (Kalender, 2006). He was interested in the large amount of potential information that is inefficiently used during conventional radiography and estimated that by taking careful measurements of X-ray transmission through a subject at many positions and at a sufficient number of angles it would be possible to determine attenuation differences of 0.5%, sufficient to distinguish between soft tissues.

Hounsfield's original design imagined the subject divided into axial slices. The X-ray beam to be used was collimated down to a narrow pencil-width beam of X-rays approximately 3 mm within the plane of the slice and 13 mm wide perpendicular to the slice (along the axis of the subject). The X-ray tube was rigidly linked to a single sodium iodide scintillation detector located on the other side of the subject, and together the X-ray tube and detector scanned across the subject. The linear transverse scanning motion of the tube and the detector across the subject was referred to as a translation.

To minimize examination time, the first generation scanners actually used 2 adjacent detectors and a 26-mm-wide X-ray beam (in the slice thickness direction) to simultaneously collect data for 2 slices. By the end of the scan 28,800 measurements (180 views x 160 rays) were obtained for each slice, taken at many angles (180) and positions (160).

The first clinical CT scanner was built and installed at Atkinson-Morley Hospital in England in September 1971. X-ray CT, introduced into clinical practice in 1972, was the first of the modern slice-imaging modalities.

1.2.2 Evolution of computed tomographic scanners

CT scan technology has continued to develop, resulting in reduced scanning times for acquisition of a single slice. Image quality and therefore diagnostic capabilities depend strongly on scan time, since voluntary and involuntary patient motion will lead to losses of image sharpness and to artefacts.

Early CT scanners were extremely slow and required enormous computer facilities to generate comparatively crude scans. Improvements in tube technology and computer hardware and software have shortened scan times and improved the resolution of scans. Reductions in scan time have reduced motion artefact and improved image quality. The incorporation of slip ring technology led to the development of spiral scanners, and more recently, multi-slice scanners with scan times of under a second have become widely available. These important technological changes have been coupled with faster computing and image processing (Kalender, 2005).

The scanner design developments have been referred to as first-, second-, third-, and fourth-generation CT systems, and have followed developments in X-ray, detector and scanner technology, as well in speed of acquisition of image data for complete volumes. Although each subsequent generation is associated with a technical advance, the most recent development of helical CT (commonly referred to as spiral CT (SCT)) and electron beam (or ultrafast) CT (EBCT) have probably been the most clinically important (Garvey and Hanlon, 2002). The introduction of spiral scanning in 1989 has meant the transition from slice-by-slice imaging to true volume imaging. CT today allows imaging of the whole body in five to 20 seconds with sub-millimetre isotropic resolution, with rotation times below one second, and has often been

referred to as the most important invention in diagnostic radiology since the discovery of X-rays. In 2006 the number of clinical installations in operation was estimated to be about 45,000, almost all of which are whole-body spiral scanners.

First generation CT scanners largely resembled Hounsfield's experimental set-up. The first commercial scanners, termed 'second generation', differed only slightly from Hounsfield's scanning system. To speed up scanning and to utilize the available X-ray information more efficiently, detectors were added which entailed changing from a pencil beam to a small fan beam.

Both the first and second generation scanners functioned according to the translation–rotation principle in which the radiation source and the detector scanned the object in a linear translatory motion, with this procedure repeated successively after a small rotational increment. One-hundred and eighty projections were sampled in one-degree steps, which was sufficient to calculate an image with 6400 pixels. Scan times were approximately five minutes and image reconstruction, which was carried out simultaneously, took the same amount of time.

The first whole-body scanners with fan beam systems entered the market in 1976, providing scan times of approximately 20 seconds per image. In the first scanners of this type both the X-ray tube and the detector rotated around the patient, and the scanner concept was termed 'third generation'. Later scanner designs involved a ring-like stationary detector fully encircling the patient so that only the X-ray tube rotated, and were termed 'fourth generation' scanners. Translation–rotation systems have now been completely replaced by rotatory systems, and the third generation design constitutes the standard approach in clinical scanners today. SCT scanning with multi-row detectors provided higher image quality and higher volume scan speed at lower cost.

Continuously rotating CT systems, based on 'slip-ring technology', were introduced in 1987 (Fuchs *et al.*, 2000). The electrical energy necessary for the X-ray tube is transferred by

slip-rings instead of cables. Consequently, it was possible to obtain continuous data acquisition. While the tube is rotating the table supporting the patient moves continuously so that a volume of tissue rather than individual slices is scanned. The data are then reformatted automatically to display the images as axial slices. High quality reconstructed images in coronal, sagittal, and oblique planes can then be acquired using a CT workstation. The advantages of spiral scanning include shorter scanning time, acquisition of thin slices enabling high quality image reconstruction and imaging of smaller objects, and CTA is possible because its speed means that reduced volumes of injected contrast material may be used with more images acquired during the period of peak enhancement. Breath-hold image acquisition with consequent reduction in image artefact is also possible.

At the same time, rotation times were reduced to one second. This technology provided the basis for advanced dynamic examinations and finally for SCT. All CT scanners produced today incorporate slip-ring technology with continuous rotation.

The introduction of four-slice CT scanners in 1998 meant a reduction of volume scan times by a factor of four compared with the typical one second systems with single-row detector, and typical rotation times of 0.5 second. This heralded the start of the 'slice race' that is currently underway between the leading manufacturers and 16-slice scanners became available in 2001, followed by 64-slice scanners in 2004. With 16-MDCT, routine acquisition of 0.75 to 1.0 mm images over the entire volume in the same or less time became possible, and evaluation of trifurcation vessel stenotic disease improved. Routine acquisition of a single dataset covering the chest, abdomen, and pelvis at high resolution (1.0-1.25 mm slice thickness) became clinically feasible. With 64-channel scanners, CT data are generally acquired with submillimetre detector configuration settings, in even less acquisition time. If desired, this allows the reconstruction of CT images with an effective section thickness smaller than one mm (0.4-0.6 mm) resulting in high-resolution isotropic 3D datasets of almost any part of human anatomy (Hallett and

Fleischmann, 2006). Whereas conventional and spiral scanners use a single row of detectors to pick up the X-ray beam after it has passed through the subject, multislice scanners have increased numbers of rows of detectors that enable volume data acquisition instead of individual slice data. In combination with fast rotation times (0.37 seconds rotation speed compared with one second rotation speed for conventional CT) faster image acquisition speed is achievable, and the development of faster computer software enables increased reconstruction and postprocessing capabilities. Together with thin section slices MDCT enables almost isotropic data collection that can be arranged in different planes without compromising the spatial resolution of the original axial images. Particular benefits have been translated to CTA, and cardiac imaging and CT coronary angiography have witnessed striking advances in CT with very high clinical impact (Berry *et al.*, 1999).

1.2.3 Computed tomography image reconstruction

CT image reconstruction involves reconstructing images mathematically from measured data and to display and to archive them in digital form. Hounsfield envisioned dividing a slice into a matrix of voxels. A matrix size of 512 x 512 is commonly used today, with each voxel approximately 0.5 x 0.5 mm. CT image reconstruction depends on quantifying the attenuation of the X-ray beam that occurs in each voxel of the reconstruction matrix. These calculated attenuation values are then represented as grey levels in a 2D image of the slice. Measurements for all rays at all positions and angles can be expressed as sums of the attenuation values in voxels through which each ray has passed.

1.2.4 Computed tomography angiography

Although the introduction of helical scanners resulted in continuous scanning at higher speeds than had previously been achievable, early limitations included single-row detector

systems and computer systems unable to process data at sufficient speeds. In the mid-1990's computer processing speeds enabled reconstruction of large image data sets using dedicated CT workstations. By the late 1990s multirow detectors were introduced to helical scanning systems, improving image resolution whilst reducing scan times. This enabled scanning through long segments of the body using acceptable volumes of rapidly delivered intravenous contrast. Developments in CTA have followed the increase in number of detectors available, and particular advances have been seen in the imaging of the peripheral vascular system and coronary arteries. For example, scanning peripheral arteries from the skull base to the common femoral arteries with collimation of 0.5 mm to one mm takes no longer than 12 to 15 seconds on a 64-row detector CT scanner, and the CTA images are typically superior to those obtained using invasive angiography.

CTA relies on the acquisition of images when the blood vessels are enhanced with intravenous radiodense contrast material. A volume data set is acquired that can be converted into 3D reconstructions using a workstation. Optimal studies can be achieved when iodinated contrast is injected at a rate between three mL/s to six mL/s. Scanning is usually started once the density of contrast within the blood vessel of interest reaches at least 150 Hounsfield Units (HU), although a target range of at least 180 to 200 HU is desirable. Scan delay may then be empirical, preceded by preliminary timing bolus, or by bolus-triggered scanning.

Compared with traditional DSA the technique is non-invasive and provides cross sectional images, allowing a 3D volume data set to be compiled and therefore multiplanar 3D image reconstruction (Rubin *et al.*, 2001; Willmann *et al.*, 2003). Compared with DSA the scans are volumetric, can show vascular anatomy from any orientation (including true cranial-caudal projection), and information beyond the contrast column is gained, including visualization and measurement of both calcified and soft plaque, thrombus, inflammatory changes, and extravascular hemorrhage. CTA is used clinically for the imaging of aortoiliac disease (Wyers *et*

al., 2003), the renal arteries to diagnose and image renal artery stenoses, and for presurgical imaging of renal anatomy in live donors for the detection of arterial or venous anomalies (Kaatee *et al*, 1997; Beregi *et al.*, 1996; Rubin *et al.*, 1995; Cochran *et al.*, 1997), peripheral vascular disease, the pulmonary arteries for diagnosis of pulmonary embolism (Bloomgarden and Rosen, 2001), carotid arteries (Phillips and Bubash, 2002; Alvarez-Linera *et al.*, 2003; Josephson *et al.*, 2004; Budoff *et al.*, 2003), and for the evaluation of coronary artery disease using ultrafast scanning with a very short rotation time and echocardiogram (ECG) triggering (Gaylord, 2002). Disadvantages include a high radiation dose, and the requirement for intravenous contrast medium.

The four main principles of CTA are achieving good arterial contrast enhancement during image acquisition, providing adequate cephalocaudal coverage of the arterial system during optimum contrast opacification, imaging of the arterial tree during the first circulation of contrast to avoid venous artefact, and efficient handling of the huge amount of acquired data using various post-processing algorithms including surface shaded display, volume rendering technique, multiplanar reconstruction and maximum intensity projection (MIP) (Burrill *et al.*, 2007).

1.2.5 Computed tomography image output

CT output occurs in three ways. Firstly planar reconstruction can be performed, the simplest of which is axial reconstruction. The plane may also be curved to give a curved planar reconstruction, and this may be accomplished in 3D for renal and coronary artery analysis. Secondly MIP shows the densest voxels and demonstrates contrast in the blood vessels, as well as calcification in the vessel wall. Lastly, volume rendering encodes different density voxels with varying colors at different intensities. Although volume rendering generates colorful 3D

renderings, in many situations these images lack important information that is found in planar reconstructions (such as accurate measurements, soft tissue, and perivascular processes).

1.2.6 Ionising radiation exposure

The main concern with MDCT scanners is the high radiation dose (Brenner and Hall, 2007). This is approximately 10 millisieverts for an abdominal CT scan, compared with 0.02 for a posteroanterior chest radiograph (www.fda.gov/cdrh/ct/risks.html). A number of methods have been used to reduce radiation dose when using MDCT, including scanning only the area of direct interest and being selective about performing precontrast scans, also known as 'scouts'. If such a scan is necessary, a low-mA protocol should be used. Radiation exposure during cardiac imaging is greater than with conventional coronary angiography, although this can be reduced using ECG pulsing to modulate the mAs of the scanner depending on the cardiac cycle.

By contrast peripheral angiography requires less radiation exposure when using MDCT as opposed to conventional DSA techniques. General dose reducing techniques have been shown to provide successful dose reduction without compromising diagnostic success when conducting MDCT angiography. Decreasing mAs has been shown not to affect the diagnostic sensitivity of MDCT angiography, with a substantial reduction in radiation dose. Reducing kVp, from 120 to 100, significantly reduces patient dose, although a reduced kVp reduces the signal-to-noise ratio. This reduction is compensated for by the attenuation level of iodine, leading to diagnostic images. While these techniques help to reduce the radiation exposure, further reductions will need to be made to compare with exposure during DSA. Other disadvantages of CTA include the use of nephrotoxic contrast media, the technical resources required, and the time necessary to perform the volume rendered reconstructions.

1.3 Investigation of the vascular anatomy of cadaveric surgical flaps

1.3.1 Vascular injection techniques

Although several vascular injection techniques exist for the investigation of the vascular anatomies of surgical flaps, 2D lead-oxide radiography has become the standard. Intravascular injection with ink (**Figure 1.2**), colored latex (**Figure 1.3**), or various substances mixed with gelatin, allows detailed dissection of tissues to be undertaken (Bergeron *et al.*, 2006). Only ink, however, allows appreciation of the vascular territory (Taylor *et al.*, 1994; Taylor and Palmer, 1987), and these methods often have to be combined with radiography as the 3D relationship of the vasculature with the surrounding tissues is lost during dissection. Although diaphanization, as described by Spälteholz and Hirsch (1907), allows visualization of the vascular anatomy of the skin and subcutaneous tissues, tissue preparation is time consuming, and considerable distortion of the anatomy occurs due to shrinkage. Radiographic investigation using a lead oxide-gelatin mixture allows detailed examination of the vascular anatomy of the integument in relation to the surrounding tissues. Red lead oxide (Pb_3O_4) is the form of lead oxide most commonly used by anatomists as its orange-red colour facilitates vascular dissection. Lead oxide in all of its forms, however, is toxic, and gloves and a mask are required when handling it at all times, together with a special facility for its disposal. Barium sulphate has recently been reappraised for vascular injection studies (Tan *et al.*, 1999), and excellent images have been obtained using mammographic radiography. It is non-toxic and consequently no specialized precautions are necessary during its preparation.

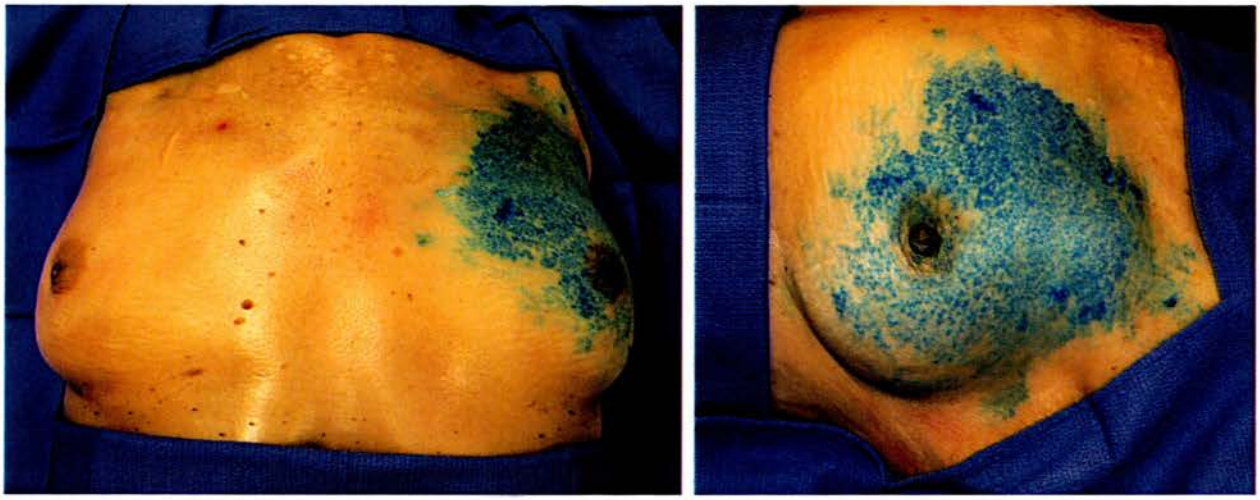

Figure 1.2 Methylene blue dye injection into the isolated left second internal mammary artery perforator to demonstrate the vascular territory of the internal mammary artery perforator flap. This perforator and its venae comitantes can also be used as recipient vessels during free flap breast reconstruction.

Figure 1.3 Red latex injection of the isolated posterior tibial artery and blue latex injection of its venae comitantes in a lower leg specimen to investigate the vascular anatomy of the posterior tibial artery perforator flap, a workhorse flap in lower limb reconstruction.

1.3.2 History of angiographic techniques for the investigation of flap vascular anatomy

The greatest treatise on the anatomy of the perforators of the human body was also the first, and was produced by Carl Manchot, a 23-year old medical student. He produced a study of the cutaneous arteries of the human body in only six months for a competition arranged by the medical faculty of the Kaiser Wilhelm University Strasbourg prior to the advent of radiography

(Manchot, 1889; Manchot, 1983). His work, however, lay untranslated in the german literature until the 1970s, when it became apparent that many of the axial pattern flaps that had recently been developed were based on cutaneous arteries that had already been described by him. Because of this Manchot's work has often been described as plastic surgery's missed opportunity (Morain, 1985).

In 1936 Salmon published his book entitled 'Artères de la peau' (Salmon, 1936; Salmon, 1988), which was a reappraisal of the works of Manchot using radiography. Salmon produced a detailed account of the cutaneous vasculature, and following on from observations by Manchot, highlighted the three-dimensionality of the composite vascular territories. In 1980 Taylor set out to reappraise the work of Manchot, and in 1982 became aware of the works of Salmon through a communication with Lamberty (Taylor, 2002). Taylor and Palmer (1987) used a modification of Salmon's lead tetroxide mixture to create a total radiographic montage of the cutaneous arteries. They described 40 angiosomes and an average of 374 major cutaneous perforators, with each angiosome supplied by the branches of a named source artery, noting that each was connected to their neighbour, usually by reduced caliber vessels, which were termed 'choke' arteries, but sometimes by true anastomotic vessels of a similar caliber. In experimental studies Morris and Taylor (1993) found that when a flap is based on the vessels of one angiosome, the adjacent angiosome could be captured with safety across the choke vessel watershed between adjacent angiosomes.

In response to the shortcomings of 2D image representation for the investigation of 3D vascular anatomy superficial to the deep fascia, as is required for the understanding and development of perforator flaps, Nakajima *et al.* (1998) described a method of 3D computer graphical reconstruction of 2D lead oxide radiographs. This enabled the classification of the components of the vascular plexus of each angiosome in 3D, which had not been previously possible, and led to the development of new flaps. Other investigators have attempted a novel

approach at 3D representation of 2D radiographs, using stereoscopic radiography to create stereographic angiographic images (Kawai *et al.*, 2004). These require special viewing techniques that involve crossing the eyes to superimpose the images until they appear in 3D.

1.4 Computed tomography angiography and venography for the investigation of flap vascular anatomy

The introduction of CT has since revolutionized many surgical specialties (Nagler *et al.*, 1997; Chow *et al.*, 2005). Masia *et al.* (2006) reported the results from preoperative planning in 66 DIEAP flaps using MDCT with 3D reconstruction. Neither false-positive nor false-negative results were found when comparing CT images with the intra-operative findings, and the information acquired allowed reduction of operating time and safer performance of surgery. Alonso-Burgos *et al.* (2006) evaluated multislice-CTA 3D volume-rendered reconstruction for preoperative planning in six patients undergoing DIEAP flap reconstruction. Accurate identification of the main perforators was achieved in all cases with a very satisfactory concordance between CTA images and surgical findings (**Figure 1.4**). The inherently high contrast resolution of CT enables detailed imaging of tissues that have undergone vascular injection with radio-opaque substances. The use of CT eliminates the superimposition of images of structures outside the area of interest, and images from a single CT procedure can be viewed in the axial, coronal, or sagittal planes. 3D volume-rendered reconstruction can also be performed to allow complex visualizations (**Figures 1.5 to 1.9**). The main advantage over conventional 2D projection radiography is the ability to evaluate the 3D relationship of a given vessel with respect to the surrounding tissues.

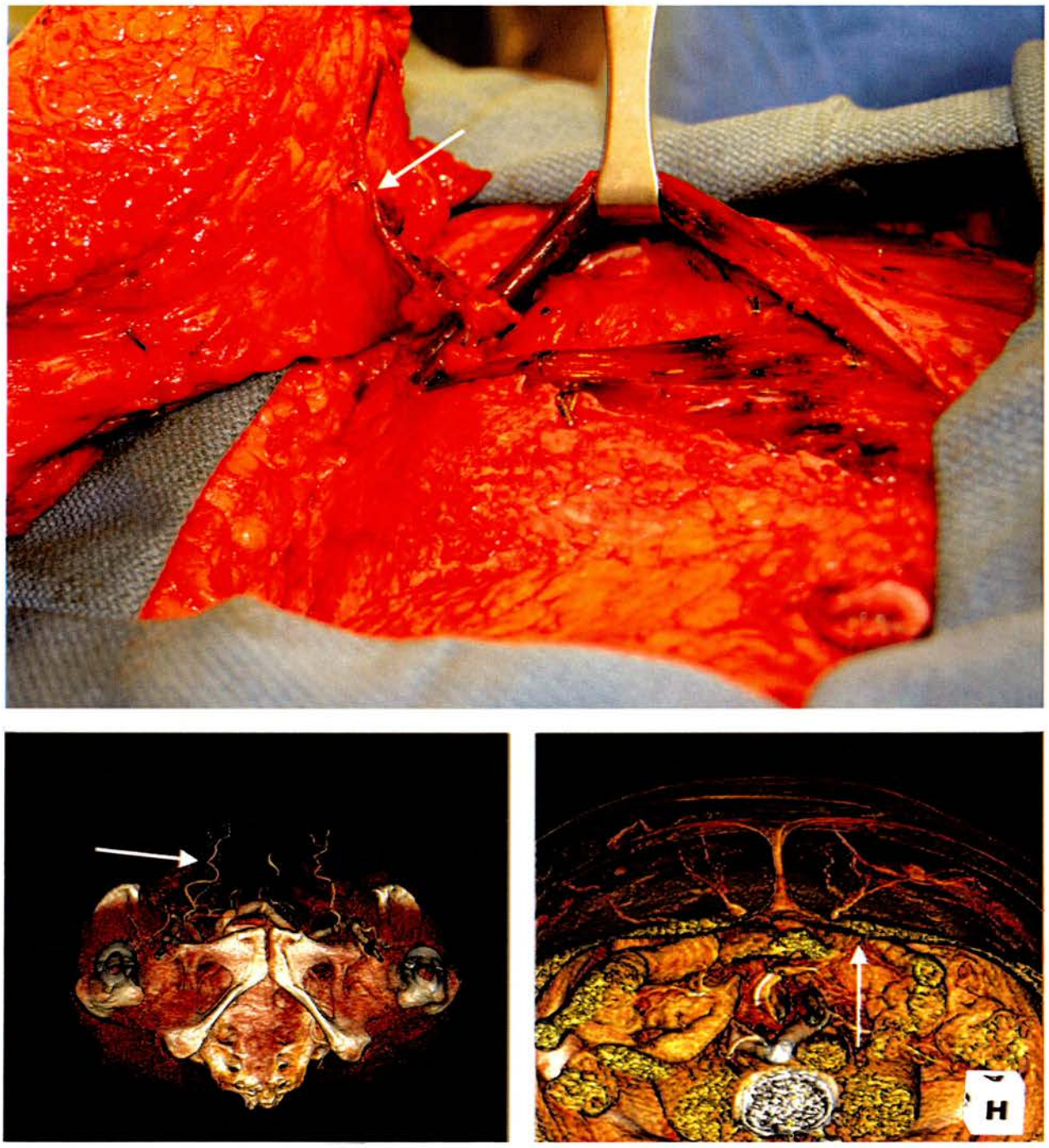

Figure 1.4 Left: Volume rendered CTA of the abdomen revealing the perforators of the deep inferior epigastric artery; Right: Compare with intraoperative findings from the same patient demonstrating the high concordance with the preoperative CTA images.

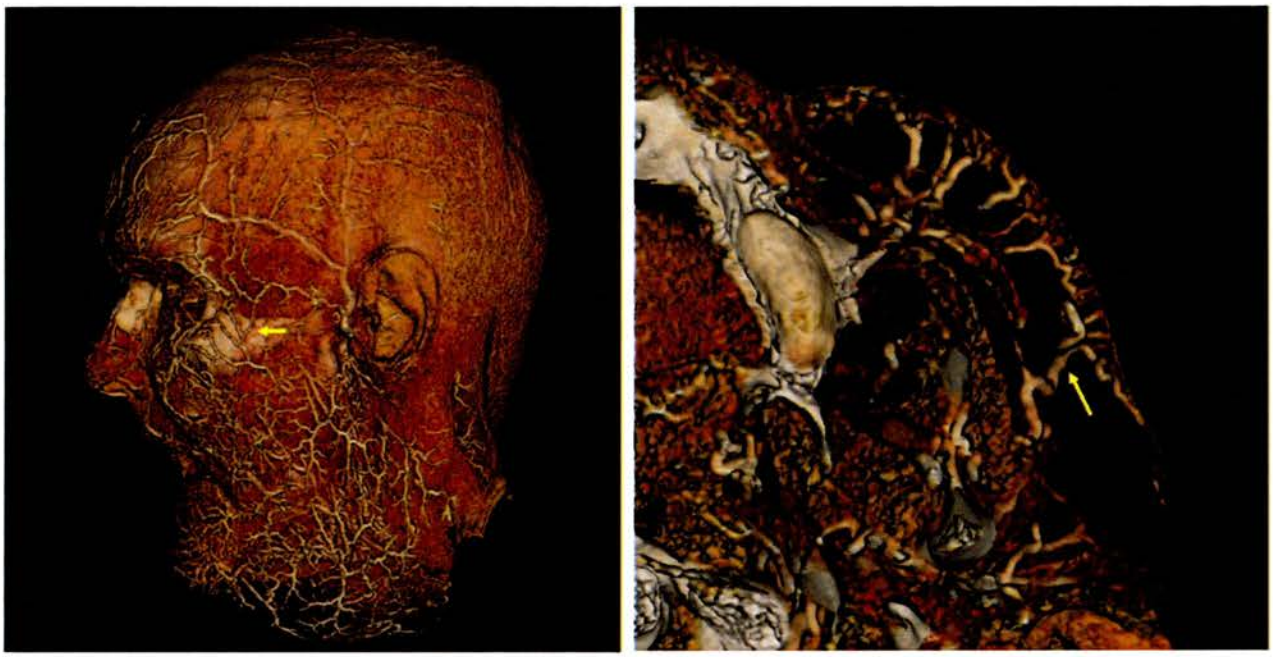

Figure 1.5 Static three-dimensional computed tomographic angiogram of a head dissection following cannulation of the internal and external carotid arteries bilaterally and injection of a barium sulphate/gelatin mixture. Note the rich vascular network and perforators originating from the facial artery and superficial temporal artery (yellow arrow).

Figure 1.6 Static CT angiogram of a hand (volar view right hand) following cannulation of the brachial artery and injection of a barium sulphate/gelatin mixture. Note the ability to distinguish the position of the arteries relative to the bones of the hand.

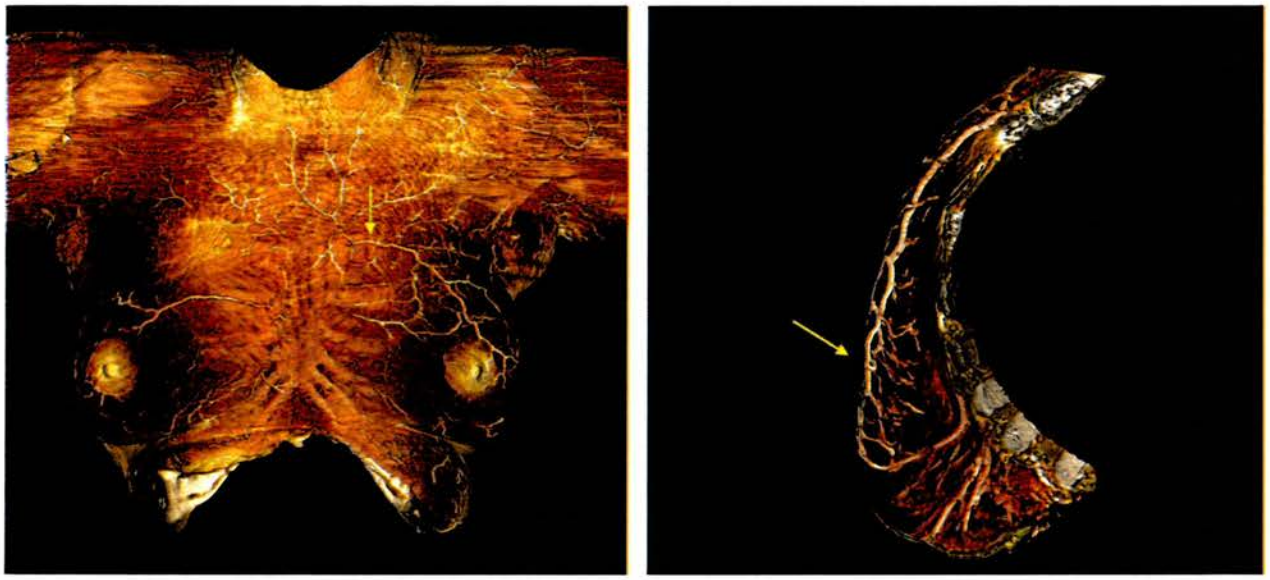

Figure 1.7 Anteroposterior (left) and lateral (right) views of a static three-dimensional computed tomographic angiogram of a chest wall following cannulation of the axillary artery and injection of a barium sulphate/gelatin mixture. Note the extensive vascular distribution of the large second intercostal internal mammary artery perforator.

Figure 1.8 (Left) Static three-dimensional computed tomographic angiogram of a right lower leg following cannulation of the popliteal artery and injection of a barium sulphate/gelatin mixture. (Right) Static three-dimensional computed tomographic angiogram of the integument of the right lower leg placed over a fiberglass cast in its anatomical position.

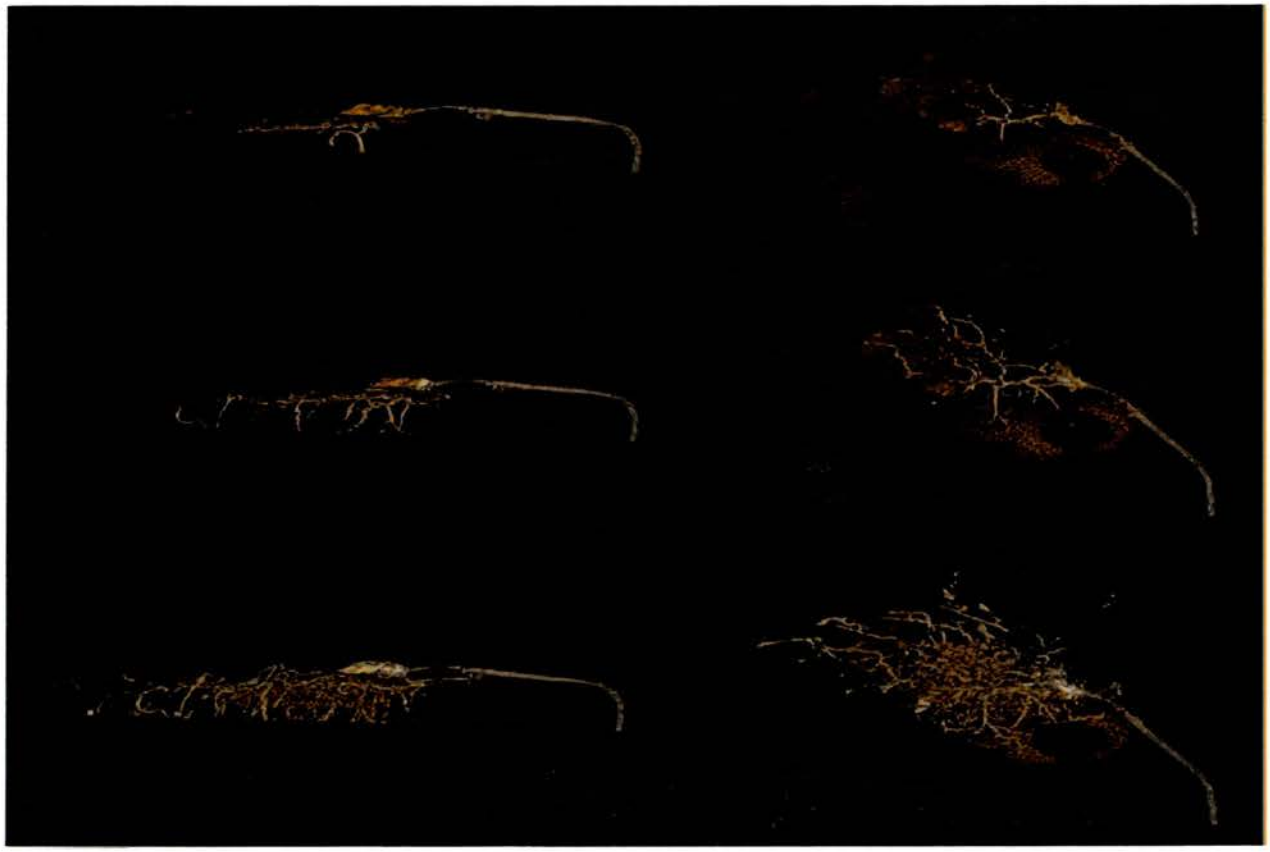

Figure 1.9 Lateral and oblique views of dynamic computed tomographic angiograms of an anterolateral thigh flap during injection of iodinated contrast medium through a cannulated perforator from the lateral circumflex femoral artery. The images were taken at 0.5ml filling increments. Note perforator branches running along the subdermal plexus and suprafascial level on the lateral views. Also note the rich vascular communication between the subdermal plexus and suprafascial plexus.

4D dynamic CTA and CTV are promising techniques that overcome many of the disadvantages of traditional radiographic techniques. Intravascular injection of iodinated CT contrast medium into a cadaveric surgical flap using a delivery pump enables perfusion of the flap to be appreciated in 3D. This allows investigation of the sequence of vascular filling, the vascular territory, the recruitment of adjacent angiosomes, and the simultaneous investigation of

multiple angiosomes within the same flap. In addition, because of the low viscosity of the iodinated contrast medium, the subdermal plexus can be imaged dynamically, which is not achievable using lead-based mixtures (Imanishi *et al.*, 2000). Another advantage is that the contrast agent can be washed out of the flap, enabling repeated investigations of different perforators within the flap under different conditions, for example before and after flap thinning.

1.5 History of surgical flap development

The evolution of flap development has followed our understanding of their vascular supply (Hallock, 2003; Timmons, 1985). The early random pattern flap, which by definition lacked an axial arteriovenous system, was constrained by rigorous length-to-width ratios to ensure viability. It was not until Milton demonstrated in the pig model that flaps made under similar conditions of blood supply survived to the same length regardless of width, and found that the only effect of decreasing width was to decrease the chance of a pedicle containing a large vessel (Milton, 1970). The axial pattern flap, introduced by McGregor and Jackson (1972) in their classic description of the groin flap, represented the next milestone in flap development (McGregor and Morgan, 1973). Defining the vascular supply to the groin flap enabled its use for the first 'free flap' by Taylor and Daniel (1973).

In the 1970s the works of Manchot were discovered and translated (Manchot, 1889; Manchot, 1983), revealing that many axial flaps were based on vessels that he had already described. Musculocutaneous flaps which were introduced by Ger (1966) and by Orticochea (1972) rapidly became popular due to their reliability and wide arcs of rotation. Descriptions of the vascular territories of these flaps were later provided by McCraw *et al.* (1977) and by Mathes and Nahai (1981). In 1981 Pontén reported that length-to-width ratios in excess of 2.5:1 could be achieved in flaps from the lower leg if the deep fascia was included in an area where local skin flaps had previously been unfavourable. The anatomical basis for these fasciocutaneous flaps

was later described by Haertsch (1981), Barclay *et al.* (1982), and by Cormack and Lamberty (1984; Lamberty and Cormack, 1986). In 1987, following reappraisal of the works of Manchot and Salmon (1936; 1988), Taylor and Palmer (1987) introduced the concept of the angiosome, defining it as a 3D anatomic territory supplied by a source artery that spans between the skin and bone, and this concept has proven invaluable in flap design.

The perforator flap concept was introduced by Kroll and Rosenfield in 1988 during their description of a new type of flap based on unnamed perforators located near the midline of the lower back region, noting that perforator flaps combined the reliable blood supply of musculocutaneous flaps with the reduced donor site morbidity of a skin flap. In 1989 this concept was crystallized when Koshima and Soeda described an inferior epigastric artery skin flap without rectus abdominis muscle for reconstruction of floor of the mouth and groin defects, noting that a large flap without muscle could survive on a single muscle perforator.

Since their introduction there have been multiple reports of new perforator flaps in the plastic surgery literature, and the indications for their use is ever expanding. The main advantage is that the muscle underlying the adipocutaneous flap is left *in situ* (**Figure 1.10**), preserving form and function at the donor site, which is the basic tenet of plastic surgery. The composition of these flaps can also be tailored to reconstruct a defect. For example the lateral circumflex femoral artery (LCFA) axis enables multiple tissue components to be raised in various proportions based on a single source vessel (Lin *et al.*, 2006), and the LCFAP-*vl* and TAP flaps can be used for resurfacing shallow defects without the bulk and unpredictable degree of atrophy associated with musculocutaneous flaps. The reduced donor site morbidity also often leads to faster recovery and reduced postoperative pain.

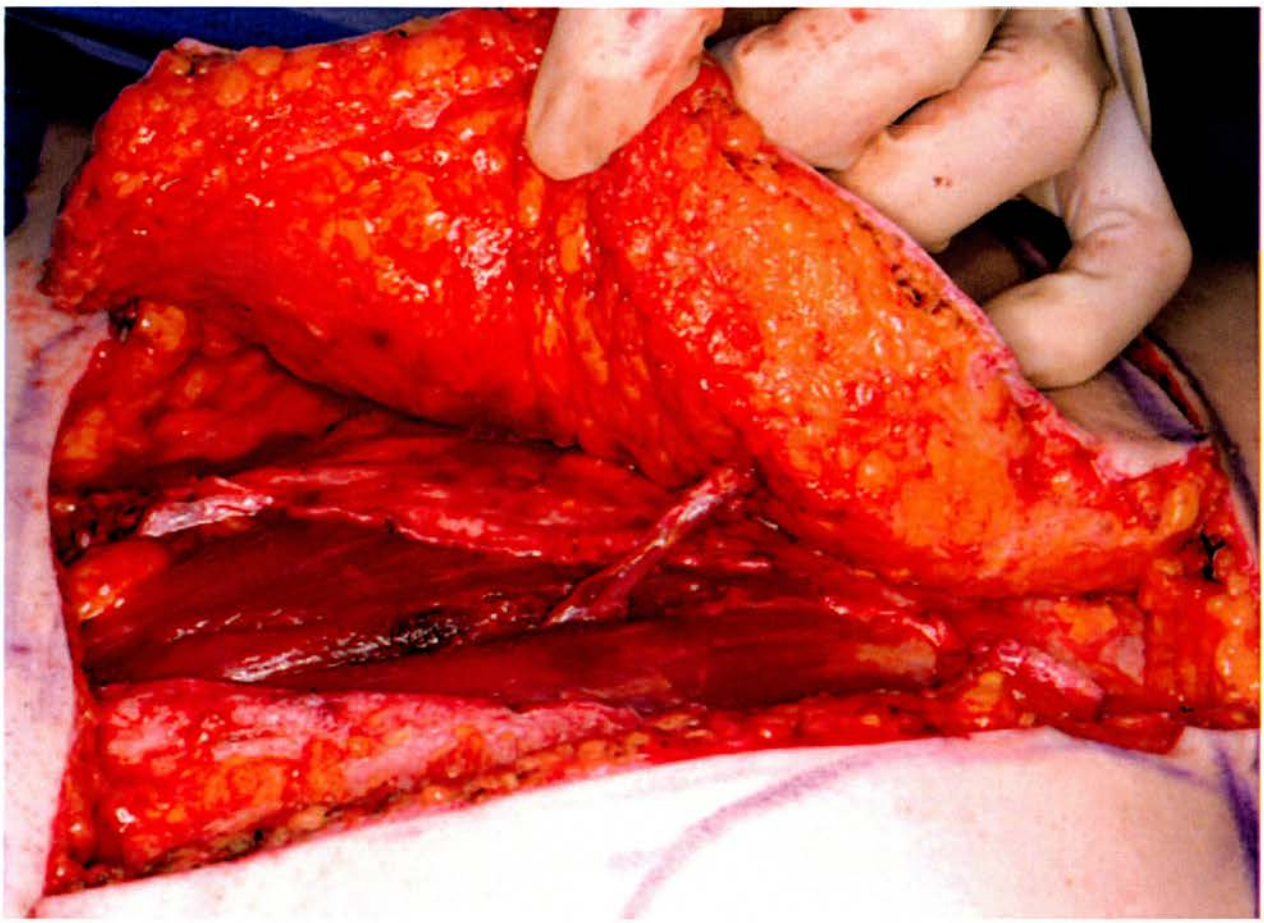

Figure 1.10 Intraoperative photograph of deep inferior epigastric artery perforator flap harvest with splitting and preservation of the underlying rectus abdominis muscle.

1.6 Perforator flap nomenclature

Ever since their conception, there has been debate over what constitutes a true perforator flap, and how a perforator should be defined (Blondeel *et al.*, 2003; Taylor, 2003). Purists state that a muscle perforator flap is the only real perforator flap, due to the additional effort and time needed to dissect the perforator out from between the muscle fibers to reduce the donor site morbidity (Wei *et al.*, 2001). A variety of terms have been used to name perforator flaps, including anatomical location (eg anterolateral thigh perforator flap), arterial supply (eg thoracodorsal artery perforator flap), or muscle of origin, and this has led confusion in the

literature.

In an attempt to introduce consistency, a standardized nomenclature has been agreed upon that describes all perforator flaps according to the main artery of origin (Geddes *et al.*, 2003; Blondeel *et al.*, 2006)

- Cutaneous flaps include all flaps previously described as axial, septocutaneous, and fasciocutaneous [Mathes and Nahai type A and B fasciocutaneous flaps (1997)].
- Cutaneous flaps are divided into either cutaneous flaps or musculocutaneous perforator flaps.
- Perforator flaps are the true musculocutaneous perforator flaps [Mathes and Nahai type C fasciocutaneous flaps (1997)] in which the source vessel to the skin arises from and passes through the underlying muscle. Flaps are named according to the source vessel, and the suffix -AP signifies a true musculocutaneous perforator flap.
- Where the flap is harvested based on septocutaneous or fasciocutaneous vessels, the suffix -s is added to the flap vessel abbreviation (eg. an anterolateral thigh flap harvested as a septocutaneous flap is abbreviated to LCFAP-*s*).
- The perforator flap nomenclature correlated to the angiosomes of the body is used according to the descriptions by Taylor and Palmer.
- When multiple flaps are based on musculocutaneous perforators of the same source artery, the muscular origin of the cutaneous vessels is abbreviated and italicized to indicate the anatomic origin of the flap (eg. LCFAP-*vl* for the vastus lateralis muscle).
- In the case of flaps based on source arteries that have numbered segmental origins, such as the posterior intercostal or lumbar arteries, the numbered source vessel requires notation. The corresponding vessel number is added after the flap abbreviation (eg. PIAP-8 flap to indicate the eighth posterior intercostal perforators).

Table 1.1 Nomenclature of the commonly used perforator flaps

Common name	New nomenclature	Source artery	Muscle of origin
ALT	LCFAP-*vl*	Descending branch of the lateral circumflex femoral artery	Vastus lateralis
TAP	TAP	Thoracodorsal artery	Latissimus dorsi
DIEP	DIEAP	Deep inferior epigastric artery	Rectus abdominis

1.7 Perforator flap hyperperfusion theory

A phenomenon universal to perforator flaps is the ability of a single perforator to support a relatively large fasciocutaneous vascular territory, which may occur due to hyperperfusion through the isolated perforator vessel. Perforator flaps are perfused through a long vessel whose calibre decreases from its origin to the skin, because all branches have been sealed, resulting in a conduit with resistances in series, rather than a tree with resistances in parallel, as in the normal systemic circulation. Rubino *et al.* (2006), using colour flow Doppler to measure the relationship between blood velocity and flow between the pedicle and perforator vessels in perforator flaps, found postoperatively that blood velocity in the perforator was significantly higher than in the pedicle, with the velocity of blood and the rate of flow reaching the skin higher in perforator flaps than in the normal circulation. Coscia and Rubino have developed a mathematical model for normal and perforator flap circulation based on Doppler and anatomical measurements to describe the rate of flow within the vessel, based on the difference between the vessel radius at the pedicle and the periphery, the length of the pedicle, the blood viscosity, and the pressure gradient.

Hyperperfusion of the LCFAP-*vl* flap was noted in its first report by Song *et al.* (1984),

and this has been later confirmed in several studies. Heitland *et al.* (2005) measured blood volume flow and velocity at the donor and recipient vessels of perforator flaps pre- and postoperatively using Duplex ultrasound and found that blood flow was twice as great as in the donor vessels, which they concluded was evidence of flap hyperperfusion. In a study by Figus *et al.* (2006) 16 DIEAP flaps were monitored postoperatively for a minimum period of 48 hours using laser Doppler flowmetry and lightguide reflectance spectrophotometry to analyse blood flow and oxygenated haemoglobin percentage in the cutaneous microcirculation of the flap. Laser Doppler flowmetry demonstrated an increase in capillary flow in comparison to the pre-operative levels, providing evidence for flap hyperperfusion. Gravvanis *et al.* (2007) evaluated blood perfusion and blood flow within 11 LCFAP-*vl* flaps using both near-infrared spectroscopy and color Doppler ultrasonography and documented evidence of hyperpefusion postoperatively.

Bhattacharya *et al.* (2005) have shown that the diameter of perforators correlates directly with their perfusion pressure, supporting the theory that the dominant perforator with the largest diameter should be sought to enable flap hyperperfusion. Other factors that may contribute to the hyperperfusion of a perforator flap include sympathetic denervation leading to vasodilatation and decrease in vascular resistance (Banbury *et al.*, 1999), and also a higher blood flow rate at the recipient vessel than at the donor pedicle (Heitland *et al.* 2005).

Morris and Taylor have demonstrated experimentally that one adjacent vascular territory may be captured reliably in a surgical flap (1993). Hyperperfusion through a single perforator, however, may allow capture of two adjacent angiosomes.

1.8 Anterolateral thigh perforator (LCFAP-*vl*) flap

1.8.1 Background

The LCFAP-*vl* flap, first described by Song *et al.* in 1984, is a versatile and reliable flap (Wei *et al.*, 2002; Celik *et al.*, 2002; Kuo *et al.*, 2002; Gedebou *et al.*, 2002) that has achieved popularity in head and neck surgery (Koshima *et al.*, 1993; Chana and Wei, 2004), as well as in reconstructive surgery of the hand and upper and lower extremities (Javid and Cormack, 2003; Wang *et al.*, 2005; Adani *et al.*, 2005; Yildrim *et al.*, 2006; Herter *et al.*, 2007; Saint-Cyr and Gupta, 2007). The flap minimizes the donor site associated with harvest of the vastus lateralis muscle (Dowden and McCraw, 1980; Drimmer and Krasna, 1987), with donor site morbidity related to the amount of muscle harvested with the skin paddle (Kimata *et al.*, 2000; Lipa *et al.*, 2005; Mureau *et al.*, 2005).

The chimeric principle allows the composition of the flap to be tailored to accurately match the requirements of the recipient site, with multiple components raised on different perforators from the lateral femoral circumflex axis (Koshima, 1991). This includes the vastus lateralis, tensor fascia lata, and rectus femoris muscles, and iliac crest (Koshima *et al.*, 1993; Lin *et al.*, 2006a; Lin *et al.*, 2006b), and can be combined with vascularised fibula for use as an osteocutanous flap (Koshima *et al.*, 1998). An adjacent flap can also be harvested and anastomosed to a branch of the LCFA, including the groin flap or medial thigh flap, according to the mosaic flap principle (Koshima *et al.*, 1994).

Reports suggest that the LCFAP-*vl* flap can be raised with or without fascia (Koshima *et al.*, 2003), and can be safely thinned as either a one-stage procedure in the Asian population, or as a two-stage procedure to resurface shallow defects (Kimura and Satoh, 1996; Kimura *et al.*, 2001; Adani *et al.*, 2005, Yang *et al.*, 2006) (**Figure 1.11**). In Western patients, however, primary flap thinning thinning has been reported to result in high rates of partial or complete flap

necrosis (Ross *et al.*, 2003; Alkureishi *et al.*, 2003; Van Landuyt, 2006). It can be used as a flow-through flap to reconstruct defects of both soft tissues and major vessels in the extremities (Koshima *et al.*, 1995), and as an adipofascial flap (Hsieh *et al.*, 2003). It can also be pedicled proximally for coverage of defects at the perineum, lower abdominal wall, and greater trochanter, and distally for coverage about the knee (Gravvanis *et al.*, 2006; Hallock, 2005; Pan *et al.*, 2004; Yildrim *et al.*, 2003). The anterior or lateral branch of the lateral cutaneous nerve of the thigh can be included to provide sensation (Ribuffo *et al.*, 2005). Primary closure of the donor site can be achieved if the width of the flap does not exceed 8cm, otherwise skin grafting or a V–Y local advancement flap can be used (Yamada *et al.*, 2001). Flap harvest is associated with little or no donor site functional deficit (Kimata *et al.*, 2000; Kuo *et al.*, 2001). Most series have been described in the Asian population where the flap tends to be approximately 7mm thick (Koshima, 2000; Nakayama *et al.*, 2002), about half the thickness of the flap in the Western population (Yu, 2004). In the Western population acoustic Doppler has a low accuracy related to body mass index (Yu and Youssef, 2006).

Clinical studies have demonstrated that the LCFAP-*vl* flap can be safely extended in size of the skin paddle. Koshima *et al.* have reported success with LCFAP-*vl* flaps of up to 30 cm in length (1995), and Yildirim *et al.* have reported successful LCFAP-*vl* flap harvest of up to 20cm in width (2003). Methods to reliably further increase the flap cutaneous territory have included mosaic and chimeric flap harvest designs. Mosaic anterior thigh flaps consist of connected anterolateral thigh-medial thigh flaps, the pedicles of which are the perforators of the lateral circumflex femoral system and the perforators from the femoral vessels (Koshima, 1991). The two adjacent flaps are simultaneously elevated with double pedicles including the lateral circumflex femoral system, and the pedicle of the medial thigh flap is anastomosed to the muscle branch or the descending branch of the lateral circumflex femoral system, and the system is joined to a single recipient vessel (Koshima *et al.*, 2004). Massive thinned flaps from the thigh

region have also been reported, with Kimura *et al.* safely performing primary thinning of flaps of up to 30 cm in length and 15 cm in width based on perforators from the LCFAP-*vl* flap and the tensor fasciae latae perforator flaps from the common pedicle of the LCFA (2006). Chimeric composite flaps, such as the combined anterolateral and anteromedial thigh flap, are combined using microanastomoses, each with an isolated pedicle and a single vascular source (Koshima *et al.*, 1993). Recently Mehrara (2007) has reported that the LCFAP-*vl* flap cutaneous paddle can be safely extended up to 480cm^2 (range 240-480cm^2, mean 322cm^2) perfused by a single perforator from the LCFA without the need for chimeric or mosaic flap anastomses.

Figure 1.11 Left: Lower leg defect; Right: Postoperative photographs following reconstruction with an anterolateral thigh flap thinned primarily, revealing good contour.

1.8.2 Anatomy

The perforators to the LCFAP-*vl* flap originate from the descending branch of the LCFA. This lies in the intermuscular septum between the rectus femoris and vastus lateralis muscles along with the motor nerve to the vastus lateralis, along a line drawn between the anterior superior iliac spine to the superolateral border of the patella (Xu *et al.*, 1988) (**Figure 1.12**). The

length of the pedicle is typically 8 to 16 cm, with a vessel diameter of larger than 2 mm. Musculocutaneous perforators are found most commonly (Wei *et al.*, 2002; Kimata *et al.*, 1998), and therefore in the majority of cases flap harvest requires a careful dissection of a suitable intramuscular perforator within the vastus lateralis muscle. Yu, in a series in a Western population, found one to three cutaneous perforators in predicable locations approximately 5cm apart and 1.5 cm lateral to the A-P line, with the perforator that is most consistently present located around the mid-point, which he termed perforator B (2004). Both Wei *et al.* (2002) and Yu (2006) have reported a learning curve, and with experience a perforator can be found in almost all cases.

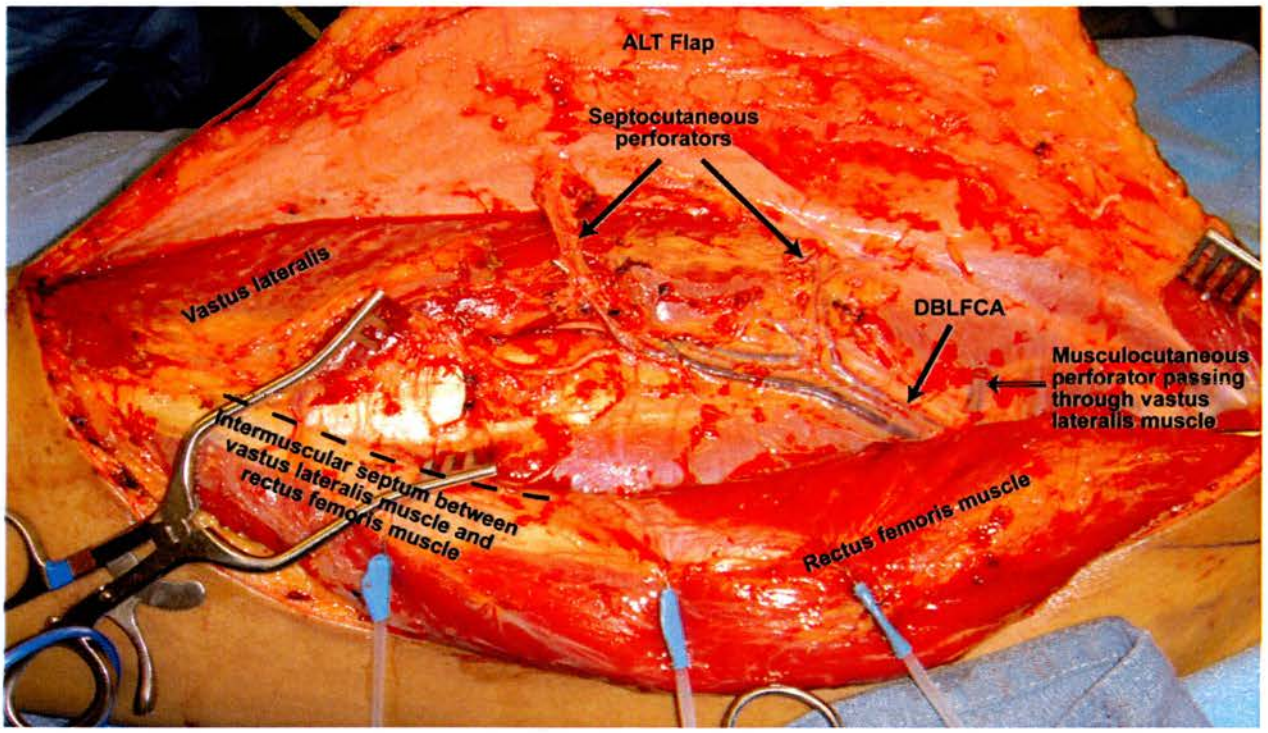

Figure 1.12 Intraoperative anatomy of the anterolateral thigh perforator flap.

1.8.3 Surgical technique

Doppler is usually used to identify the perforators preoperatively, with the flap usually designed about perforator B. A longitudinal skin incision is made on the medial side of the flap and dissection is carried out at the suprafascial level. Entering the intermuscular septum distally between the rectus femoris and vastus lateralis muscles allows direct visualization of the descending branch and location of the perforators. One or more appropriate musculocutaneous or septocutaneous perforators are selected and dissected through the vastus lateralis muscle or its investing fascia and epimysium. Some authors advocate leaving a cuff of muscle around the perforator to minimize damage and spasm during dissection. A visible pulse and an audible arterial and venous Doppler signal must be heard before completing the final skin incision of the flap. The dissection continues until the descending branch of the LCFA and its vena comitans are isolated with careful preservation of the motor nerve. The lateral femoral cutaneous nerve is incorporated if a sensate flap is required. Koshima advocates that the descending branch should be transected distal to the branch to the rectus femoris muscle to prevent possible ischemic necrosis of the rectus femoris muscle (Koshima *et al.*, 1993).

1.9 Thoracodorsal artery perforator (TAP) flap

1.9.1 Background

The latissimus dorsi musculocutaneous flap is traditionally a workhorse for local and distant reconstruction of the chest wall, breast, head and neck, and limbs (Schneider *et al.*, 1977; Muhlbauer and Olbrisch, 1977; McCraw *et al.*, 1977; Bostwick *et al.*, 1978; Barton *et al.*, 1983; Haughey and Fredrickson, 1991; Davis *et al.*, 1992; Pinsolle *et al.*, 2006; Apffelstaedt, 2002; Delay *et al.*, 1998). The flap was first described by Tansini in 1896 as a skin rotation flap

pedicled in the axilla for reconstruction of mastectomy defects, where high rates of distal flap necrosis prompted cadaveric appraisal of the vascular anatomy of the region (Maxwell, 1980). In 1906 the latissimus dorsi musculocutaneous flap was described, demonstrating increased reliability of the skin paddle, and in 1912 D'Este described a superiorly based latissimus dorsi skin flap for reconstruction of the mastectomy defect. Adoption of Halstedian doctrines, where breast reconstruction following mastectomy was avoided for fear of increasing the chance of tumour recurrence, prevented the reintroduction of the latissimus dorsi musculocutaneous flap for breast reconstruction until the description in 1976 by Olivari, followed by descriptions by Schneider, Hill, and Brown (1977), Muhlbauer and Olbrisch (1977), McCraw, Dibbell, and Carraway (1977), and Bostwick, Vasconez, and Jurkiewicz (1978).

Although the functional sequelae following harvest of the latissimus dorsi muscle are well tolerated by compensation via the teres major (Brumback *et al.*, 1992; Russell *et al.*, 1986; Laitung and Peck, 1985), previous questionnaire-based and functional assessment based studies of women who have undergone pedicled full-width latissimus dorsi musculocutaneous flap breast reconstruction have revealed postoperative functional deficit (Fraulin *et al.*, 1995; Russell *et al.*, 1986; Adams *et al.*, 2004). Fraulin *et al.* found that following unilateral pedicled latissimus dorsi post-modified radial mastectomy breast reconstruction there was a significant difference between operated and non-operated shoulders for power and endurance measurements of adduction and abduction, as well as for work simulations of ladder climbing, painting above shoulder level, and push-up from a chair (Fraulin *et al.*, 1995). Using a postal questionnaire evaluation for patients following post-mastectomy latissimus dorsi breast reconstruction, Adams *et al.* found that activities of reaching overhead and lifting groceries were significantly impaired, as was swimming (Adams *et al.*, 2004). In an attempt to minimise the postoperative functional sequelae, Tobin *et al.* (1981 a and b) developed the split latissimus dorsi muscle flap, utilising the dual blood supply of the descending and transverse branches of the thoracodorsal artery, and

this has recently been reappraised by Schwabegger *et al.* (2003), who found full strength on manual evaluation at 2 months postoperatively.

To reduce the donor site morbidity from latissimus dorsi musculocutaneous flap harvest the TAP flap was described by Angrigiani *et al.* in 1995. It is versatile and reliable in experienced hands (Guerra *et al.*, 2004; Heitmann *et al.*, 2003; Schwabegger *et al.*, 2002; Kim *et al.*, 2002; Thomas *et al.*, 2005; Kim, 2003; Koshima *et al.*, 1999; Angrigiani *et al.*, 1995; Spinelli *et al.*, 1996), with a long pedicle and a large flap cutaneous territory that can be reliably perfused by a single perforator. It can be harvested with minimal donor site morbidity and is indicated for defects of the head and neck, trunk, and upper and lower extremity, as well as for use as a pedicled flap for breast reconstruction (Hamdi *et al.*, 2004). The flap may also be harvested with a cuff of latissimus dorsi muscle where there are multiple small caliber perforators to protect the perforators (Hamdi *et al.*, 2004 and 2006). There is also potential for use of both the perforator and muscle flap to reconstruct two distinct defects, or as a chimeric flap pedicled on the thoracodorsal vessels (Kim, 2005; Van Landuyt *et al.*, 2005), and it can also be used as a flow-through flap (Koshima *et al.*, 1999). An osteocutaneous flap can be raised with a segment of vascularised scapula (Momeni *et al.*, 2006).

Although inherently thin (**Figure 1.13**), some authors have demonstrated that the TAP flap can be reliably thinned between the superficial and deep adipose layers (Kim *et al.*, 2002; Kim and Kim, 2003; Kim *et al.*, 2001). There is versatility in the orientation of the flap design (Koshima *et al.*, 1999), and primary closure is achievable in flaps of up to 10cm in width. For a sensate flap a lateral branch of the intercostal nerve can be included.

Underutilisation of the TAP flap may be related to confusion regarding the location of reliable perforators from the thoracodorsal artery. In the original flap description, Angrigiani *et al.* found that the descending branch provided 2 to 3 perforators, with the proximal perforator found approximately 8cm below the posterior axillary fold and 2 to 3 cm from the lateral border

of the muscle, with distal perforators spaced 2 to 4 cm apart (Angrigiani *et al.*, 1995), and these findings have been confirmed by other anatomical and clinical studies (Guerra *et al.*, 2004; Heitmann *et al.*, 2003; Thomas *et al.*, Spinelli *et al.*, 1996. Schwabegger *et al.*, 2002). Schwabegger *et al.* (2002) found that perforators were frequently not found in a line along the muscle fibres, and also that the dominant perforator was located more caudal to the axillary fold than previously described. The use of unidirectional Doppler ultrasound is associated with a high range of false positive results for identifying TAP flap perforators (Blondeel *et al.*, 1998), and colour Duplex scanning is considered to be more reliable (Schwabegger *et al.*, 2002; Lin *et al.*, 2006). The skin paddle is generally designed based on aesthetic considerations of the donor and recipient site (Millard, 1981; Ruetschi *et al.*, 1981).

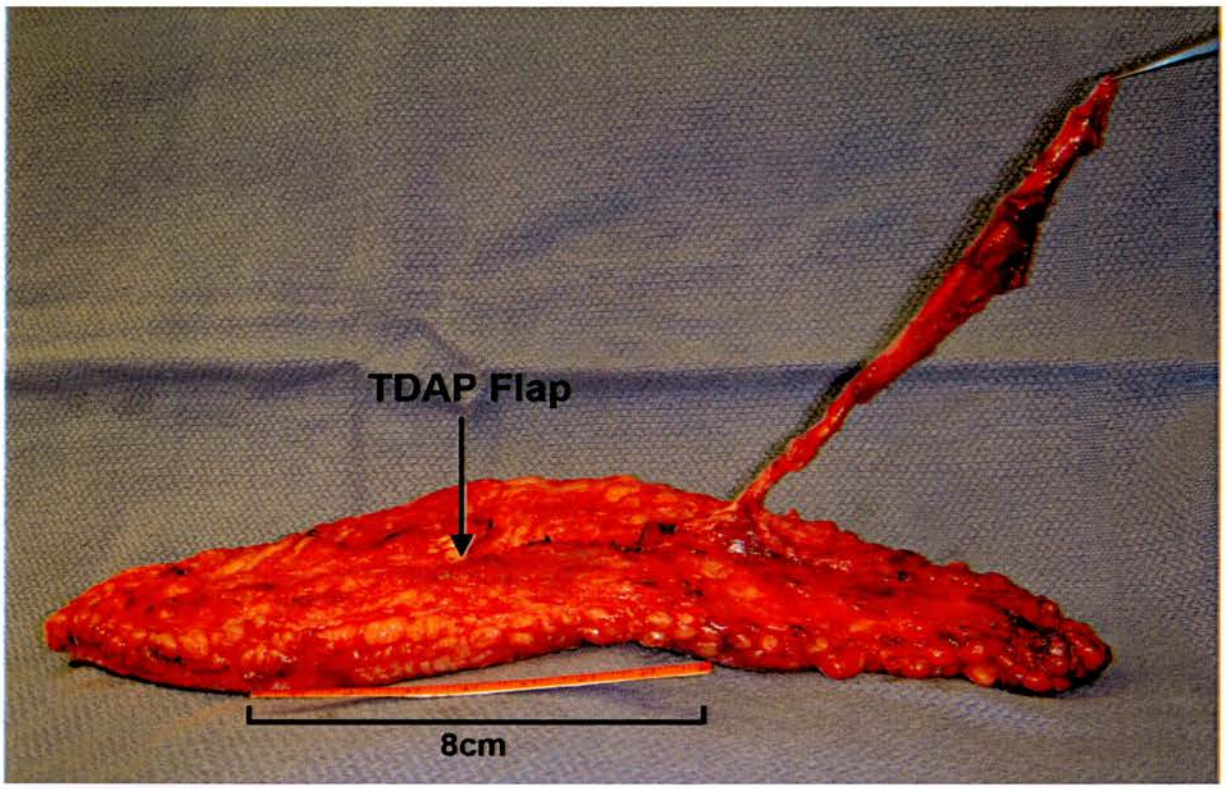

Figure 1.13 Intraoperative harvest of a thoracodorsal artery perforator flap demonstrating the inherent thinness and pliability of the flap.

1.9.2 Anatomy

The thoracodorsal artery reliably divides into descending (or lateral) and transverse (or medial) branches on the latissimus dorsi muscle, with the thoracodorsal nerve dividing to follow the artery (Bartlett *et al.*, 1981; Friedrich *et al.*, 1988). The descending branch of the thoracodorsal artery is known to have the largest and most reliable perforating vessels, and is found descending along a line at approximately 2cm behind the anterior border of the latissimus dorsi muscle edge (Guerra *et al.*, 2004; Heitmann *et al.*, 2003; Thomas *et al.*, 2005) (**Figure 1.14**). Perforators are located within 8 cm of the neurovascular hilus, 4cm inferior to the tip of the scapula, with the first perforator always the largest and most consistent. In an anatomical study Thomas *et al.* found septocutaneous perforators from the thoracodorsal artery supplying the skin, in addition to the musculocutaneous perforators, in 60 percent of specimens. The septocutaneous perforators originated as a single branch from the thoracodorsal artery that was identified near the lateral border of the muscle, reaching the skin without penetrating the latissimus dorsi. An inverse relationship was found between the size and number of musculocutaneous versus septocutaneous perforators, and the ratio of the musculocutaneous to septocutaneous perforators was 3:2 (Thomas *et al.*, 2005).

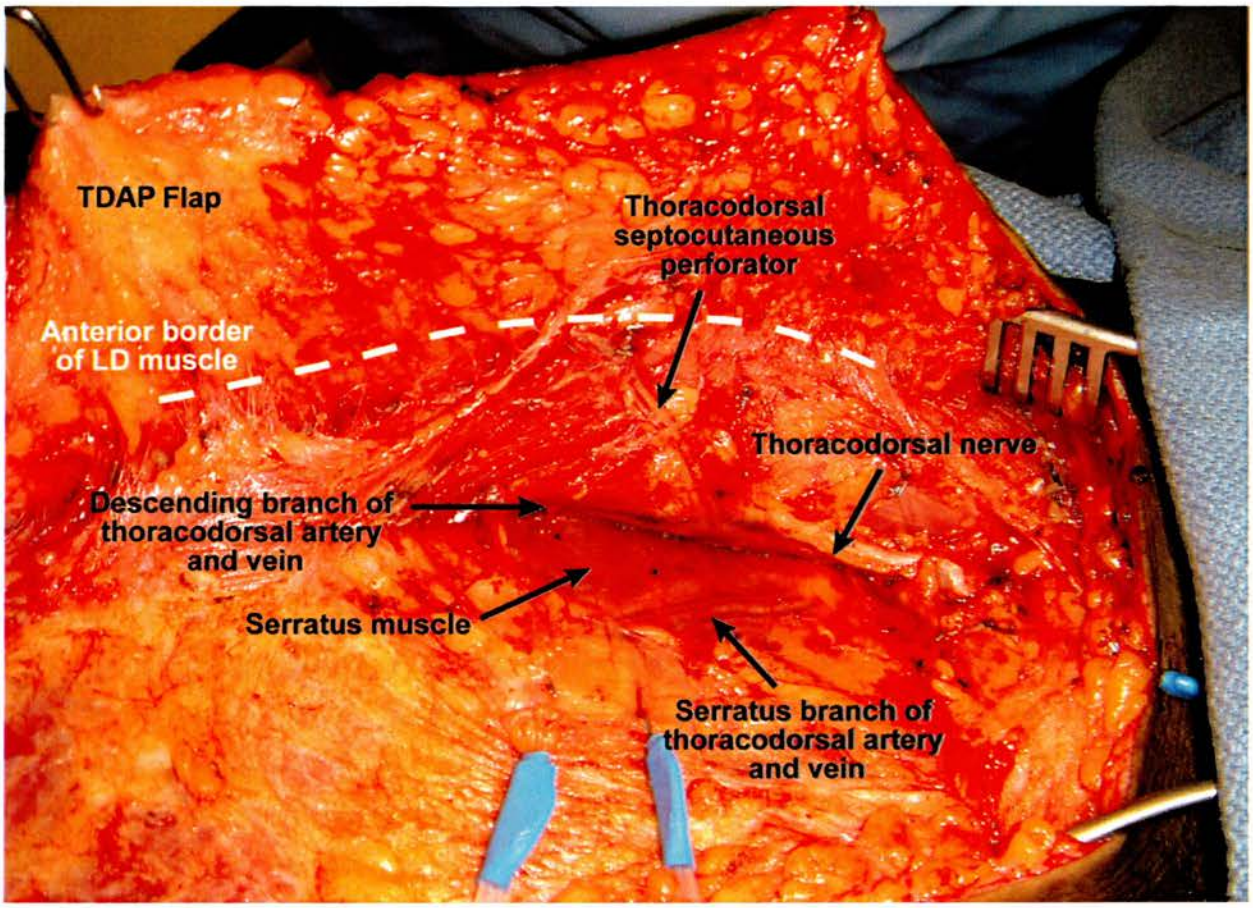

Figure 1.14 Intraoperative photograph of a thoracodorsal artery perforator flap demonstrating the anatomy of the flap.

1.9.3 Surgical technique

The flap is raised with the patient in the lateral decubitus position. An incision anterior to the anterior border of the latissimus dorsi muscle enables incorporation of either a septocutaneous and musculocutaneous perforator, and dissection continues until the perforator cleavage line is identified on the muscle, which appears white due to the presence of the lateral thoracodorsal nerve. If the perforators are small then a muscle-sparing technique can be used. Care is taken to preserve the thoracodorsal nerve and the delicate venae comitantes, and the distal end of the thoracodorsal pedicle, close to the origin of the muscle, is ligated and dissected

toward the axilla. The major branches of the thoracodorsal and subscapular vessels are then ligated up to the axillary artery and vein until the desired pedicle length is achieved.

1.10 Deep inferior epigastric artery perforator (DIEAP) flap

1.10.1 Background

The deep inferior epigastric artery perforator (DIEAP) flap is utilized for autologous breast reconstruction (**Figure 1.15**). Although Holmstrom demonstrated that the flap could be reliably perfused using a single medial row perforator in 1979, Koshima and Soeda first described the flap in 1989. The authors noted that a large adipocutaneous vascular territory could be reliably perfused on a single perforator, and reduced donor site morbidity has been noted compared with the transverse rectus abdominis musculocutaneous (TRAM) flap (Blondeel *et al.*, 1997; Futter *et al.*, 2000). Allen and Treece first described the use of the free flap for breast reconstruction in 1994.

Although breast reconstruction remains its primary indication, the DIEAP flap has been described as a free flap for reconstruction of defects in the head and neck (Neligan and Lipa, 2006) and lower limb (Van Landuyt *et al.*, 2005), and it may also be thinned in one stage (Koshima *et al.*, 1992). For breast reconstruction the DIEAP flap offers distinct advantages to patients compared with the TRAM flap in terms of decreased donor-site morbidity and shorter recovery periods. The DIEAP flap has proven reliability and a low complication rate (Granzow *et al.*, 2006; Gill *et al.*, 2004; Hamdi and Rebecca, 2006), although its harvest requires a high level of surgical expertise with a significant learning curve. Contraindications include a history of previous abdominoplasty or multiple abdominal scars. Acoustic Doppler may produce a very high proportion of false positive results due to its relatively high sensitivity locating very small perforators (Giunta *et al.*, 2000). CTA has been used for DIEAP (Alonso-Burgos *et al.*, 2006;

Masia *et al.*, 2006) flap presurgical imaging, and a high concordance with surgical findings and a reduction in operating time have been reported.

The SIEA is encountered during harvest of transverse lower abdominal flaps, and large calibre vessels may allow the harvest of an SIEA flap (**Figure 1.16**), which is associated with the least abdominal morbidity of the abdominal flap techniques. Anatomical and clinical studies suggest that this flap cannot safely be extended across the midline (Blondeel *et al.*, 2000; Wolfram *et al.*, 2006; Chevray, 2004; Hester *et al.*, 1984; Taylor and Daniel, 1975; Granzow *et al.*, 2006), but the mechanism of perfusion has not yet been elucidated.

Figure 1.15 Left: Preoperative photograph of a patient undergoing bilateral mastectomy and secondary deep inferior epigastric artery perforator flap breast reconstruction; Middle: Abdominal markings for flap harvest, with crosses marking the perforator locations from presurgical CT imaging; Right: Postoperative photograph following breast reconstruction.

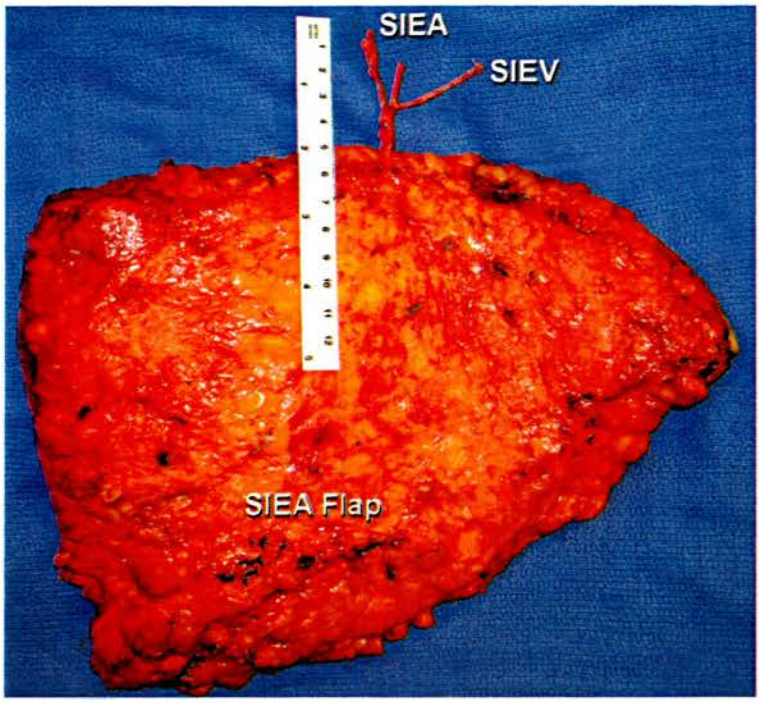

Figure 1.16 Superficial inferior epigastric artery flap harvest.

1.10.2 Anatomy

The deep inferior epigastric artery (DIEA), which is the most significant artery supplying the skin of the anterior abdominal wall, provides a pedicle that is 7.5 to 20.5 cm in length and 3.3 +/- 0.4 mm in diameter with two accompanying venae commitantes (Offman *et al.*, 2005). It forms two main branches in the majority of cases, with the lateral branch giving off a lateral row of perforators in the lateral third of the muscle, and the medial branch giving rise to a medial row of perforators in the medial third of the muscle and an umbilical branch (Moon and Taylor, 1988). Several studies have noted that dominance of the lateral branch is more common, and that the lateral division gives rise to more perforators, which have a shorter intramuscular course (Munhoz *et al.*, 2004; El-Mrakby and Milner, 2002), than the medial branch. There are generally 5+/-2 perforators concentrated in the periumbilical region. Blondeel has noted clinically that the use of medial perforators is imperative if zone IV is required (Blondeel, 1999).

The superficial inferior epigastric vein (SIEV) is larger than the deep inferior epigastric vein, suggesting that in normal physiological conditions venous drainage occurs predominantly through the superficial system (Carramenha e Costa *et al.*, 1987). The deep and superficial systems are connected by the venae commitantes of the arterial perforators. The SIEV has multiple lateral branches to the outer parts of the flap, but fewer medial branches of smaller caliber.

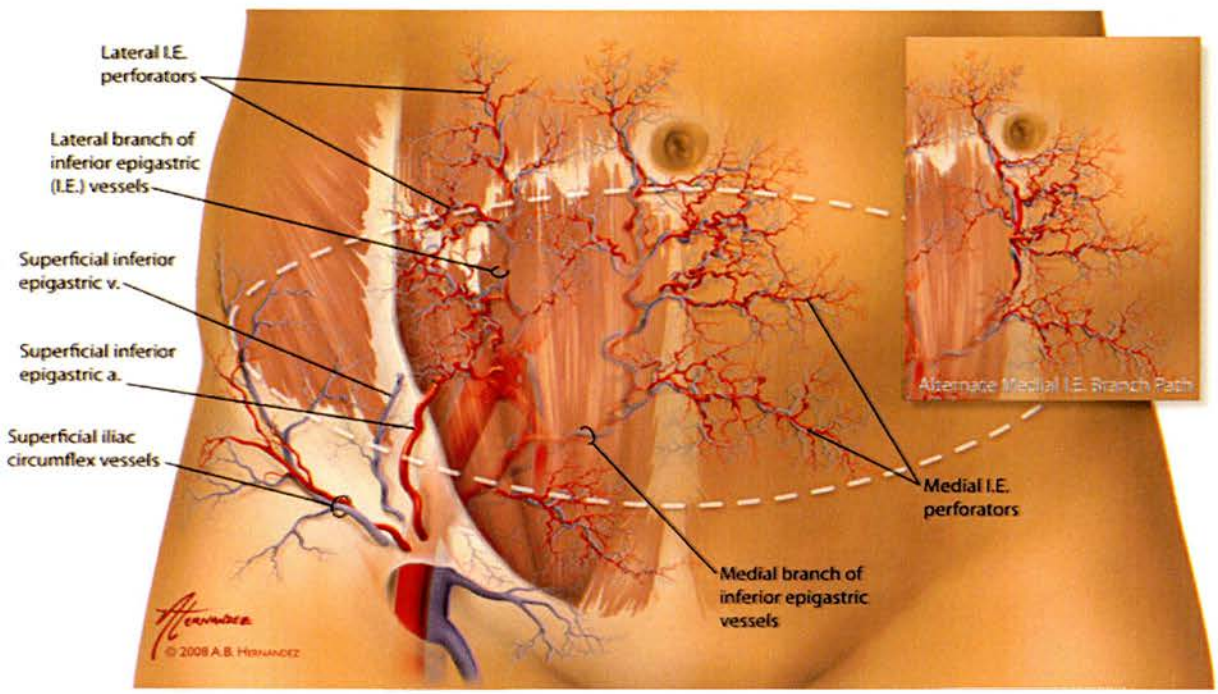

Figure 1.17 Anatomical illustration of the cutaneous blood supply to the lower abdomen. The deep inferior epigastric artery divides into two branches in the majority of cases. The lateral branch gives off a lateral row of perforators in the lateral third of the muscle, and the medial branch gives rise to a medial row of perforators in the medial third of the muscle.

1.10.3 Perfusion zones

Perfusion of the transverse lower abdominal flap has caused much controversy (Scheflan and Dinner 1983a and 1983b; Hartrampf *et al.*, 1982, Dinner *et al.*, 1983; Ohjimi *et al.*, 2005; Hallock, 2001; Keller , 2006; Holm *et al.*, 2006). Scheflan and Dinner (1983a; 1983b) originally described the perfusion zones of the lower abdominal transverse skin flap in the pedicled TRAM, reporting that the flap was perfused as a centrally perfused ellipse with declining perfusion at the edges. Hartrampf *et al.* (1982) are credited with popularizing this theory, with the perfusion zones being named after Hartrampf. Less than a year after their first description, however, Dinner *et al.* (1983) corrected their original report, noting that the ipsilateral flap circulation was consistently stronger than the contralateral circulation. Unfortunately this correction was unnoticed by the plastic surgery community, and this has caused much confusion to surgeons when fashioning flaps based on the lower abdominal skin paddle. *In vivo* angiography (Ohjimi *et al.*, 2005) of free TRAM flaps has supported the observation that the ipsilateral circulation is consistently stronger than that seen contralateral to the midline. This was supported by findings by Hallock (2001) using laser Doppler to assess the perfusion in the free TRAM flap, noting that the contralateral skin territories had significantly decreased flow when compared with all ipsilateral territories. These findings have also been confirmed for the DIEAP flap. Keller (2006) used near-infrared spectroscopy to measure the perfusion in each zone of the free DIEAP flap and found that the ipsilateral circulation was consistently stronger than that contralateral to the midline, and Holm *et al.* (2006) used laser-induced fluorescence of indocyanine green angiography to demonstrate tissue perfusion intraoperatively for DIEAP flaps and found that the lower abdominal adipocutaneous flap behaves as two halves separated by the midline.

Anatomical studies support these findings. The skin paddle crosses four vascular territories as described by Taylor and Palmer (1987), with choke vessel watershed areas between

the adjacent perfusion zones. Thus a step-wise progression of perfusion across the adjacent perfusion zones is observed, originating from the perforator arteries on the ipsilateral side (Holm *et al.*, 2006).

Zone IV, which is the greatest distance from the perforator, is routinely discarded by some surgeons as it is the most likely part of the flap to suffer from fat necrosis secondary to ischaemia (Gill *et al.*, 2004; Cheng *et al.*, 2006; Blondeel *et al.*, 2000). Studies of the angiosomes of the abdomen have provided a possible explanation for these clinical findings. The transverse lower abdominal flap perfused by the DIEA has a large potential vascular territory with choke anastomoses across the midline with the contralateral DIEA, as well as laterally across choke vessel anastomoses with the territories of the superficial inferior epigastric (SIEA) and lateral branches of the posterior intercostal arteries (Offman *et al.*, 2005). This suggests that in order to reach zone IV, which is the most distal part of the flap and the least well perfused due to the greatest distance from the perforator vessel, the blood flow has to pass through two sets of choke vessel anastomoses (Moon and Taylor, 1988; Blondeel, 1999).

Blondeel noted in a clinical series that all flaps with compromised vascularisation of zone IV in the study were nourished by lateral row perforators, and therefore advised that the use of medial perforators is imperative if zone IV is required (Blondeel, 1999). In a very large clinical study of DIEAP flap outcomes Gill *et al.* (2004) have suggested that where multiple perforators are required to perfuse the flap, there is no strong centralized blood supply and flap survival is dependent on small-diameter vessels, which may compromise the viability of zone IV, and the complication rate was directly proportional to the number of perforators used. Blondeel *et al.* (2000) later suggested that the viability of zone IV may be related to its venous anatomy, and in a study of the venous system of the DIEAP flap performed in 15 cadaver and three abdominoplasty specimens they found that large lateral branches crossing the midline were found in only 18 percent of cases, whereas 45 percent had indirect connections through a deeper

network of smaller veins and 36 percent had no midline crossing branches. Clinically in a large series they noted that diffuse venous congestion occurred in approximately two percent of DIEAP flaps and in all these cases a particularly large SIEV had been noted during flap harvest.

Studies of the DIEAP flap have therefore concluded that perfusion of zone III adjacent to the territory of the vascular pedicle, known as zone I, is stronger than that of zone II, even though these zones are an equal distance from the pedicle. Thus authors suggest that the classic Hartrampf zones should be rearranged for the DIEAP flap, switching zones II and III (Holm *et al.*, 2006; Rickard, 2001).

1.10.4 Surgical technique

Standard abdominoplasty markings are made with a flap approximately 12 cm wide at the midline and extending laterally to the anterior superior iliac spines, and a two-team approach is employed. If a large perforator from the internal mammary artery and vein are found then these may be prepared for anastomosis, otherwise the internal mammary vessels are commonly exposed through the 3rd interspace or via excision or partial resection of the third intercostal cartilage. The superior and inferior skin incisions are made and the superficial inferior epigastric vessels are identified first. If these are found to be of sufficient caliber they are followed down to their origin from the common femoral artery and a superior inferior epigastric artery (SIEA) flap is performed instead. SIEA flap harvest has the advantage of staying superficial to the deep fascia and therefore results in minimal donor site morbidity. Disadvantages include anatomical variability (Taylor and Daniel, 1975; Reardon *et al.*, 2004), and some authors report that only the ipsilateral zones of the flap are reliably perfused (Wolfram *et al.*, 2006; Chevray, 2004; Hester *et al.*, 1984; Granzow *et al.*, 2006). Often only the superficial inferior epigastric vein (SIEV) is present of sufficient size and this is dissected for several centimeters for use as a backup for the venous drainage of the flap if venous congestion is present after anastomosis of the deep inferior

epigastric vein. Dissection then proceeds from lateral to medial. The DIEAP flap may be raised on more than one perforator from the same perforator row with atraumatic longitudinal separation of the rectus muscle fibres. If no suitable perforator is found then the contralateral portion of the flap is raised. When a suitable perforator is found, the perforator is dissected off the rectus sheath and "unroofed" followed by intramuscular dissection and ligation of all intramuscular branches. Maintenance of a bloodless field is crucial for safe perforator flap dissection. The segmental intercostal nerves run medially, superficial to the pedicle, and care must be taken to preserve them. Dissection then continues until a pedicle of sufficient length and calibre are obtained. Sensory nerves that are found with the perforators can be harvested and anastomosed to an intercostal nerve (Blondeel, 1999; Yap *et al.*, 2002). The anastomosis is performed and the flap inset, with de-epithelialisation depending on the amount of native breast skin that has been preserved. Zone IV is routinely discarded by many surgeons (Gill *et al.*, 2004). Ultimately abdominal flap selection should be performed on a case-by-case basis to suit the anatomy and recipient site requirements of the individual (Granzow *et al.*, 2007; Chevray, 2004).

1.11 Summary

Perforator flaps have evolved from a desire to minimize the donor site morbidity of flap harvest. The mechanism by which the cutaneous perforators perfuse the skin remains poorly understood, and vascular anatomical studies of the integument superficial to the deep fascia have been limited to 2D static investigations. 3D and 4D evaluation of the vascular regions of the workhorse perforator flaps, including the LCFAP-*vl*, TAP, and DIEAP flaps, may further our understanding of their perfusion and aid more reliable flap design. In particular perforator flaps are at risk of venous congestion, and designing these flaps with knowledge of their venous architecture may reduce the risk of this phenomenon.

The vascular architecture of the LCFAP-*vl* flap, the effect of thinning on vascular perfusion, the anatomical basis of the adipofascial flap, and the vascular basis of the extended flap, remain poorly understood. Knowledge of these may aid optimal design of the flap with respect to the LCFA territory and the concomitant venous drainage pattern, reducing the risk of venous congestion. In particular, reports suggest that the LCFAP-*vl* flap can be safely thinned in the Asian population (Koshima *et al.*, 1993; Kimura and Satoh, 1996; Kimura *et al.*, 2001; Yang *et al.*, 2006). In Western patients, however, thinning has been reported to result in high rates of partial or complete flap necrosis (Ross *et al.*, 2003; Van Landuyt, 2006), yet the reason for this is poorly understood,

The arterial and venous anatomies of the TAP flap have yet to be elucidated, and knowledge of these may help improve the reliability of the flap. In particular reports suggest that the flap can be reliably thinned between the superficial and deep adipose layers (Kim *et al.*, 2002; Kim and Kim, 2003; Kim *et al.*, 2001), although the anatomical basis for this remains unknown. The locations of the perforators from the thoracodorsal artery remain contentious (Angrigiani *et al.*, 1995; Guerra *et al.*, 2004; Heitmann *et al.*, 2003; Thomas *et al.*, Spinelli *et al.*, 1996. Schwabegger *et al.*, 2002).

The vascular anatomy of the DIEAP flap remain poorly understood, and many surgeons routinely discard zone IV of the flap due to concerns regarding inadequate arterial perfusion (Gill *et al.*, 2004; Cheng *et al.*, 2006; Blondeel *et al.*, 2000). Blondeel *et al.* (2000) have suggested that the high rates of ischaemic complications in this region may relate to the poor venous drainage. Blondeel (1999) also suggests that a medial row perforator should be selected if the entire flap is required.

The arterial and venous anatomies of the SIEA flap also remain poorly understood. Clinical experience has suggested that the flap cannot safely be extended across the midline (Blondeel *et al.*, 2000; Wolfram *et al.*, 2006; Chevray, 2004; Hester *et al.*, 1984; Taylor and

Daniel, 1975; Granzow *et al.*, 2006), although the anatomical basis for this phenomenon remains poorly understood.

1.12 Aims

The aims of this thesis were to develop novel static and dynamic 3D perforator flap models to better analyze the vascular tree and pattern of blood perfusion. The workhorse perforator flap anatomical regions, including the LCFAP-*vl*, TAP, and DIEAP flaps, were selected for study. 3D and 4D CTA and CTV techniques were utilized for the first time to enable investigation of the anatomy and perfusion of individual perforator complexes in the axial, coronal, and sagittal views in the cadaveric perforator flap. Dynamic and static imaging of perforators and their accompanying venae comitantes was also performed, enabling the sequence and direction of filling of the perforator branches in the flap to be evaluated in 3D. The viscosity of the contrast medium was similar to that of blood and was continuously injected at a constant pressure using a precision delivery pump, enabling closer modeling of *in vivo* perfusion characteristics than had been achievable previously. The contrast medium could also be washed out of the flap, allowing multiple investigations of the arterial and venous systems of the same flap to be performed under different conditions, such as before and after flap thinning. Washout of the contrast was achieved without changing the vascular territory for a standard fill volume or dilating the linking vessels between adjacent vascular territories. Software was also developed that could quantify the contrast density in the suprafascial, subcutaneous, and subdermal plexuses in any part of the flap at a given time, enabling objective evaluation of flap perfusion. This research will help to determine the overall vascular territories of perforator flaps, and also to understand the vascular systems within the specific circulatory regions, which may improve the reliability of these workhorse perforator flaps.

The thesis is organized in the following manner in order to address these aims:

In chapter two the materials and methods of the novel static and dynamic 3D perforator flap models are described.

In chapter three a detailed 3D and 4D appraisal of the arterial and venous anatomy and perfusion of the LCFAP-*vl* flap using the novel computed tomographic technique is presented. Changes in flap perfusion following thinning and harvest of an adipofascial flap were also examined. Software was used to evaluate the contrast density within each plexus of the flap with respect to the perforator. The vascular basis of the extended LCFAP-*vl* flap was also investigated.

In chapter four the vascular anatomy of the TAP flap was examined using 3D and 4D CTA and CTV, including evaluating the effect of flap thinning between the deep and superficial adipose layers. Coloured latex injections and flap dissections were also performed in order to establish the location, calibre, and intramuscular length of the perforators from the thoracodorsal artery.

In chapter five the arterial and venous anatomies of the DIEAP flap are described. Histological evaluation of all of the perforators within the flap was performed to evaluate whether anatomical differences exist between the medial and lateral row perforators. The vascular basis of the SIEA flap was also investigated.

Chapter 2

MATERIALS AND METHODS

In this chapter the materials and methods used for the studies within this thesis will be described.

2.1 Flap preparation

Flaps were harvested from fresh adult cadavers acquired through the Willed Body Program at The University of Texas Southwestern Medical Center, in Dallas, Texas. Perforator flaps harvested included the following: LCFAP-*vl*; TAP; DIEAP. Each flap was harvested, prepared, and CT scanned by posthumous day five.

All surgical landmarks relevant to the flap were marked and each perforator flap was dissected based on the largest perforator originating from the main vascular pedicle.

2.1.1 Methodology

For the examination of surgical flaps the desired perforator or source artery and its largest vena comitans were cannulated using 24-gauge butterfly catheters (0.7mm diameter) (**Figures 2.1 and 2.2**). At the level of the deep fascia the resistance from the valves within the vein was found to be insignificant, allowing perfusion of the venous bed via retrograde injection. A dilute methylene blue solution was infiltrated into the flap to identify vascular leaks, which were then either coagulated using bipolar diathermy, with care taken to avoid thermal damage to the vasculature within the flap, or ligated using silk sutures. The use of surgical clips was avoided to prevent CT imaging artefacts. Following occlusion of all leaking points, each flap was irrigated

with warmed saline (37°C) containing heparin (10 U/ml) until the effluent from the venous system was colourless.

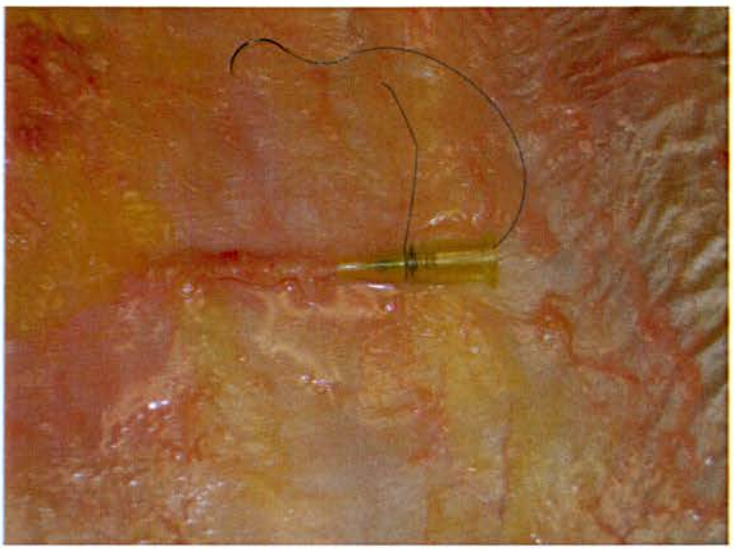

Figure 2.1 Cannulation technique of a perforator.

Figure 2.2 Left: DIEAP flap harvested with preservation of both DIEAs and demonstration of all of the perforators. Right: DIEAP flap with cannulation of perforators of the DIEA.

2.1.2 Dynamic computed tomography scan protocol

To maintain shape and orientation during various radiographic studies surgical flaps were held in custom built imaging trays. Each tray was constructed from 3/8 inch thick panels of low radiographic opacity polystyrene foam. The trays featured sills contoured to the flap profile to define and maintain the flap shape, and the flap was placed skin downwards to avoid pressure on the pedicle. The tray was then placed on a specially constructed rig angled at 60°, and then placed on the table in the CT scanner (**Figure 2.2**). This enabled the CT gantry to be tilted to its maximum 30° angle and therefore the flap was effectively exactly parallel with CT scanner coil, minimising the scan time. At 60° the flap was stable within the rig. For example, on the GE Lightspeed 16-slice scanner with the scanner set to perform helical scans at a 0.5 seconds rotation time, 10 mm collimation for 0.625 mm slices, and a 0.938 pitch setting, a four-centimeter thick flap is scanned in about three seconds.

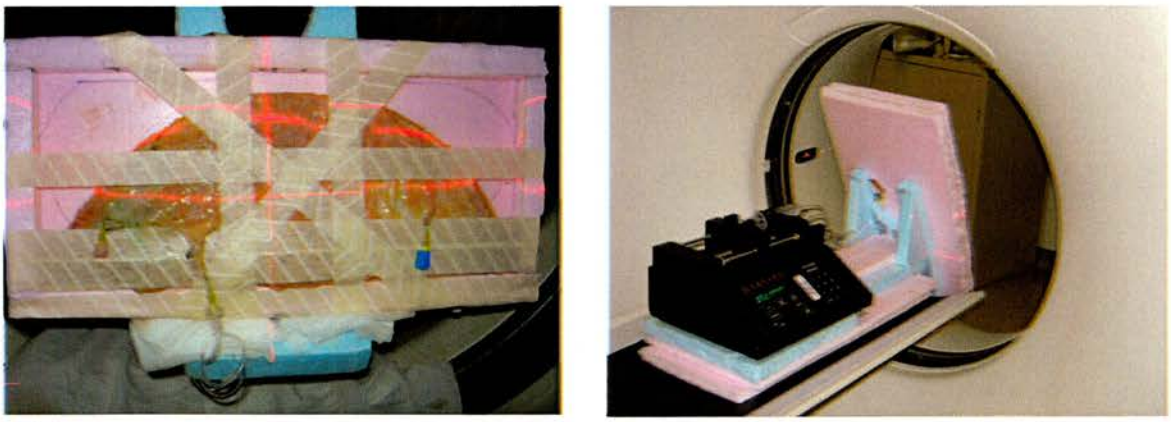

Figure 2.3 Deep inferior epigastric artery perforator flap secured within the rig and placed in the CT scanner. The flap is placed skin down to avoid pressure on the cannulated perforator complex. This tray was then placed on a specially constructed rig angled at 60°, and then placed on the table in the CT scanner. This enabled the CT gantry to be tilted to its maximum 30° angle and therefore the flap was effectively exactly parallel with CT scanner coil, minimising the scan time. At 60° the flap was stable within the rig.

A 30 cc syringe was filled with Omnipaque 300 (iohexol; 300 mg/ml) heated to 37°C to reduce the viscosity (www.amershamhealth-us.com/shared/pdfs/pi/Omnipaque.pdf) and improve vascular filling. Plastic tubing was placed between the syringe and the perforator cannula, supported with tape to gently lift the perforator away from the flap surface and improve the imaging of the suprafascial braches, whilst reducing tension on the perforator. The volume of CT contrast medium typically required to achieve optimal filling of the vascular territories was found to be only three milliliters although this varied depending on the flap type.

The optimal injection rate to allow for good visualization of local vascularity and to offer adequate time resolution was found to be 0.5ml/minute, and this could be

achieved using a Harvard precision pump. At this rate arterial injection did not lead to later filling of the venous system, and therefore avoided obscuring the images. The injection rate could be slowed down further to evaluate the early perforator vascular filling pattern. Scans were repeated at a 0.1 ml fill increment (i.e., every 12 s at 0.5 ml/min) over the first one milliliter of the contrast injection, and at 0.5 ml fill increments thereafter. Given a three milliliter injection on a four centimeter thick flap, the acquired data set comprises 14 volume sets of 33 slices each. An equation was developed using a Microsoft Excel spreadsheet (Microsoft Corp., Redmond, WA, USA) to calculate the approximate time delay for various injection rates to account for the filling of dead-space prior to the start of imaging.

During scanning, the extent of flap vascularity was usually unknown, and therefore slice reconstructions were performed with a circular field of view (FOV) set to encompass the flap size. The achievable in-plane resolution of a CT scan, however, is inherently limited by the square 512x512 reconstruction pixel array and the FOV. On a GE Lightspeed scanner, the minimum FOV diameter is 20 cm resulting in a pixel size of 0.6 mm, therefore, only vessels with diameter > 1.2 mm are clearly discernable. The choice of filter in the reconstruction algorithm also had large effects on the resolution of the CT image. To permit higher resolution images in regions of interest, raw CT image data was saved for retrospective reduced FOV reconstructions (Wolbarst, 2004).

Between scanning the flaps were irrigated with warmed normal saline to completely remove the contrast medium, and the next perforator or vena comitans was injected using the same protocol. Repeated scanning sequences followed by large volume washouts were performed in control flaps followed by vascular territory measurement using the CT workstation prior to the start of the study, and revealed that the area of the vascular territory was unchanged following repeated washouts, and that the diameter of

the large linking vessels also remained unchanged. This indicated that the vessel walls were elastic, and that vasodilatory mechanisms seen *in vivo* did not occur in the cadaveric flaps, as expected.

2.1.3 Static computed tomography scan protocol

For static imaging a barium sulphate/gelatin mixture was used for vascular injection. Normal saline (100ml) was warmed to 40°C, and then 3g of powdered gelatin was added slowly followed by 40g of barium sulphate, stirring continuously using a magnetic stirrer (Tan *et al.*, 1999). Following vascular injection the flap was refrigerated to 4°C for 24 hrs to allow the gelatin to set. The flap was then frozen at -20°C, without producing image artefacts, to allow parallel placement with respect to the coil of the CT scanner, shortening the scanning time.

In static scans time was not an issue, and a higher image quality helical or axial scanning mode was used. Narrowing the beam collimation reduced cone beam artefacts, and slower rotation times at a fixed tube current produced lower noise images. The tilted table jig geometry was also used, and using a one second rotation time, a 1.25 mm collimator setting and a 0.938 pitch setting, about one minute was required to produce a set of 0.625 mm slices on a four centimeter thick flap. Scans were performed at 80 kVp when using iodinated contrast agents or barium sulphate to optimize contrast, and 120 kVp was used for lead oxide contrast to minimize beam hardening artefacts (typically scans were performed at approximately 200 mA).

2.1.4 Choice of radiographic contrast agents

Radiographic contrast depends on differences in X-ray transmission through the tissue components being imaged. Materials with high atomic number amplify X-ray

attenuation due to the strong dependence of photoelectric absorption on atomic number (Bushberg *et al.*, 2002). Thus injected iodinated and ingested barium based non-toxic contrast agents have found utility in general radiography to produce contrast between similar soft tissue organ compartments. Over the diagnostic X-ray energy range when comparing the attenuation in contrast materials relative to soft tissue for Omnipaque, barium, and lead oxide based solutions, the high atomic number of lead results in relatively high attenuation over the full diagnostic X-ray energy range, whereas attenuation for the Omnipaque and barium solutions is similar over the energy range, with pronounced peaks at the 33 keV and 37 keV K-shell binding energies respectively (**Figure 2.3**).

Lead oxide is highly toxic and its preparation requires the use of a mask, gloves, and special facilities are required for disposal. On the other hand, iodinated and barium solutions are non-toxic, and special precautions are not necessary. Iodinated solutions can also be washed out by irrigation with warmed saline. These properties are advantageous when studying the same perforator flap before and after thinning. When comparing volume-rendered CT scan images of flaps injected with a barium sulphate or lead oxide mixture, it was found that the barium-based solution was able to penetrate the subdermal plexus, producing images of a higher quality than were achievable even with a lead oxide solution over a range of concentrations. In this study barium sulphate was therefore used for the majority of vascular injection studies where a static scan was desired, and Omnipaque where dynamic scanning was performed.

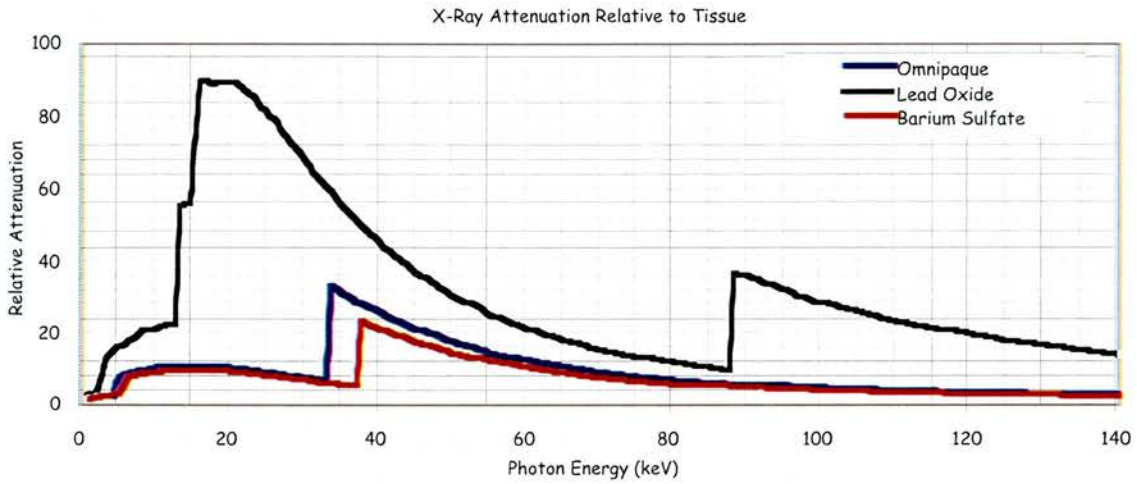

Figure 2.4 X-ray Attenuation Relative to Tissue (per unit volume) for Omnipaque 300 (Iohexol, 300 mg/ml) Barium Sulphate (100 mg $BaSO_4$: 100 ml H_2O), and Lead Oxide (100 mg PbO: 100 ml H_2O) over the Diagnostic X-ray Energy Range (~10 – 120 keV).

2.1.5 Analysis software

To determine the vascular density of the different layers of the perforator flap, custom-built software was developed to evaluate regional contrast concentration based on the CT HU numbers using Image-J. The analyses included measurements of radial, angular and depth distribution of the contrast within the perforator flap. Relative contrast density analyses were performed radially with respect to the perforator entrance into the flap enabling the filling pattern and vascular density of each layer of the flap to be assessed objectively. The 3D CT workstation was used to measure distances, angles, and perimeters directly from 2D or 3D images.

2.2 Ethics committee approval

All the studies contained within this thesis were fully approved by the ethics committee of UT Southwestern. All intraoperative photographs were obtained with written patient consent.

2.3 Materials used in experimental procedures

2.3.1 Chemicals and solutions used

The following chemicals were used for the studies in this thesis:

Lead oxide powder (PbO)

Barium sulphate powder

Gelatin powder

Methylene blue dye

Eosin dye

Coloured latex (Ward's; Rochester; NY)

Heparin sulphate (10U/ml)

Omnipaque 300 (iohexol; 300 mg/ml; Amersham, Princeton, NJ)

2.3.2 Instruments

The following instruments were used for the studies in this thesis:

GE Lightspeed 16-slice scanner (General Electric, Milwaukee, WI)

24-gauge butterfly catheters (0.7mm diameter; BD Insyte; Becton Dickinson S.A., Madrid, Spain)

Styrofoam (Dow Chemical Company, Midland, MI)

Harvard precision pump (PHD 2000, Harvard Apparatus, Inc.)

Photographic documentation was performed using a Nikon D80 system, with images downloaded into Adobe Photoshop ($CS2_{TM}$).

2.4 Statistical analysis

Data are described as percentages, medians with ranges, and means with the standard error of the mean as appropriate. Microsoft Excel (Microsoft Corp., Redmond, WA, USA) software was used for statistical analysis. Where the two groups of variables follow Gaussian distributions, the student's t-test was used at 95 percent confidence intervals, and two-tailed P-values given, and where the variables do not satisfy normality testing using the Kolmogorov-Smirnov test, the Wilcoxon Mann-Whitney U-test was used at 95 percent confidence intervals, and two-tailed P-values given.

Contrast density analysis was performed using custom built software using the Interface Description Language visualization and analysis platform (ITT Visual Information Solutions; www.ittvis.com/idl).

Chapter 3

Anterolateral Thigh Perforator (LCFAP-*vl*) Flap

The aim of this chapter is to describe the methodology, and to report and discuss the results of 3D and 4D analysis of the arterial and venous anatomies and perfusion of the LCFAP-*vl* flap.

3.1 MATERIALS AND METHODS

3.1.1 Flap harvest and preparation

Eighteen flaps harvested from nine fresh adult cadavers were used in the study. A line was drawn between the anterior superior iliac spine and the superolateral border of the patella, and the midpoint of this line was clearly marked to indicate the position of the 'B' perforator (Yu, 2004). The flap was designed with the superior border 2cm below and parallel with the inguinal ligament, the inferior border at the superior border of the patella, and these lines were connected in the midaxial lines. The flaps were raised to incorporate the deep fascia, and all perforators encountered were preserved, with dissection proceeding to identify their source arteries.

Immediately following flap dissection the largest arterial perforator (perforator B in all cases) was cannulated and prepared as above. Other perforators within the LCFA angiotome (the fascioadipocutaneous vascular territory) (Behan and Wilson, 1975; Behan, 1992) were also cannulated, as were perforators from the superficial femoral

artery. For study of the venous system the largest vena comitans of the arterial perforator was cannulated and prepared as above.

3.1.2 Computed tomography imaging

Dynamic imaging was performed and an injection volume of 3ml was found to provide adequate filling of the venous system. Following injection the flaps were then irrigated with warmed saline to remove the contrast medium, and either thinned or harvested as an adipofascial flap. Flaps were thinned to 6-8mm, preserving a 5cm radius about the perforator. For the adipofascial flap the skin and dermis were excised at a uniform depth, preserving all the adipose layer of the flap. Static images were also obtained.

3.1.3 Flap microdissection

The arterial and venous systems were injected with different coloured latex solutions through the perforator and its vena comitans. Dissection was then performed under an operating microscope to investigate the relationship between the lateral circumflex femoral arterial and venous vascular territories, as well as to investigate the direction of the valves within the venous system.

3.1.4 Contrast density analysis

Contrast density analysis was performed radially with respect to the perforator entrance into the flap to enables the filling pattern and vascular density of each layer of the flap to be assessed objectively. The CT workstation was used to make measurements directly from the 2D flap image, including distances, angles, and area.

3.2 RESULTS

3.2.1 Anatomy and perfusion of the arterial system

After the perforator and its branches had filled down to level of the skin, recurrent vessels were seen to fill via flow through the subdermal plexus (**Figures 3.1 and 3.2**). The adipofascial flap did not demonstrate recurrent flow or filling of the linking vessels at the suprafascial level. These recurrent vessels perfused large diameter linking vessels that formed a suprafascial plexus and enabled filling of perforator complexes in the adjacent angiotomes. The linking vessels were seen to provide branches that descended to the subdermal plexus to perfuse the skin between adjacent angiotomes, as well as linking with one-another via horizontal branches (**Figures 3.2 to 3.5**). The large diameter linking vessels were found to lie at the suprafascial surface of the deep fascia, or in the adipose layer within two millimetres of the deep fascia in all cases, and were related to the lateral femoral cutaneous nerve and the anterior cutaneous branch of the femoral nerve. Importantly these linking vessels were morphologically distinct from the perforator complexes, and did not perforate the deep fascia. Injection of a perforator in an adjacent angiotome confirmed the bidirectional nature of these large-diameter linking vessels.

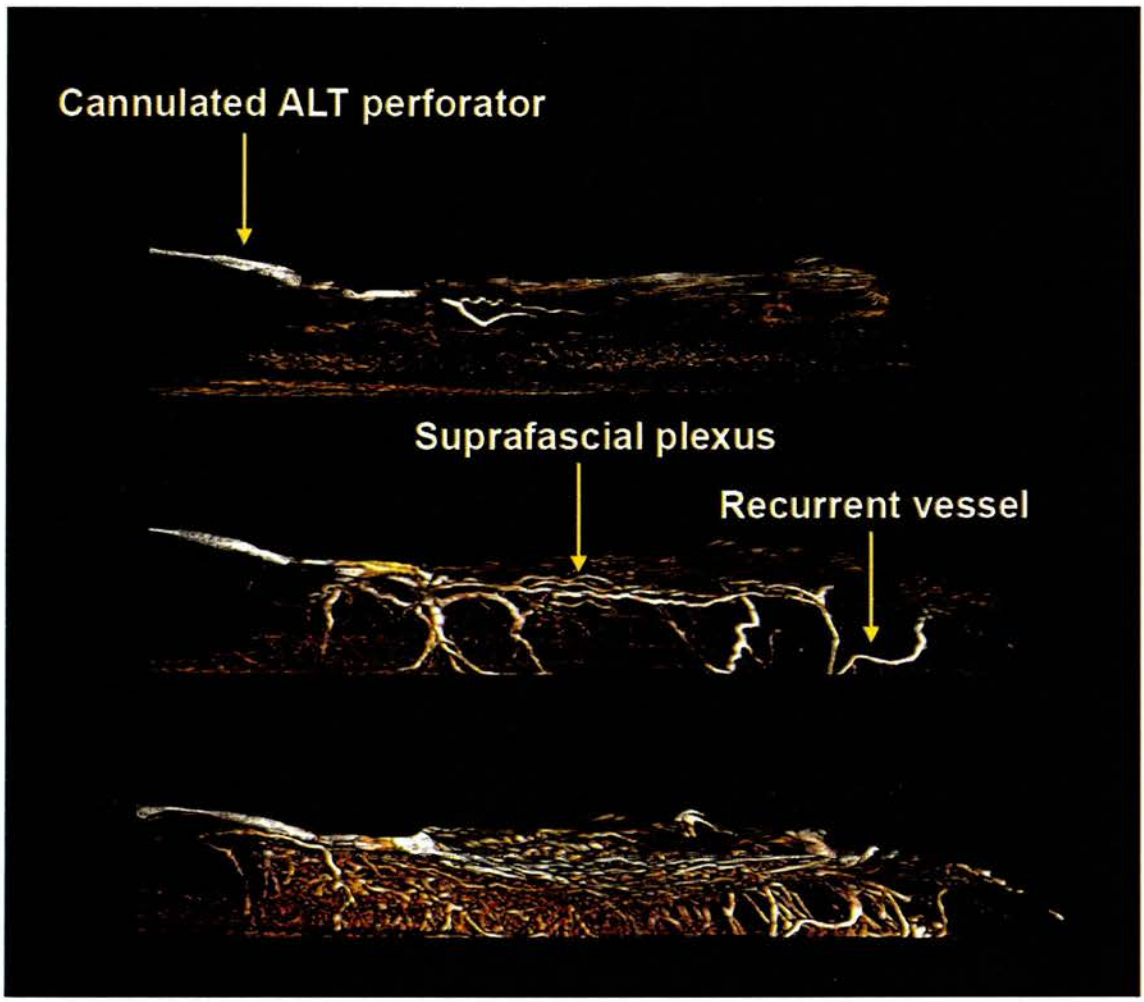

Figure 3.1 Lateral dynamic computed tomographic angiographic images of a type III perforator complex in an anterolateral thigh (ALT) flap. Images are acquired at 0.5-ml injection intervals and clearly show the dense suprafascial plexus and recurrent flow through the subdermal plexus.

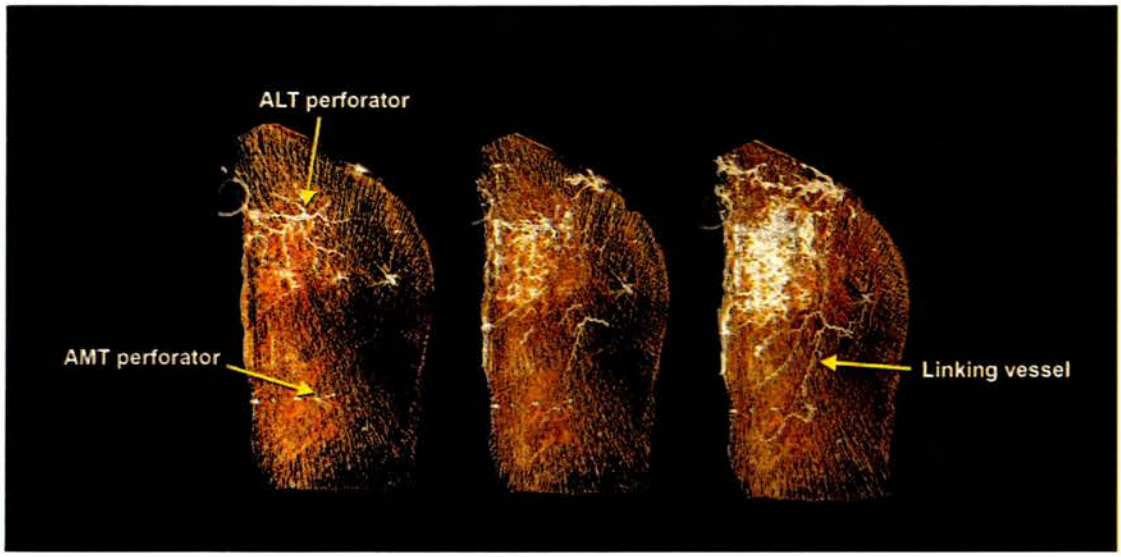

Figure 3.2 Anteroposterior views of large-diameter linking vessels between the vascular territories of the anterolateral thigh (ALT) perforator (lateral femoral circumflex angiotome) and the anteromedial thigh (AMT) perforator (superficial femoral angiotome), with illustrations.

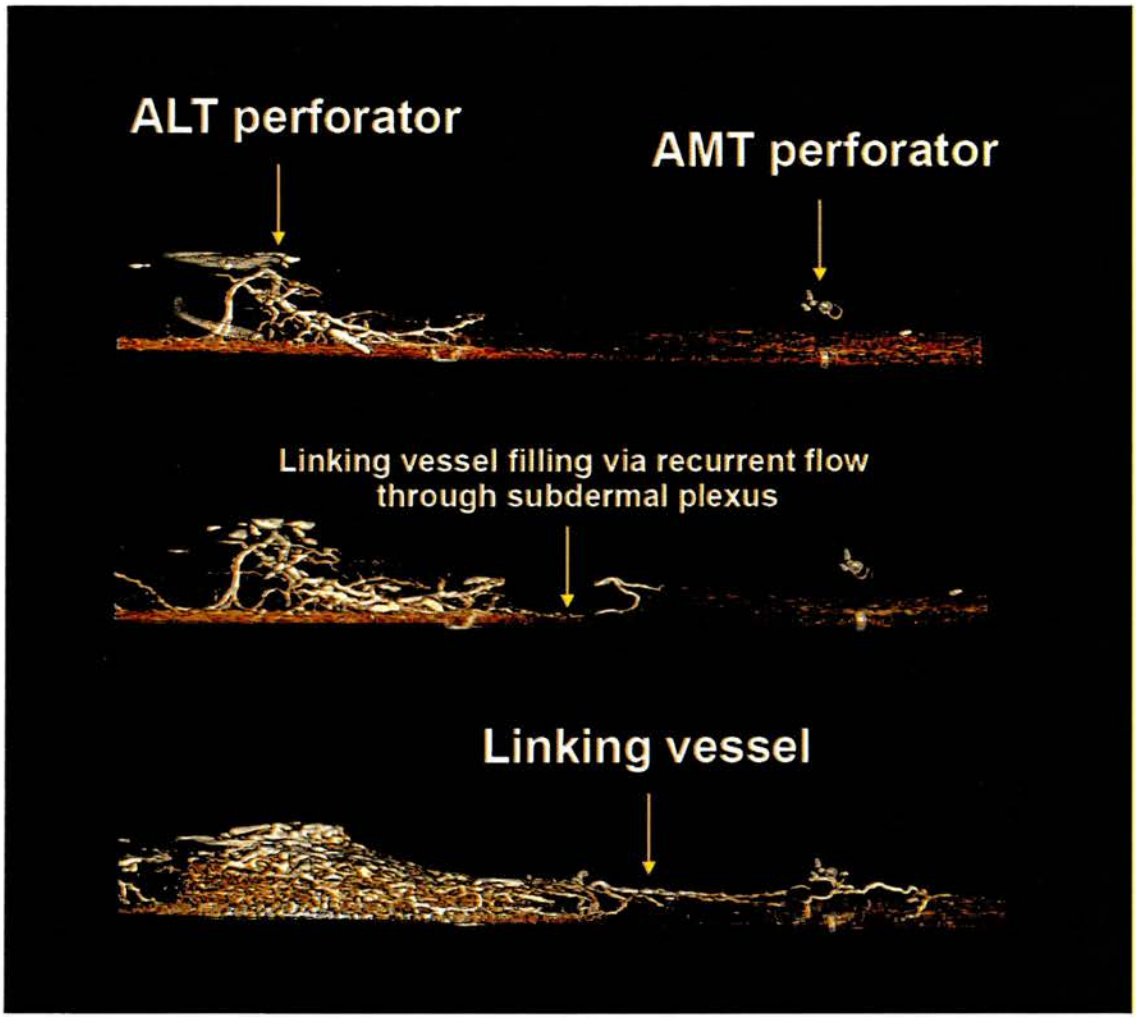

Figure 3.3 Lateral views of large-diameter linking vessels between the vascular territories of the anterolateral thigh (ALT) perforator (lateral femoral circumflex angiotome) and the anteromedial thigh (AMT) perforator (superficial femoral angiotome), with illustrations. Note on the lateral view how branches from the linking vessels perfuse the subdermal plexus between adjacent angiotomes.

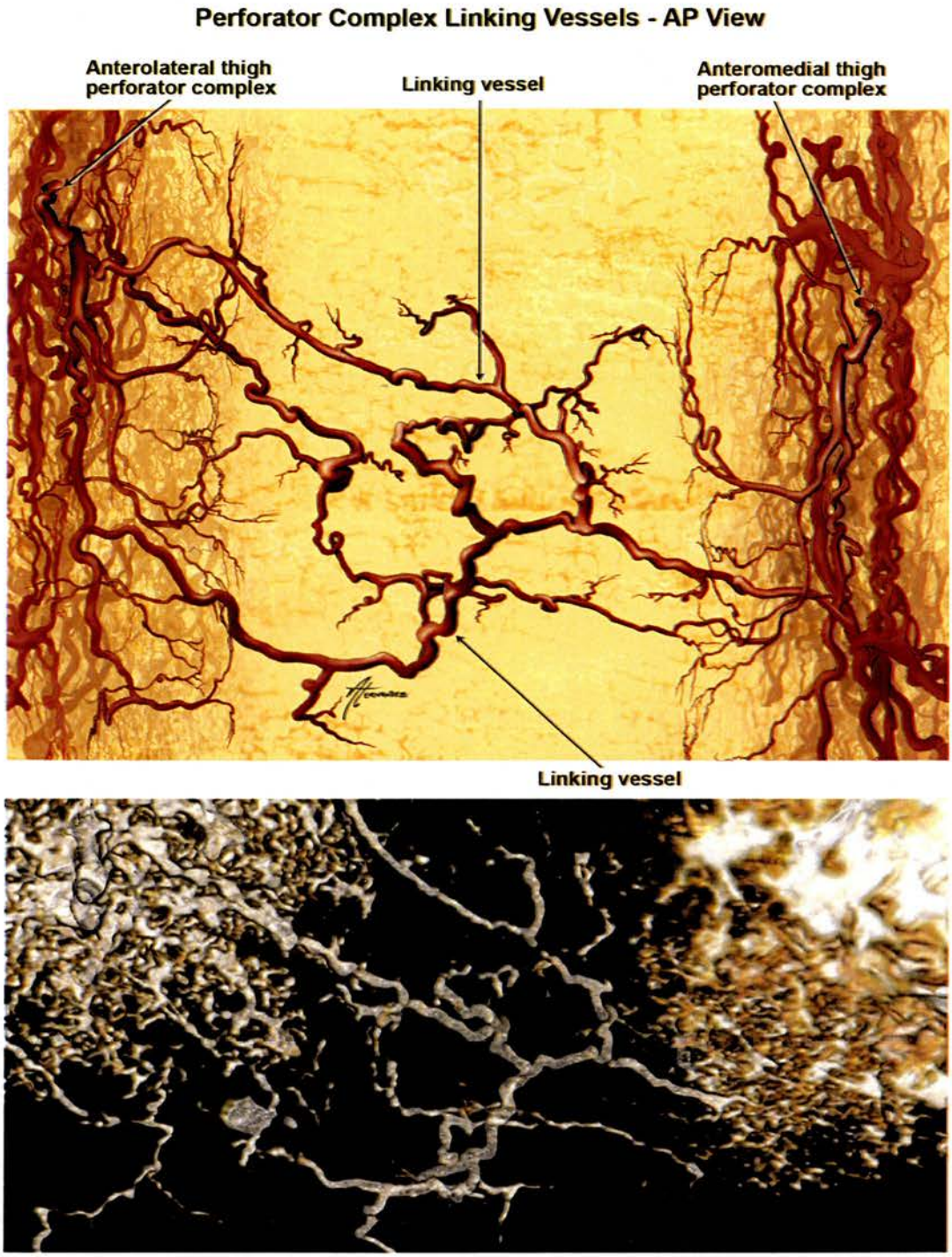

Figure 3.4 Illustration and corresponding computed tomographic angiogram demonstrating anteroposterior view of large linking vessels communicating between the anterolateral thigh perforator and the anteromedial thigh perforator.

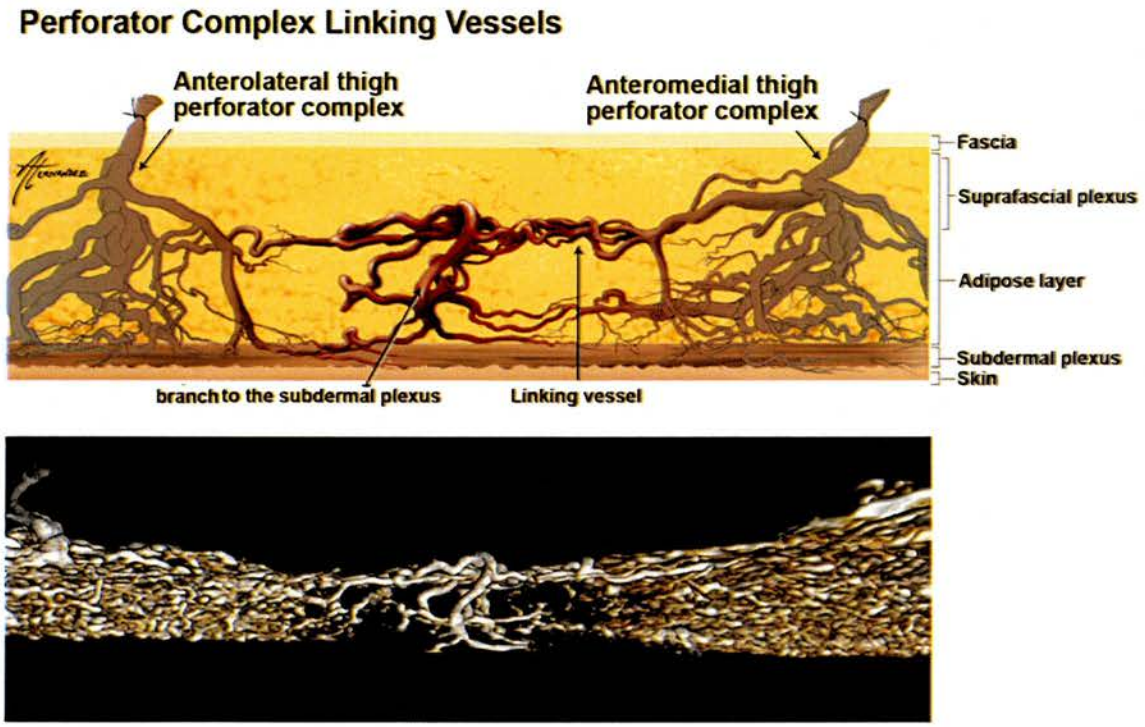

Figure 3.5 Illustration and corresponding computed tomographic angiogram demonstrating lateral view of large linking vessels communicating between the anterolateral thigh perforator and the anteromedial thigh perforator and a branch to the subdermal plexus.

Within the same angiotome perforator complexes were linked by a dense network of branches from the subdermal, subcutaneous, and suprafascial plexuses. The angiotome of a given perforator was perfused prior to filling of the adjacent vascular territories via linking vessels, supporting the angiosome theory (Taylor and Palmer, 1987; Taylor and Palmer, 1992) (**Figure 3.6**).

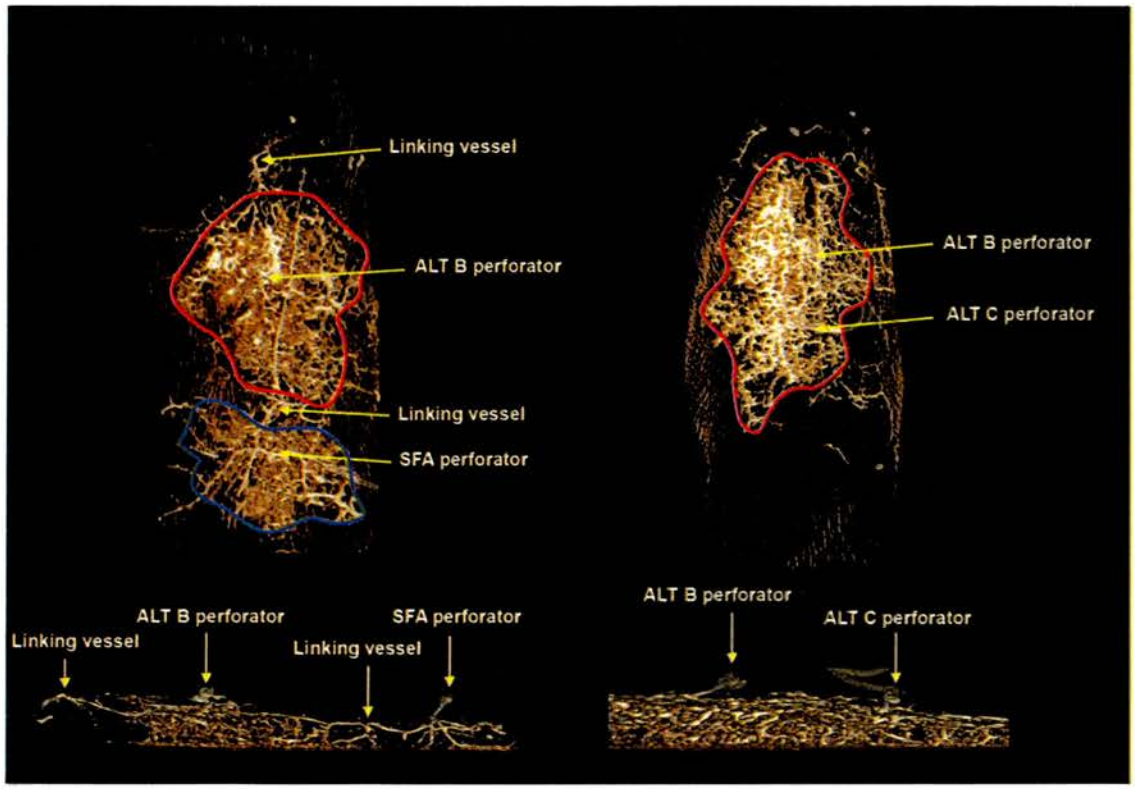

Figure 3.6 Anteroposterior and lateral dynamic computed tomographic angiograms showing the dense communicating vessels between perforators of the same vascular territory compared with those of adjacent territories. (Left) The anterolateral thigh (ALT) B perforator and an anteromedial thigh perforator have each been injected with 1.5ml of contrast. The large-diameter linking vessels can clearly be seen spanning between the adjacent angiotomes at the level of the suprafascial plexus, with branches to the subdermal plexus (it is important to note that the linking vessel complex is morphologically distinct from a perforator complex). (Right) Both the anterolateral thigh B and C perforators have been injected with 1.5ml of contrast. The lateral view shows the dense communicating branches between adjacent perforators of the same angiotome (vascular territory of the descending branch of the lateral circumflex femoral artery) through subdermal, subcutaneous, and suprafascial plexuses. This further supports the angiosome theory. SFA, superficial femoral artery.

The mean axiality of the arterial vascular territory was 183 degrees (corrected for the left thigh; range 90 to 207) with respect to the lower limb. This demonstrates that the vascular territory is orientated inferolaterally with respect to the perforator and follows the axial direction of the limb (**Figure 3.7**).

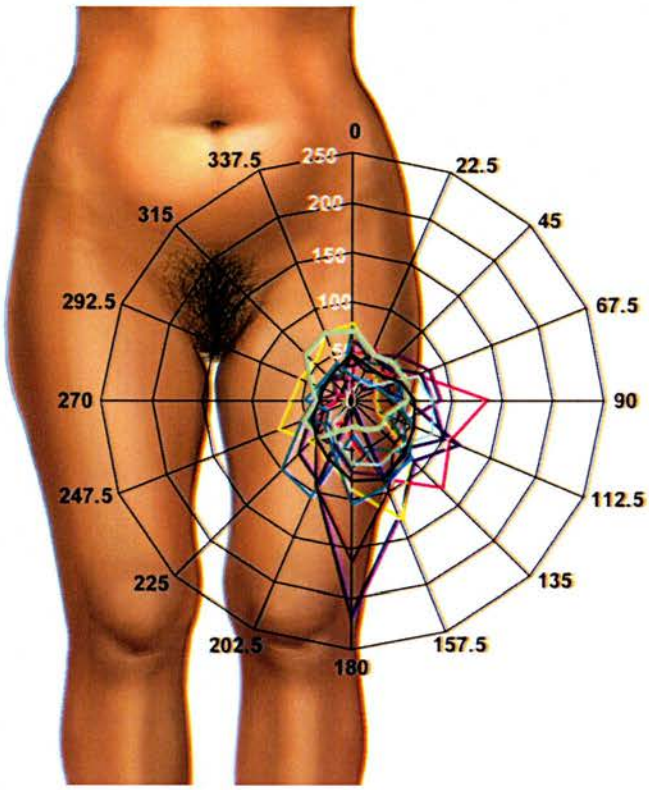

Figure 3.7 Polar plot of the arterial vascular territories of the descending branch of the lateral circumflex femoral artery by means of injection of the anterolateral thigh B perforator (corrected for left thigh). The black line represents the mean. Note that the territories are axial with respect to the axiality of the limb.

3.2.2 Perforator morphological pattern

Three distinct morphological patterns of the perforator and its branching pattern were evident: Type I - the branches of the perforator coursed obliquely through the

adipose layer to reach the subdermal plexus. There were no branches at the suprafascial level (**Figure 3.8**); Type II - the branches of the perforator coursed obliquely through the adipose layer to the subdermal plexus, and branches coursed out horizontally to form a suprafascial plexus (**Figure 3.9**); Type III - the perforator divided into several branches at the suprafascial level, coursing horizontally for variable distances before diving vertically down to the subdermal plexus (**Figure 3.10**).

In our series of 18 flaps, 9 were categorised as a type III, 6 as a type I, and 3 as a type II. No relationship was found between complex type and flap thickness.

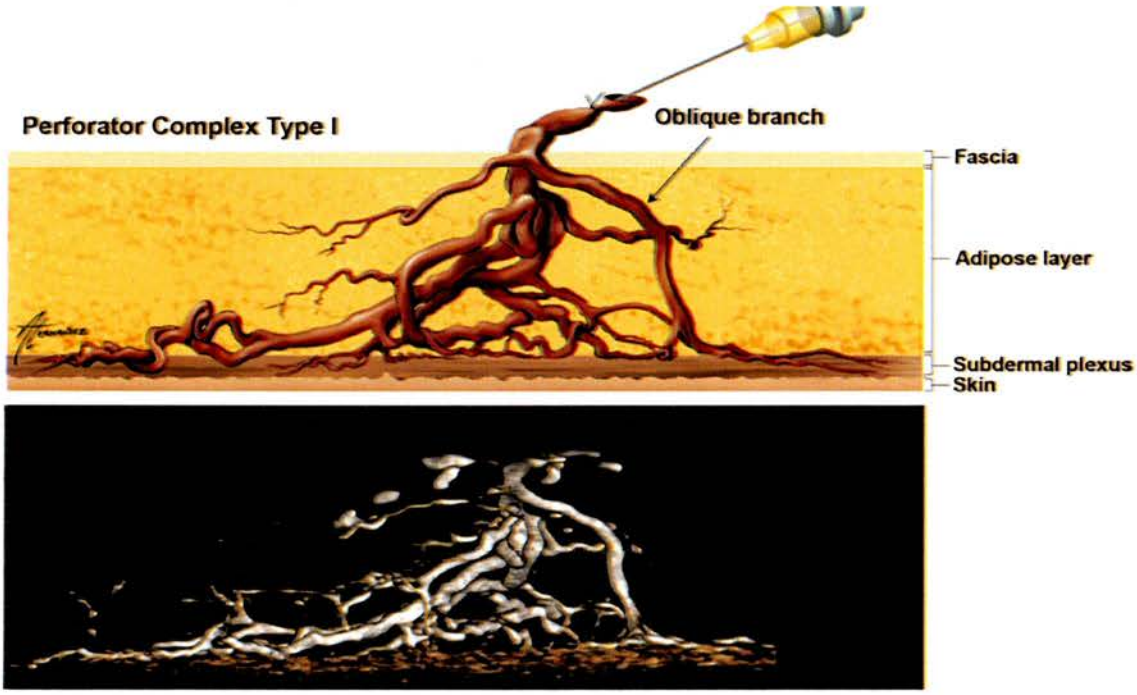

Figure 3.8 Type I perforator complex with illustration. Note that the branches of the perforator course obliquely through the adipose layer to reach the subdermal plexus, without a component at the suprafascial layer.

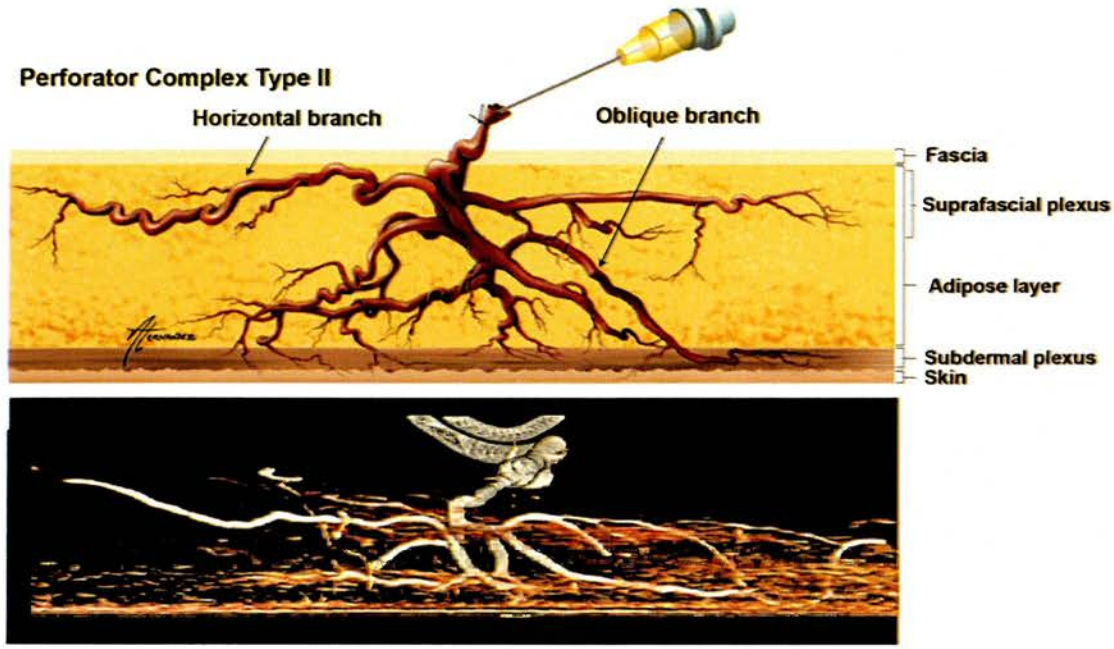

Figure 3.9 Type II perforator complex with illustration. Branches of the perforator course obliquely through the adipose layer to the subdermal plexus, and there are also branches that course out horizontally to form a suprafascial plexus.

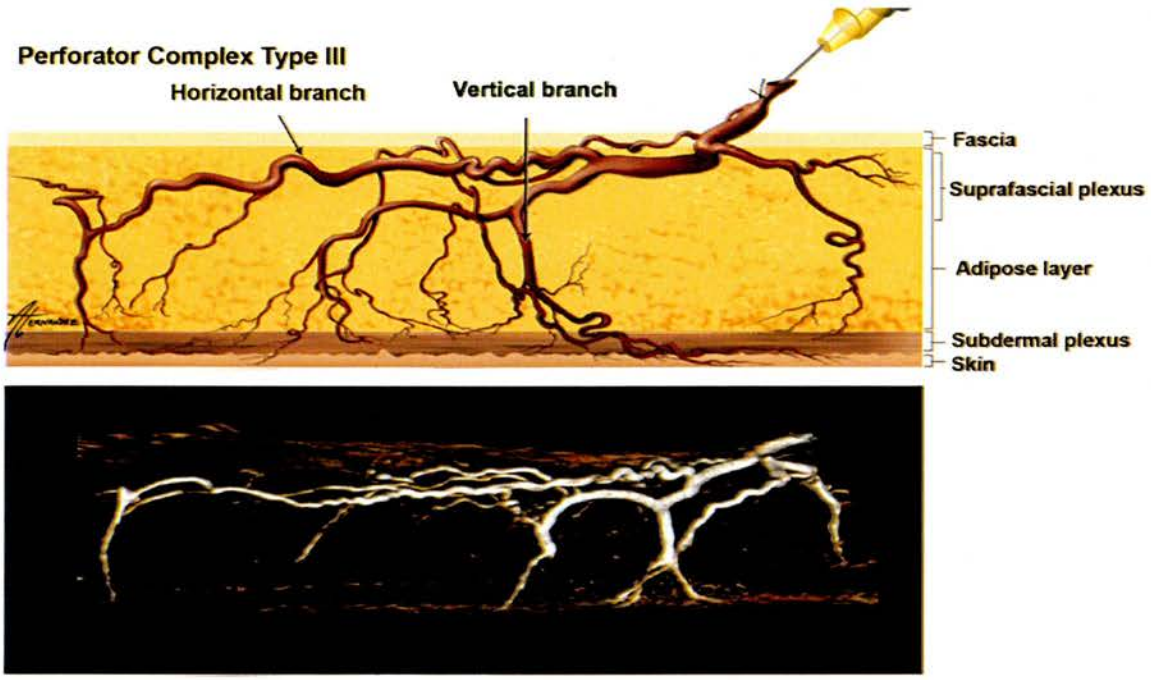

Figure 3.10 Type III perforator complex with illustration. The perforator divides into several branches at the suprafascial level, coursing horizontally for variable distances before coursing vertically to the subdermal plexus.

3.2.3 Flap thinning

Flap thinning was seen to disrupt vessels in the suprafascial plexus. Although the different perforator morphological patterns describe the branching pattern from the main perforator stem, all flaps, regardless of complex type, had a dense suprafascial plexus perfused mainly by recurrent flow through the subdermal plexus. Ligation of vessels in the suprafascial plexus prevented filling of adjacent perforator complexes within the same angiotome, as well as the large diameter linking vessels that enable perfusion of adjacent angiotomes (**Figures 3.11 and 3.12**). The angle of thinning, or the depth of thinning, as

long as the subdermal plexus was preserved, was not seen to significantly change the effect of thinning.

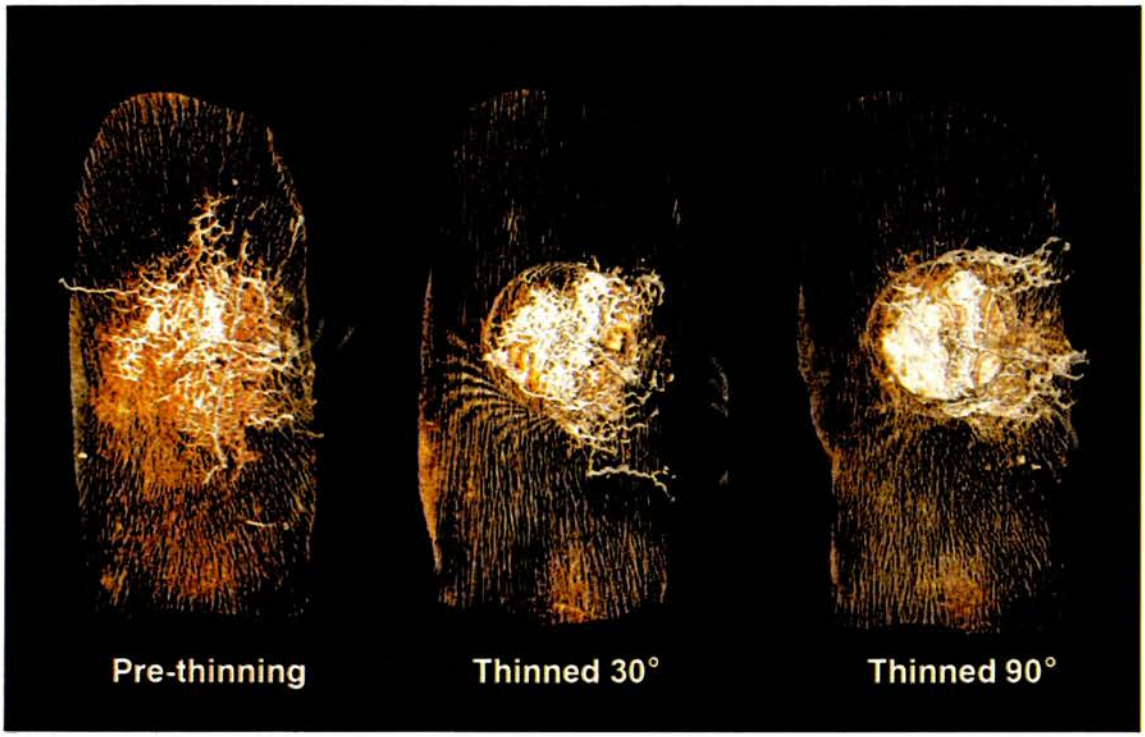

Figure 3.11 Anteroposterior views of a type II perforator complex with progressive flap thinning and injection of 1.5 ml of contrast. A 5-cm radius about the perforator has been preserved (wire circle) and thinning has been performed at 30 degrees to the horizontal followed by 90 degrees to the horizontal, with washout of the contrast between successive stages. Note how the vascular territory is reduced by any angle of thinning because of the interruption of filling at the level of the suprafascial plexus and the linking vessels. Thinning should therefore be avoided if a large flap is planned.

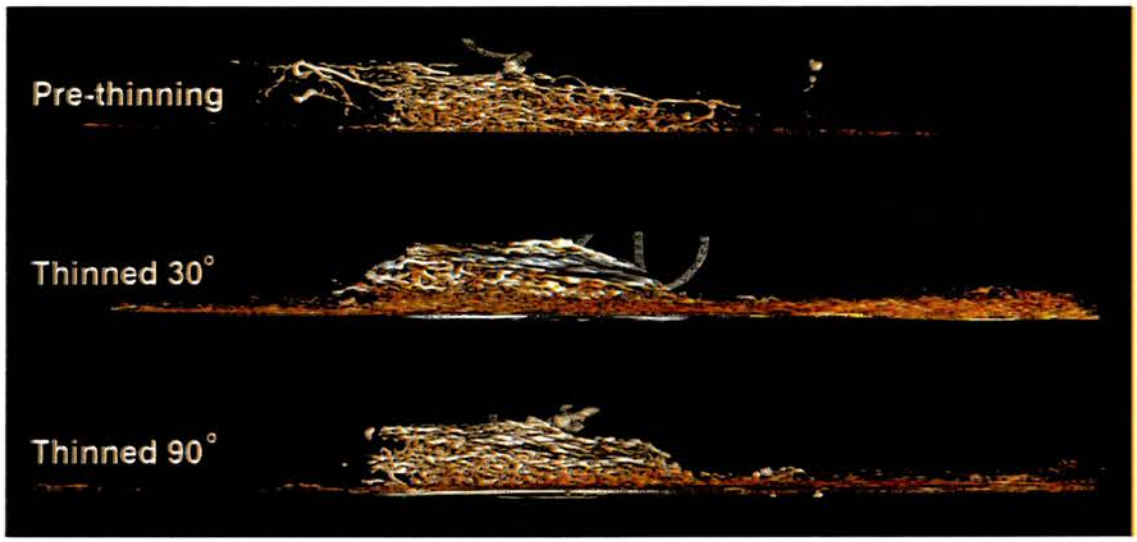

Figure 3.12 Lateral views of a type II perforator complex, with progressive flap thinning and injection of 1.5 ml of contrast. Note how the vascular territory is reduced by any angle of thinning because of the interruption of filling at the level of the suprafascial plexus and the linking vessels.

The mean percentage decrease in the area of the vascular territory following flap thinning was 40.5 percent, and a decrease in flap vascular territory was seen for all perforator complex types (**Table 3.1**). The type I perforator, with an oblique branching pattern and an absence of vessels at the level of the suprafascial plexus from the main stem of the perforator, had the largest flap vascular territory both before and after flap thinning (**Table 3.2**).

Table 3.1 Flap thinning data

	Mean (range)
Flap thickness before thinning (cm)	2.0 (1.7-2.4)
Flap thickness after thinning (cm)	0.71 (0.65-0.82)
Vascular territory before thinning (cm^2)	129.4 (67.1-172.5)
Vascular territory after thinning (cm^2)	73.1 (46.2-109.6)
Change in vascular territory (%)	40.5 (20.3-65.5)

Table 3.2 Flap thinning data by complex type

Complex Type	**Mean Flap Territory before Thinning (cm^2)**	**Mean Flap Territory after Thinning (cm^2)**	**Mean Decrease in Vascular Territory (%)**
I	146.3	85.8	40.0
II	90.5	62.2	31.3
III	95.0	46.2	51.3

3.2.4 Anatomy and perfusion of the venous system

At the level of the deep fascia the valves of the venae comitantes were overcome with minimal resistance during flap injection. During injection a delay occurred before the venous system began to fill, indicating the presence of contraflow valves. There was a superficial venous system that was seen to fill the venae comitantes of the perforators of the LCFA. The superficial system consisted of large diameter veins arranged in a

polygonal network on the subdermal plexus (**Figures 3.13 and 3.14**). Superficial venous drainage occurred in a medial direction towards the long saphenous vein, which appeared to be the main drainage vessel for the integument of the anterior thigh. Harvest of the LCFAP-*vl* flap does not usually include the long saphenous vein, although it might be beneficial to include in a very large flap for venous superdrainage. Planning of the flap more laterally to the perforator entrance into the flap would therefore optimise venous drainage within the flap.

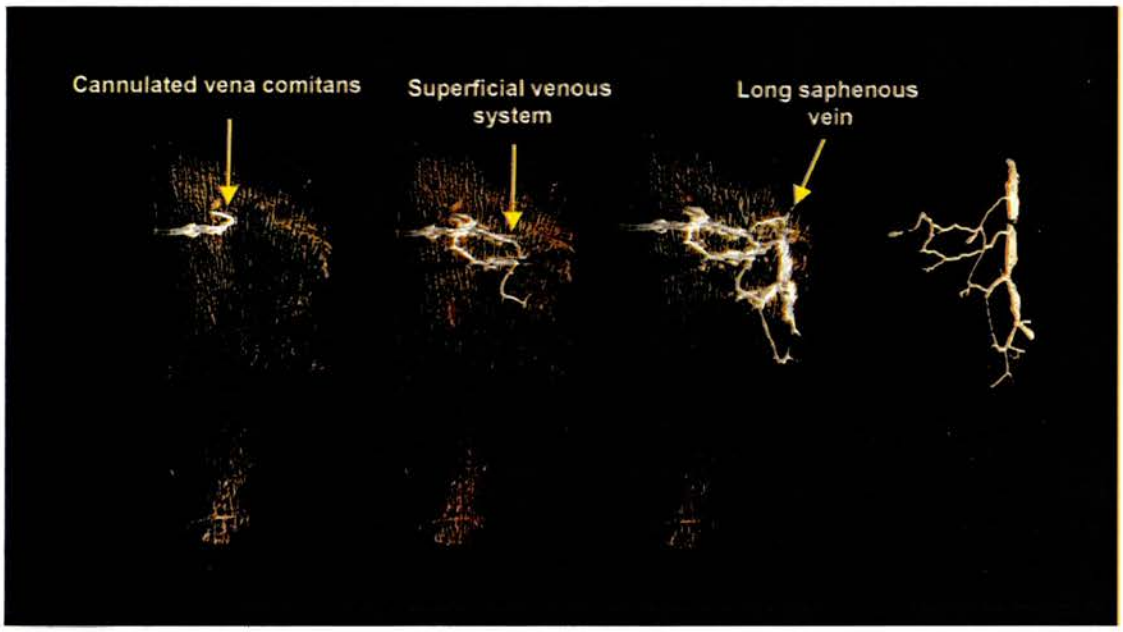

Figure 3.13 Anteroposterior views of dynamic filling of the venous system after cannulation of the vena comitans of the B perforator, with images acquired at 1-ml filling increments. The image on the right is a static study performed after injection with a barium sulphate/gelatin mixture. Note that drainage in the superficial venous system occurred medially toward the long saphenous vein. Note also that the superficial venous system is situated on the subdermal plexus and that filling of the venae comitantes of adjacent perforators occurred, draining into the deep venous system.

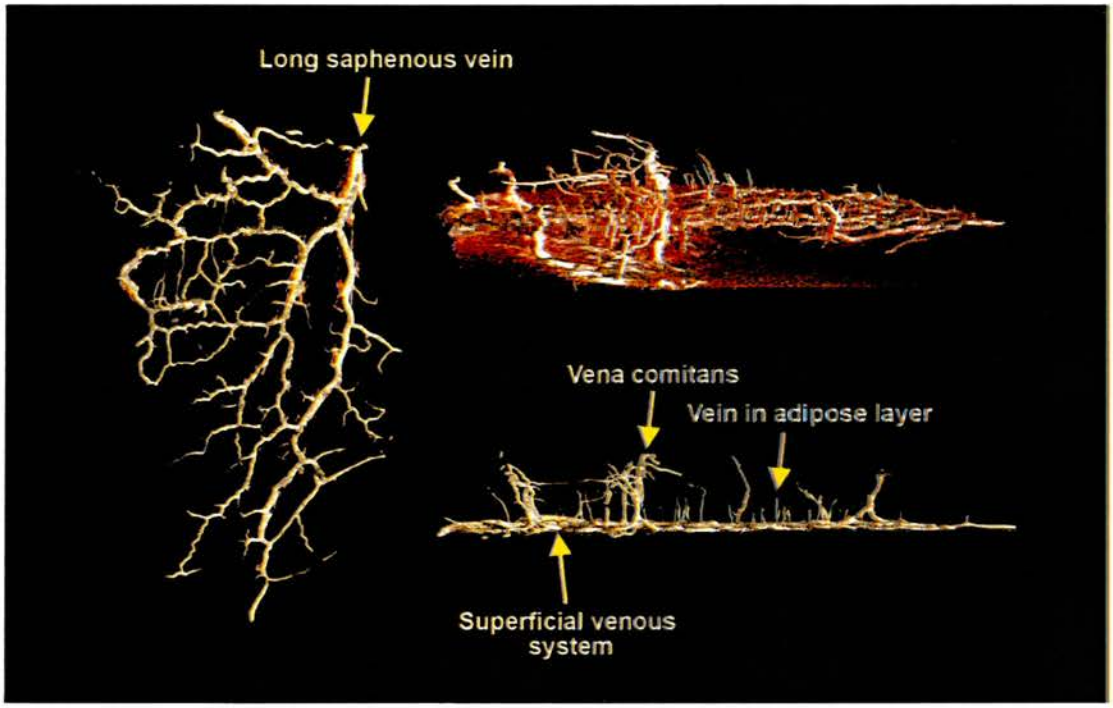

Figure 3.14 Anteroposterior, oblique, and lateral static three-dimensional views of the venous system after injection of the vena comitans of the B perforator with a barium sulphate/gelatin mixture. Note the polygonal configuration of the superficial venous system and also the presence of small veins draining the adipose layer.

In the thicker flaps veins draining the adipose layer could be clearly seen (**Figure 3.14**). Microdissection revealed that the superficial venous system is arranged as distinct venous vascular territories with valves preventing flow between adjacent vascular territories.

3.2.5 Contrast density analysis

Analysis revealed a linear relationship between the fill interval and the density of contrast in each layer of the flap following injection of the arterial system, demonstrating that perfusion of each layer is proportionally the same irrespective of the volume of

contrast injected into the flap. Analysis of the mean contrast density for each layer of the flap with respect to perforator revealed that the contrast density in the subcutaneous and suprafascial plexuses were similar at the perforator entrance, and decreased linearly with respect to distance from the perforator. The contrast density at the subdermal plexus was lower than at the other layers at the perforator entrance, declining at a slower rate than in the other layers. Contrast was still present in the subdermal plexus at the periphery of the vascular territory, indicating random pattern flow (**Figure 3.15)**.

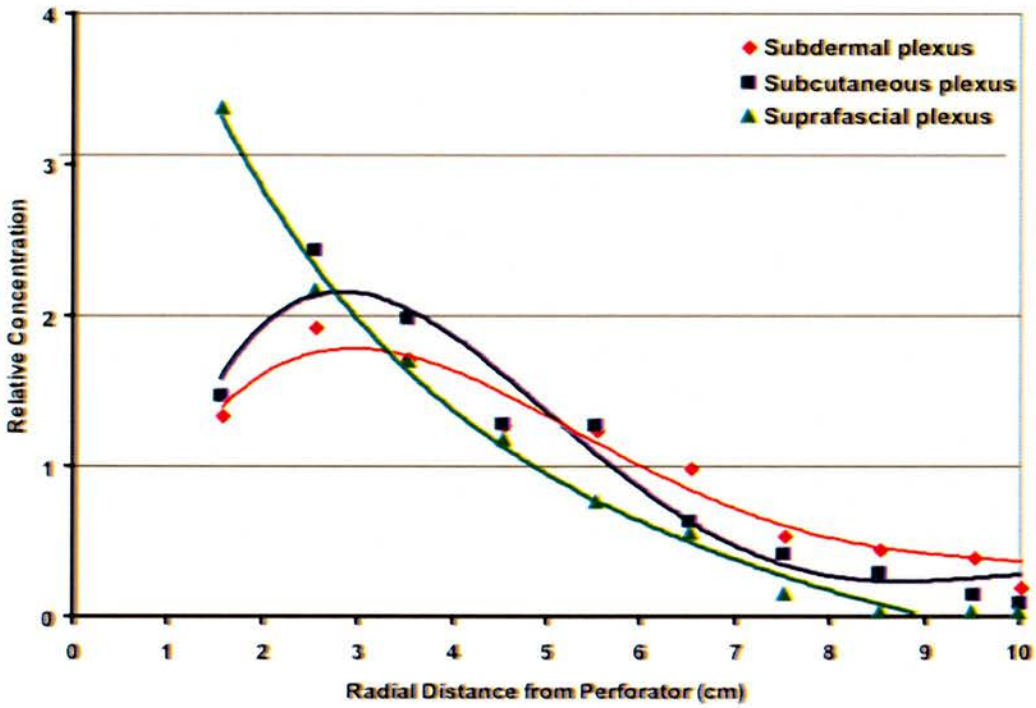

Figure 3.15 The contrast density analysis graph shows the mean contrast density for all flaps in the octant of flap axiality with respect to the perforator in the subdermal, subcutaneous, and suprafascial plexuses. Note that the contrast densities in the subcutaneous and suprafascial plexuses are similar at the perforator entrance and decrease linearly with respect to distance from the perforator. The contrast density at the subdermal plexus is lower than at the other layers at the perforator entrance, declining at a slower rate than in the other layers. Contrast is still present at the subdermal plexus at the periphery of the flap vascular territory when there is no contrast in the suprafascial plexus, indicating random pattern flow.

3.3 SUMMARY

This was the first study to use 3D and 4D CT imaging to evaluate the microanatomy of the arterial and venous system of the LCFAP-*vl* flap. Three distinct morphological patterns of the 'B' perforator and its branching pattern were evident. The perforator complex type and flap thickness were unrelated, indicating that the patterns may occur at random. Previous studies by Kimura *et al.* (2001) and Alkureishi *et al.* (2003) had evaluated the perforator morphological patterns. Kimura *et al.* (2001) classified the patterns of the perforator vessels within the adipose layer into three types according to their relationship to the residual fat within a radius of 2 cm about the perforator. The type 1 perforator was the most common and extended almost perpendicularly into the subdermal plexus while remaining in the residual fat; type 2 perforators branched off into the adipose tissue and extended sideways to the flap, protruding from the cut edge of the residual fat; type 3 perforators, which were the least common, extended across the deep fascia and gradually into the adipose layer. The limitations of this study are that the vessels were only investigated within a 2cm radius of the perforator, and intraoperative dissection may have missed small branches of the perforator. Alkureishi *et al.* (2003) by contrast found that large branches from the perforator were seen to form an arterial plexus at the level of the deep fascia, which communicated with the subdermal plexus supplying the skin, and further branches arose from the perforator and travelled obliquely through the fat to reach the subdermal plexus, rather than these patterns being mutually exclusive as Kimura *et al.* (2001) had suggested. This study utilised specimens that had undergone diaphanization, and the shrinkage of the tissues during this process may have disrupted the relative positions of the perforator and its branches. The type I complex defined in this study most closely matches the type II complex described by Kimura et al., but the type I or type III complexes as described

were not seen. This study has found that these patterns were mutually exclusive in the type II and type III perforator complexes.

Dynamic flap imaging before and after flap thinning to 6-8mm with preservation of a 5cm radius revealed a mean reduction in flap vascular territory of 40 percent, supporting findings of previous studies (Nojima *et al.*, 2005) in the same patient population. Flap thinning was seen to disrupt the vessels of the suprafascial plexus, which were found at the undersurface of the deep fascia or within two millimetres of the fascia within the adipose layer. This prevented perfusion of adjacent perforator complexes within the same angiotome, and disrupted the large diameter linking vessels that were seen to perfuse adjacent angiotomes. Alkureishi *et al.* (2003) also found that the suprafascial plexus and the oblique vessels supplying the subdermal plexus are likely to be damaged or removed during thinning, and may explain the observed reduction in subdermal plexus filling in the anatomical thinned specimens, advising that one-stage thinning of the ALT flap may not be safe in the Western population.

Flow within the large diameter linking vessels that coursed between neighbouring perforator complexes at the suprafacial level was seen to be bidirectional. Importantly these linking vessels also sent branches down to the subdermal plexus to perfuse the skin between adjacent perforator complexes, which may explain how the skin between adjacent vascular territories is perfused. Vessels without a change in calibre connecting adjacent vascular territories were noted by Taylor and Palmer in their study of the angiosomes of the body (1987), and provides further evidence for the dynamic nature of the angiosome (McGregor, 1992; Taylor and Palmer 1987; Taylor and Palmer, 1992). This linking vessel network therefore appears to be an important part of flap perfusion, and enables the capture of adjacent vascular territories, and appears to be related to the nerves within the flap at the suprafascial level. Vascular connections between adjacent

perforators within the same angiotome were noted to be denser than those between neighbouring vascular territories, and injection of a single perforator in the LCFAP-*vl* flap resulted in perfusion of the entire LCFA vascular territory prior to perfusion of the neighbouring superficial femoral artery angiotome, further supporting the angiosome theory.

Analysis of the relationship between the complex type and effect of thinning on flap perfusion found that the angle of flap thinning was not important when considering the effects of thinning. The type I perforator complex had the largest flap vascular territory after flap thinning due to the absence of horizontal branches from the main perforator stem at the level of the suprafascial plexus. If flap thinning is desired, therefore, this complex type should be selected. The effects of flap thinning on perfusion do not appear to be related to the cadaveric model used in this study, but appears to be a stereotyped pattern of perfusion based on the suprafascial plexus. A cadaveric model is unable to accurately determine the area of subdermal plexus perfused via random-pattern flow and which ultimately determines the area of the flap that would survive following flap thinning. If a large flap is desired, however, these factors are unimportant, and thinning may result in peripheral flap necrosis.

The phenomenon of recurrent flow through the subdermal plexus was first noted by Moon and Taylor (1988) in lead-oxide projection radiographic studies of the transverse abdominal adipocutaneous paddle perfused by the deep superior epigastric artery, and was seen by Alkureishi *et al.* (2003) in their study of the arterial anatomy of the LCFAP-*vl* flap in specimens following diaphanization. This is the first study in which it has been demonstrated dynamically, and it appears to be an important mechanism of flap perfusion. Harvest of an adipofascial flap resulted in perfusion of the flap only within the limits of the perforator complex itself due to the absence of recurrent flow through the

subdermal plexus, demonstrating the essential role of the subdermal plexus in mediating this phenomenon.

Venous drainage of the lateral circumflex femoral angiotome consists of a superficial system that lies on the subdermal plexus and is arranged as a polygonal network, which drain medially towards the long saphenous vein or into the venae comitantes of the perforators of the LCFA, supporting findings by Kawai *et al.* (2004). Planning the flap more laterally to the entrance of the perforators into the flap may therefore optimise venous drainage, and the long saphenous vein could be included with a separate anastomosis where a very large flap is planned. Flap microdissection revealed the presence of distinct venous vascular territories, with flow from one to another prevented by the presence of valves arranged in a contraflow direction. This is in accordance with findings by Taylor *et al.* (1990) in their study of the venosomes of the body.

This study was restricted to patients from the Western population, where the adipose layer is known to be significantly thicker than that of the Asian population (Koshima *et al.*, 1993; Yu, 2004; Nakayama *et al.*, 2002). Although the complex types in this study were unrelated to flap thickness, it is possible that the microvascular anatomy of the flaps differ between the two populations, explaining the differences in outcomes reported following flap harvest in the Asian and Western populations.

Chapter 4

Thoracodorsal Artery Perforator (TAP) Flap

The aim of this chapter is to describe the methodology, and to report and discuss the results of 3D and 4D analysis of the arterial and venous anatomies and perfusion of the TAP flap.

4.1 MATERIALS AND METHODS

4.1.1 Flap harvest and preparation

Twenty-five flaps in total were harvested from fresh adult cadavers. With the arm abducted to 90 degrees and the elbow flexed to 90 degrees, the posterior axillary fold, tip of the scapular, and anterior edge of the latissimus dorsi muscle were clearly marked. The entire hemiback flap was elevated with the latissimus dorsi muscle extending from the lower six thoracic, lumber, and superior sacral vertebrae, inferior angle of the scapula, iliac crest, and posterior axillary line.

Ten flaps were used for the dynamic CT imaging studies. Dissection was performed under an operating microscope following injection of a dilute methylene blue solution into the thoracodorsal artery. All flap perforators and their accompanying venae commitantes were identified and preserved. The largest arterial perforator, which was the first perforator from the descending branch of the thoracodorsal artery in all cases, was cannulated and the flap prepared as above. The largest vena comitans of the arterial perforator was also cannulated and prepared as above.

4.1.2 Computed tomography imaging

Adequate filling of the perforator complex was achieved with only 1.5ml of contrast at an optimal injection rate of 0.25ml/min, and a volume of 3ml of contrast was required to provide adequate filling of the venous system.

The flaps were then irrigated with warmed saline to remove the contrast medium, and the flaps were thinned between the superficial and deep adipose layers, preserving a 5cm radius about the perforator. Static CT imaging was also performed.

4.1.3 Latex injection study

In fifteen specimens the ipsilateral arm was placed in 90 degrees of abduction, with the elbow in 90 degrees of flexion, and the posterior axillary fold, inferior angle of the scapula, and the lateral border of the latissimus muscle were clearly marked. A hemi-back skin paddle design was harvested, in the midline from T7 to the sacral vertebrae, across the iliac crest, 5cm anterior to the lateral border of latissimus up to the axilla, and cephalad to the tip of the scapula. Dissection was performed with identification and preservation of the neurovascular pedicle. The distances between the landmarks marked on the flap were measured before and after flap harvest to confirm that changes in dimension had not occurred during flap harvest due to elastic recoil of the integument. The thoracodorsal artery was cannulated and irrigated with warmed (37°C) normal saline until the effluent was clear, and any leaks were sealed using bipolar cautery. In fifteen flaps this was followed by manual injection of 10ml of coloured latex. The specimens were then left at room temperature for 24 hours to allow the latex to cure. The adipocutaneous flap was harvested from cepahalad to caudal in a subfascial plane. The location of the neurovascular hilus, the branching point of the thoracodorsal artery, and all perforators with an external diameter ≥0.5mm were measured in relation to the

posterior axillary fold, the anterior border of the latissimus muscle, and the inferior angle of the scapular. The intramuscular lengths of the perforators from the deep fascia to either the descending or transverse branches of the thoracodorsal artery were also recorded.

4.1.4 Histology

Haematoxylin and eosin and Hart's elastin stains were performed for all of the perforators from two of the flaps. Paraffin processing, embedding, sectioning and histological stains were performed by standard procedures (Shehan and Hrapchak, 1980; Woods and Ellis, 1996). The perforator locations were recorded and the thickness of the smooth muscle in the tunica media was measured using microscopy and the presence of nerves were noted.

4.2 RESULTS

4.2.1 Anatomy and perfusion of the arterial and venous systems

Once filling of the oblique branches of the perforator had occurred, recurrent branches were observed to fill via flow through the subdermal plexus. The recurrent branches directly perfused other perforators within the same vascular territory, as well as forming long linking vessels found either at the level of the subdermal plexus or within the superficial adipose layer that enabled perfusion of adjacent angiotomes (**Figures 4.1 to 4.3**).

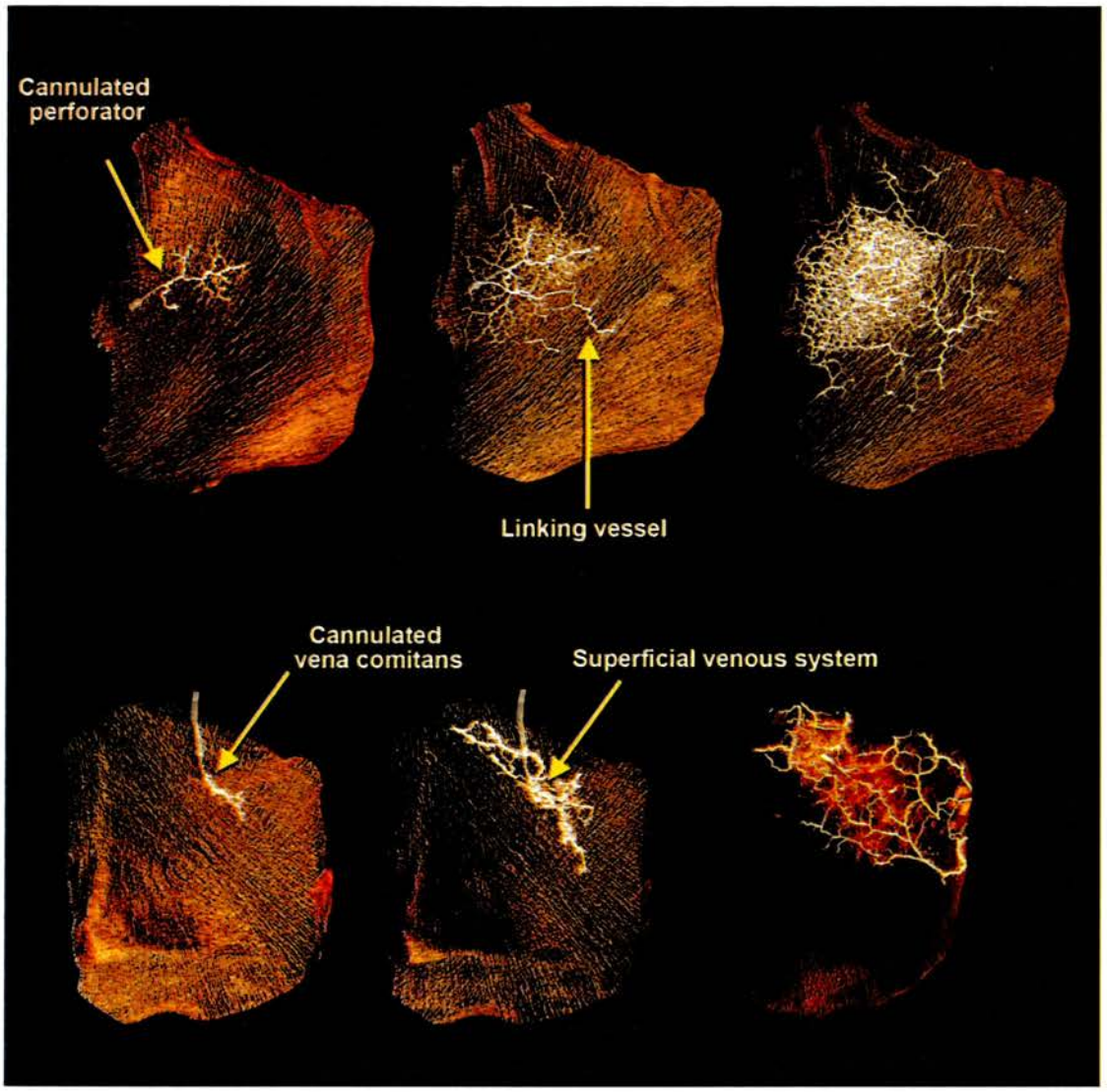

Figure 4.1 (Above) Anteroposterior dynamic computed tomographic angiograms of the most proximal perforator from the descending branch of the thoracodorsal artery at 0.5-ml filling increments. The flap is cut to follow the shape of the latissimus dorsi muscle. Note the large vascular territory and the dense network of linking vessels with the dorsal intercostal artery perforators. (Below) Anteroposterior images of dynamic filling of the venous system following cannulation of the vena comitans of the most proximal perforator from the descending branch of the thoracodorsal artery, with images acquired at 1-ml filling increments. The final image has been acquired following injection with a

barium sulphate/gelatin mixture. The superficial venous system was arranged in a polygonal configuration at the level of the subdermal plexus, and flow into the deep venous system could be seen to occur through the venae comitantes of adjacent perforators within the same angiotome. Note that drainage in the superficial venous system occurred both superolaterally towards the axilla and inferomedially/ medially toward the vertebral venous plexus, coursing progressively deeper within the flap as the veins approached the midline.

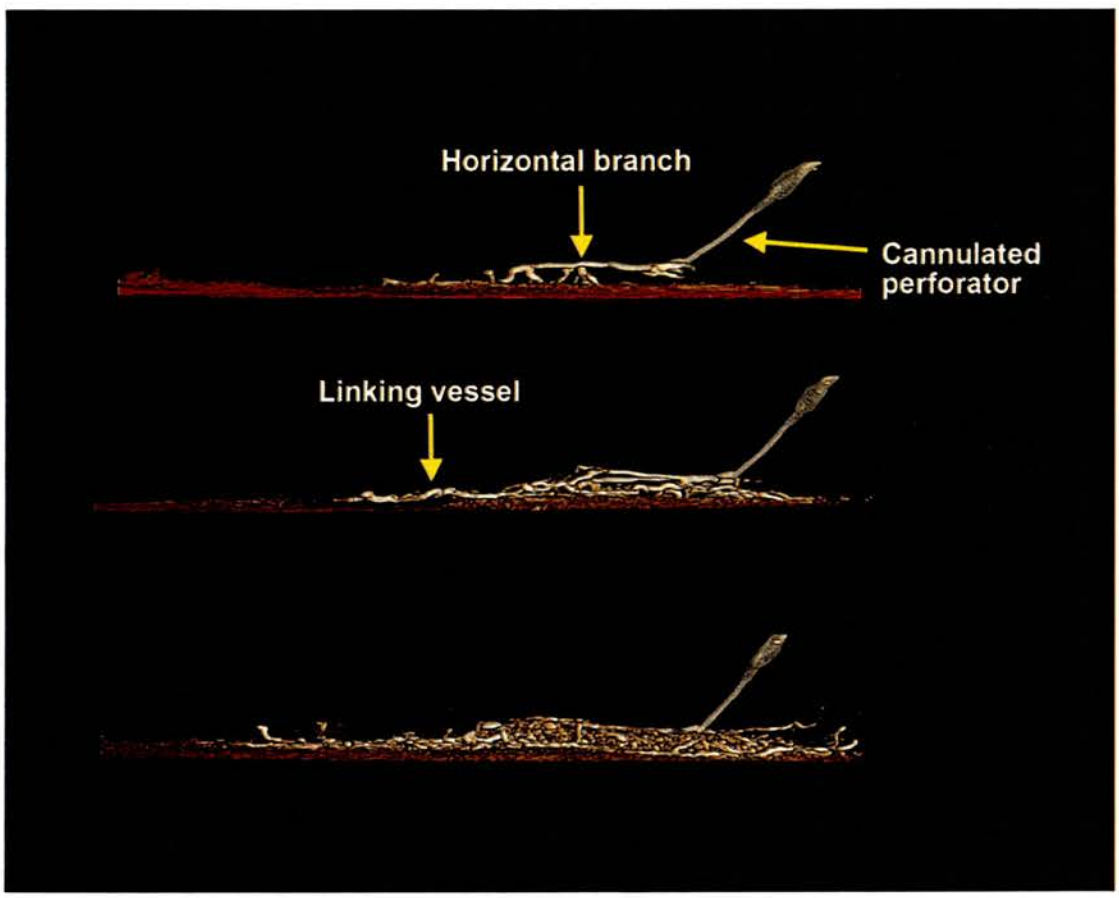

Figure 4.2 Lateral dynamic computed tomographic angiograms of the most proximal perforator from the descending branch of the thoracodorsal artery at 0.5-ml filling

increments. Note that the linking vessels are found deep within the flap at the level of the subdermal plexus, enabling thinning to be performed safely.

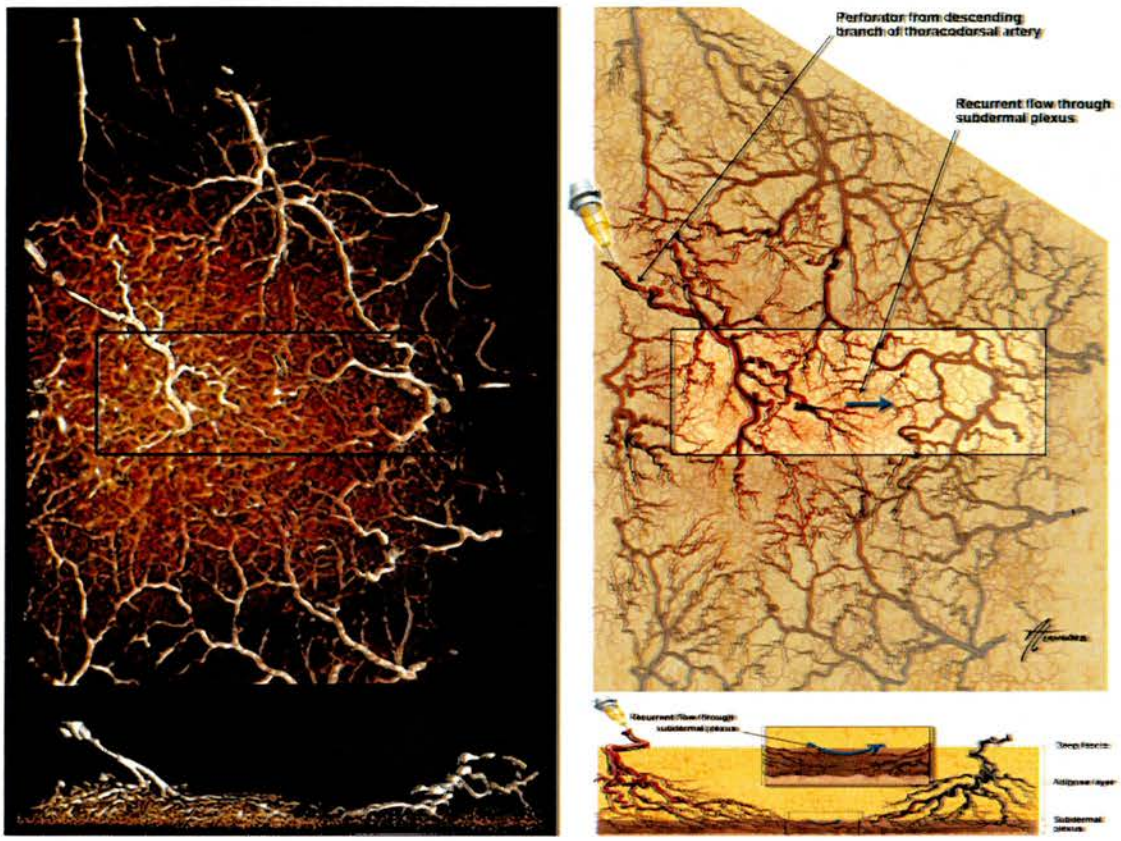

Figure 4.3 3D static images after cannulation of the most proximal perforator from the descending branch and injection with a barium sulphate/gelatin mixture, with illustration. Note the filling of the adjacent dorsal intercostal artery perforators by means of recurrent flow through the subdermal plexus, with an absence of a suprafascial plexus. This enables the flap to be thinned without disrupting its vascular supply.

A distinct superficial venous system was observed, linked with the thoracodorsal vein by the venae comitantes of the perforators of the thoracodorsal artery. The superficial system consisted of large diameter veins arranged in a polygonal network on

the subdermal plexus. Superficial venous drainage occurred in an inferomedial/medial direction towards the midline and superolaterally towards the axilla through large diameter veins, and therefore the flap should be orientated in an inferomedial direction centered on the perforator (**Figure 4.1**). The superficial veins became progressively deeper as they coursed towards the midline before termination at the vertebral venous plexus, and were accompanied by the large diameter arterial linking vessels.

4.2.2 Perforator morphological patterns

Dynamic 3D imaging of individual perforators revealed two distinct morphological patterns, which were termed types I and II according to their branching patterns: Type I - the perforator entered the deep fascia immediately and divided into several long oblique branches within the adipose layer that coursed down to the subdermal plexus (**Figure 4.4**); Type II - the perforator was found to give rise to horizontal branches at the suprafascial level and each branch coursed at this level for a short distance before entering the flap as multiple long oblique branches through the adipose layer down to the subdermal plexus (**Figure 4.5**). The maximum distance from the perforator to the point at which the horizontal branches entered the subcutaneous fat was found to be 4.1cm.

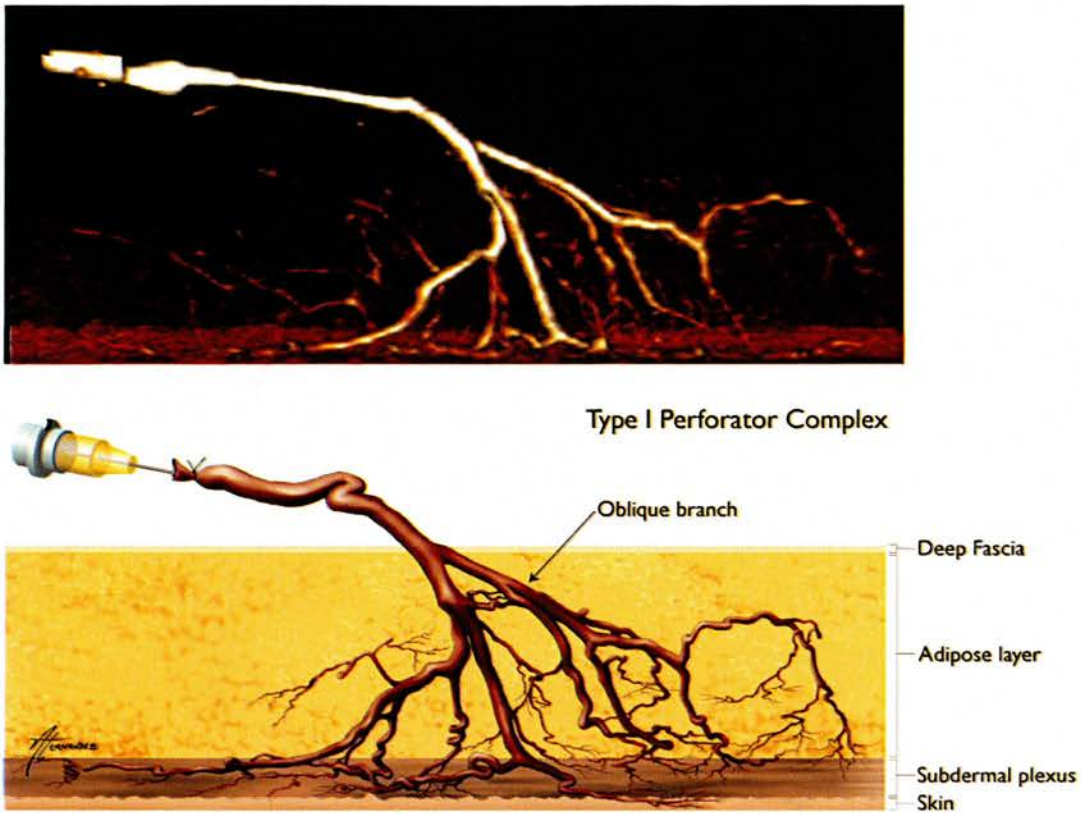

Figure 4.4 Type I perforator complex with illustration. Note that the branches of the perforator course obliquely through the adipose layer to reach the subdermal plexus, without a component at the suprafascial layer.

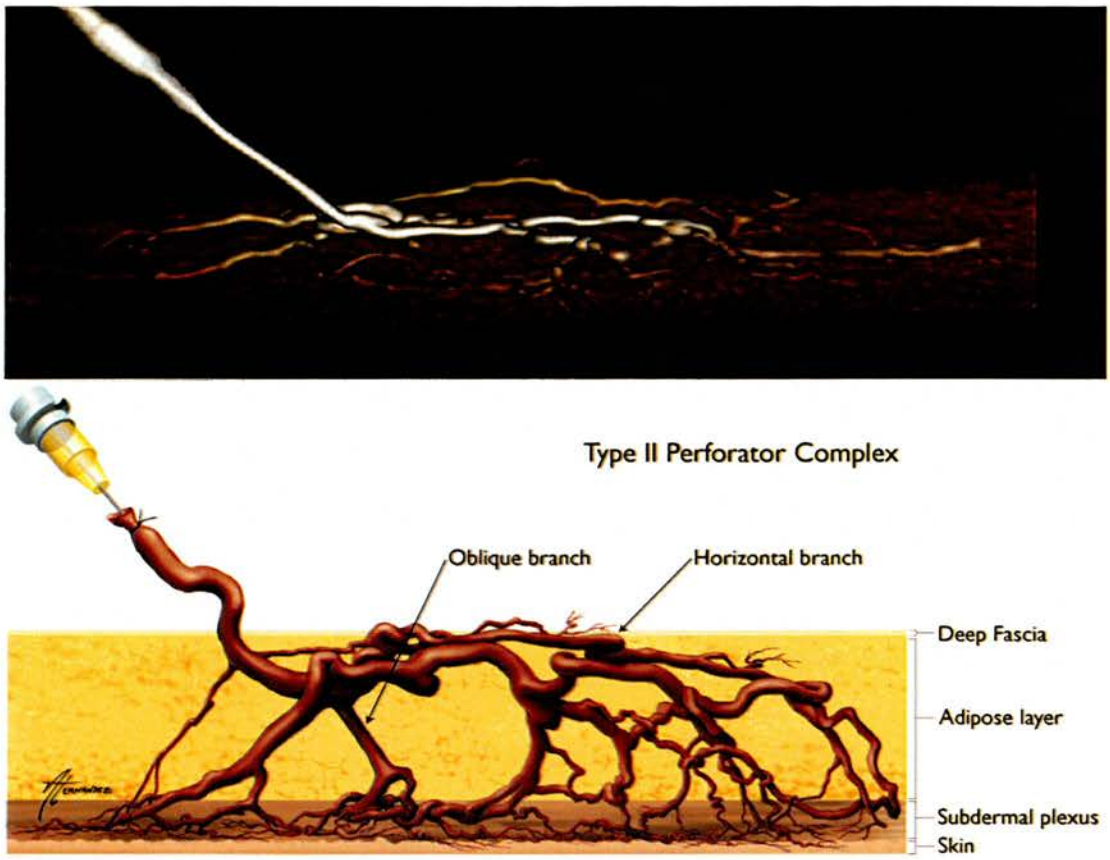

Figure 4.5 Type II perforator complex with illustration. The perforator divides into several branches at the suprafascial level, coursing horizontally for variable distances before coursing obliquely to the subdermal plexus. The maximal length of the horizontal component was measured at 4.1 cm, and this would therefore be the recommended radius to preserve during flap thinning unless the branches are visualized directly.

Five of the flaps had a type I perforator complex and five had a type II complex. Further analysis revealed that there was no relationship between flap thickness and perforator complex type.

At maximum filling the mean vascular territory was found to be 141.1 cm^2 (range, 81.7 to 197.9; σ_M=13.1) The axiality of the vascular territory was found to be inferomedial, following the shape of the latissimus dorsi muscle (**Figure 4.6**).

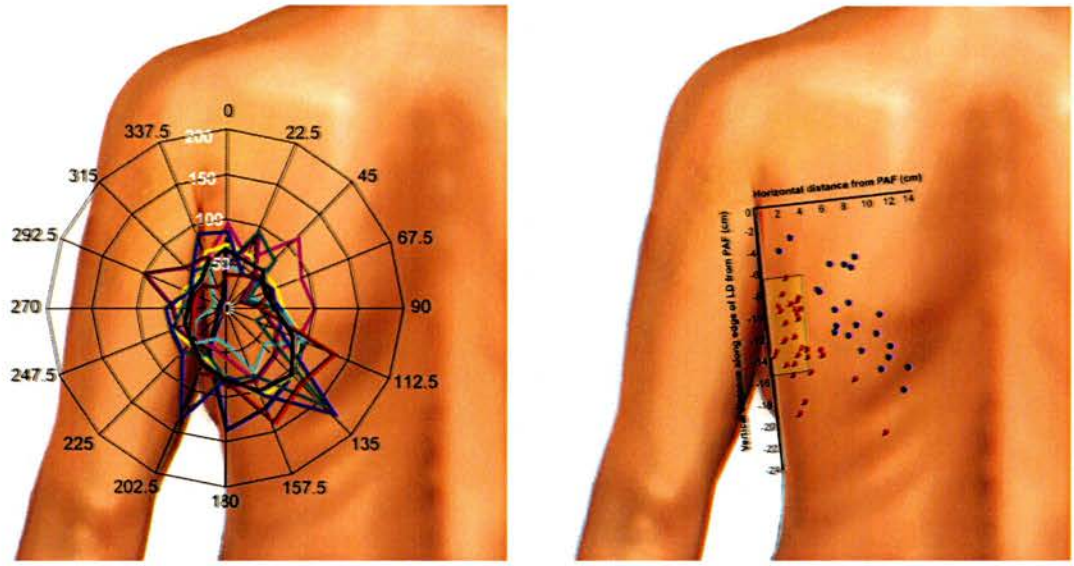

Figure 4.6 Left: Polar plot of the arterial vascular territories about the most proximal perforator from the descending branch of the thoracodorsal artery. Each color represents the vascular territory for each flap about the first perforator from the descending branch, measured from the 2D images on the CT workstation. The black line represents the mean vascular territory for all of these values. Note that the territories are axial with respect to the latissimus dorsi muscle. (Right) Scatter plot of the perforators from the descending (red) and transverse (blue) branches of the thoracodorsal artery with respect to the posterior axillary fold. The yellow area represents the region in which the most proximal, and largest, perforator from the descending branch was found in all specimens. This area was found within 3 cm of the lateral edge of the latissimus muscle from 6.6 to 15.4 cm caudal to the posterior axillary fold. A mean of 3.6 musculocutaneous perforators (range, 1 to 8) were found, with a mean of 2.5 (range, 1 to 7) originating from the descending branch and 1.1 (range, 0 to 3) originating from the transverse branch. The mean intramuscular length of perforators was 2.8 cm (range, 1.3 to 4.7) from the descending branch and 3.1 cm (range, 1.2 to 6) for the transverse branch.

4.2.3 Flap thinning

No change in the vascular territory of the thoracodorsal artery was observed after thinning as all vessels were found within the superficial adipose layers (**Table 4.1**). It should be noted that the perforator complexes of adjacent angiotomes may be disrupted by thinning and may prevent perfusion peripheral to these complexes if branches in the subcutaneous layer are not present (**Figure 4.7**).

Table 4.1 Flap data (n=10)

	Mean (range; σ_M)
Flap thickness (cm)	1.3 (0.7-2.7; 2.6)
Change in flap thickness after thinning (%)	27.4 (25.6-29.3; 1.9)
Vascular territory (cm^2) (unchanged before and after thinning)	141.1 (81.7-197.9; 13.1)

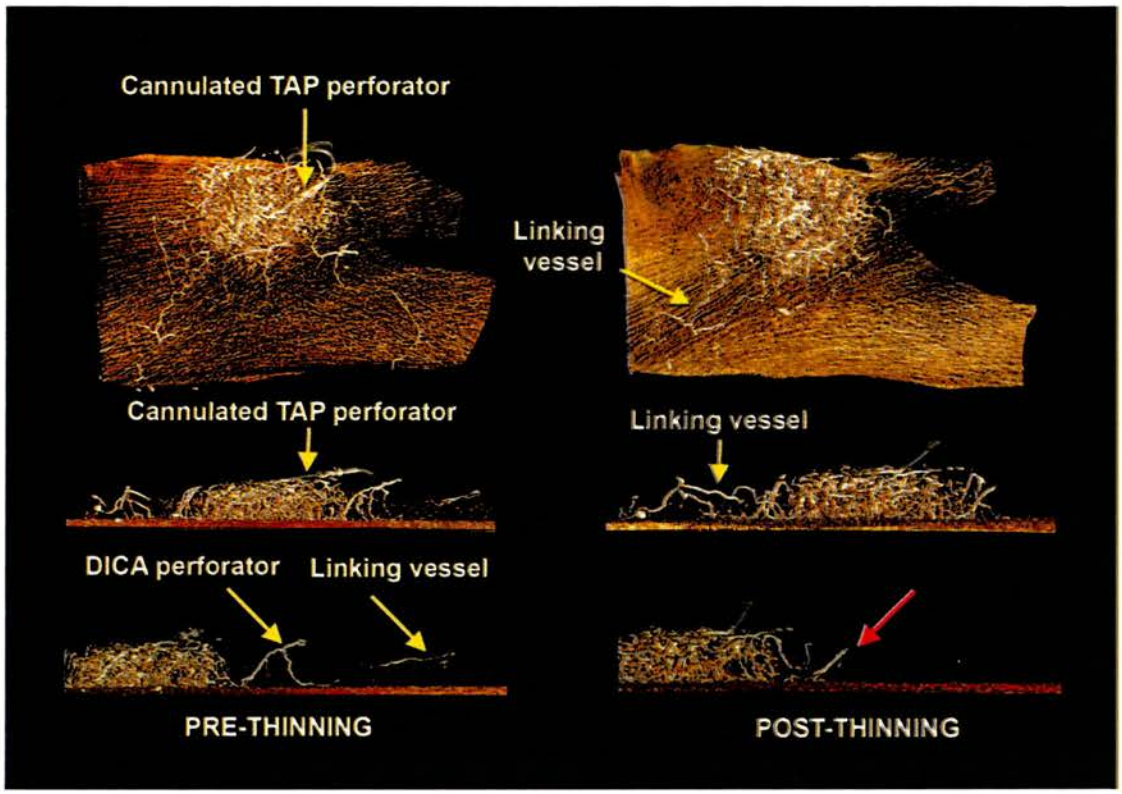

Figure 4.7 Anteroposterior and lateral views of a type I perforator complex before (left) and after (right) thinning between the deep and superficial adipose layers and injection of 1.5 ml of contrast. A 5-cm radius about the perforator has been preserved, and thinning has been performed at 90 degrees to the horizontal, with washout of the contrast between successive stages. The vascular territory is unaffected by flap thinning, as the linking vessels lie within the superficial adipose layer or at the level of the subdermal plexus. However, flow through the linking vessels is mediated through adjacent perforator complexes (the dorsal intercostal artery perforators), and these may be interrupted by flap thinning (red arrow), preventing the vascular territory from extending beyond this unless bypassing vessels are present in the superficial adipose layer.

The maximum radius from the perforator at which the transverse suprafascial branches entered the adipose layer was 4.1cm. It is therefore recommended that a radius of least this distance should be preserved around the perforator to avoid damaging these vessels.

4.2.4 Latex injection study

The thoracodorsal artery bifurcated into transverse and descending branches at the neurovascular hilus in all specimens, at a mean distance of 5.1cm (range, 2.1 to 7.5; σ_M=0.43) from the posterior axillary fold, 2.2cm (range, 1.3 to 3.1; σ_M=0.17) from the lateral edge of the latissimus dorsi muscle (**Table 4.2**). The mean length of the descending branch was 15.2cm (range 13.2 to 19.0cm).

Table 4.2 Results from latex injection and microdissection study (n=15)

	Mean (range; σ_M)
Distance from the posterior axillary fold to the first perforator from the descending branch (cm)	10.6 (6.6-15.4; 0.88)
Distance from the neurovascular hilus to the first perforator from the descending branch (cm)	6.0 (3-13.3; 0.82)
Distance between the first and second perforators from the descending branch (cm)	3.4 (0.5-7.6; 0.61)
Distance between the second and third perforators from the descending branch (cm)	1.2 (0.7-2.5; 0.33)

A mean of 3.6 musculocutaneous perforators ≥0.5mm (1 to 8) were found per flap, with 70% originating from the descending branch, and perforators from the transverse branch found in 10 of 15 flaps. The descending branch yielded a mean of 2.5 perforators per flap (range 0 to 7), and the transverse branch 1.1 perforators per flap (range 0 to 3). At least one perforator originated from the descending branch in all dissections. A second perforator was observed in 12 dissections, a third in 5, and a fourth in 3 specimens (**Figure 4.6**). The most proximal perforator from the descending branch was noted to have the largest diameter in all specimens, and was found within 3cm of the lateral edge of the latissimus muscle from 6.6 to 15.4cm caudal to the posterior axillary fold. At least one perforator in each flap >0.5mm was found within a 5.9 x 4.3cm area located between 9.5 and 15.4cm from the posterior axillary fold within 4.3cm of the lateral border of the latissimus muscle. 58% of all perforators from the descending branch, and 39% of all perforators from the thoracodorsal artery were found in this region. In 8 of 15 flaps the most proximal perforator from the descending branch was found in this region, and in the remainder it was the second. From the bifurcation of thoraocdorsal artery at least one perforator was found from 5 to 10cm, within 4.3cm of the lateral border of the latissimus muscle. 61% of all perforators from the descending branch were found in this region, and 41% of perforators from the thoracodorsal artery. A direct extramuscular branch from the thoracodorsal artery was observed coursing over the lateral edge of the muscle to give rise to septocutaneous perforators was noted in 8 of 15 dissections. No anatomical concordance in perforator location was seen between specimens harvested from the same cadaver.

At 5cm from the posterior axillary fold the descending branch was found at a mean of 2.0cm (range 1.4 to 2.5cm) from the lateral edge of the latissimus dorsi muscle, at 10cm at a mean of 2.4cm (1.3 to 3.3cm), and at 15cm at a mean of 2.9cm (range 2.0 to

3.8cm). The mean length of the descending branch was 15.2cm (range 13.2 to 19.0cm). The descending branch gave off one or more medial branches, the first of which had the largest caliber and was found at a mean of 2.1cm from the bifurcation (range 1 to 3.1cm) (**Figure 4.8**).

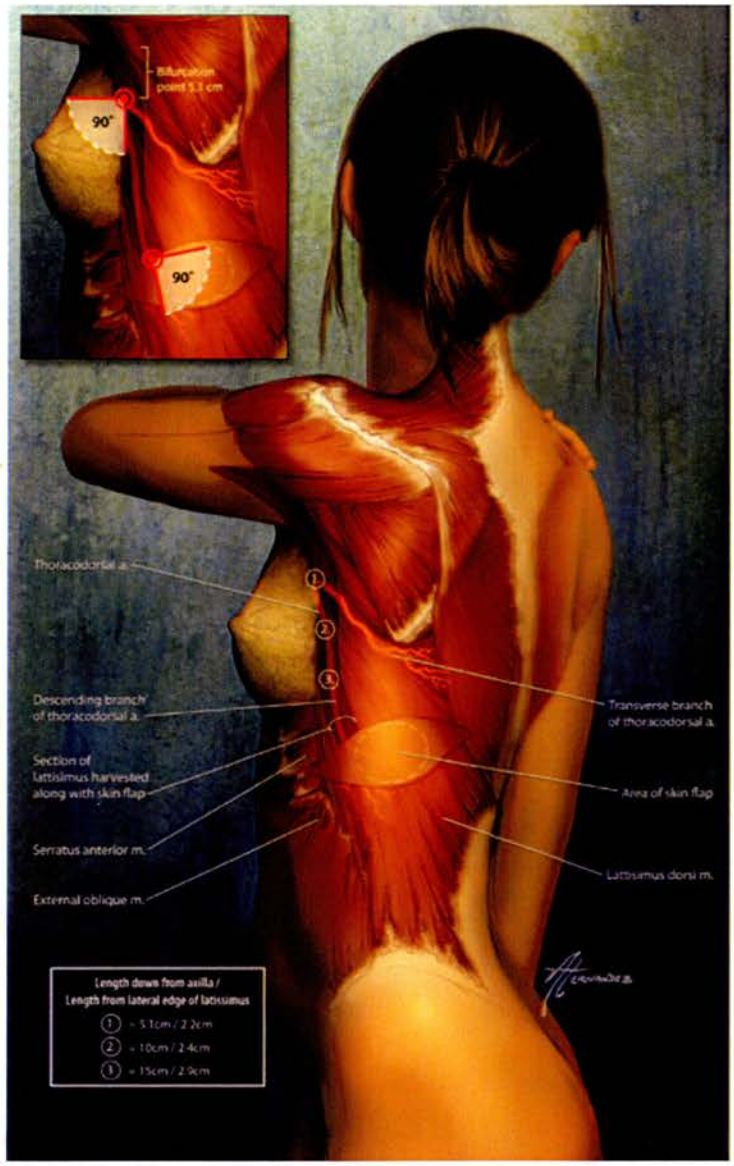

Figure 4.8. Illustration demonstrating the mean position of the descending branch of the thoracodorsal artery in relation to the lateral edge of the latissimus dorsi muscle. This can be confirmed intraoperatively by using an intraoperative Doppler on the surface of the muscle, or by direct inspection of the underside of the flap. Note that a small portion of muscle can be harvested along with the artery to protect it, and that when used as a pedicled flap for breast, chest, neck, or upper arm coverage two pivot points exist: one pivot point at the muscle-skin paddle juncture and the second located at the bifurcation point.

4.2.5 Histology

The first perforators from the descending and transverse branches were found to have the largest vessel diameters and thickest tunica media layers (**Table 4.3**). A branch of the thoracodorsal nerve and two venae comitantes were found to accompany all perforators (**Figure 4.9**).

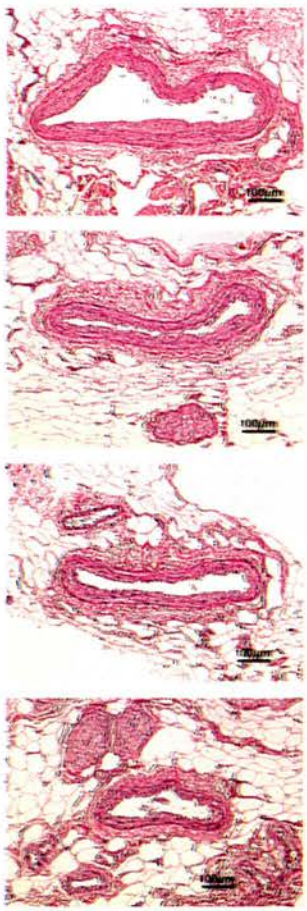

Figure 4.9. Haematoxylin and eosin stain histology of all of the perforators from the descending branch of the thoracodorsal artery (n=2). Note that the first perforators from the descending and transverse branches were found to have the largest vessel diameters and thickest tunica media layers, with a proportional decrease in size with increasing distance from the bifurcation. Note also that a branch of the thoracodorsal nerve and two venae comitantes were found to accompany all perforators.

Table 4.3 Measurements of the internal diameter and thickness of the tunica media for the perforators of the thoracodorsal artery (n=2)

	Mean external diameter (mm)	**Mean thickness of tunica media (μm)**
First perforator from descending branch	0.50	50
Second perforator from descending branch	0.45	45
Third perforator from descending branch	0.30	40
First perforator from transverse branch	0.60	50

4.3 SUMMARY

This was the first study to evaluate the microanatomy and perfusion of the TAP flap using dynamic 3D imaging techniques. Perfusion in the TAP flap was found to occur via vessels at the level of the subdermal plexus or within the superficial adipose layer. The relative absence of a suprafascial plexus may be related to the very thin deep fascial layer superficial to the latissimus dorsi muscle. The linking vessels between the thoracodorsal and dorsal intercostal angiotomes were situated within the superficial adipose layer and allowed thinning between the deep and superficial adipose layers without disrupting the perfusion of the flap.

Two distinct morphological perforator complex types were found. In the type I complex the perforator branches immediately entered the flap as multiple long oblique branches through the adipose layer down to the subdermal plexus, whereas in the type II perforator complex there was a significant suprafascial plexus around the perforator. No relationship was found between the morphological pattern of the perforator and flap thickness, suggesting that these patterns may occur at random. The maximum distance

from the perforator to the point at which the horizontal branches entered the subcutaneous fat was found to be 4.1cm, and therefore this is the radius that should be preserved about the perforator when flap thinning is performed, although these vessels may also be visualised at the level of the deep fascia and avoided.

Linking vessels were found to occur within the superficial adipose layer, enabling flap thinning to be safely performed between the deep and superficial adipose layers. This was evidenced by no change in the flap vascular territory following thinning between the adipose layers whilst preserving a 5cm radius about the perforator. The flap was found to be inherently thin prior to thinning with a mean flap thickness of 1.3cm, and thinning between the superficial and deep adipose layers was found to reduce the mean thickness by a further 27 percent.

Dynamic imaging of the venous system through injection of the vena comitans of the perforators revealed the presence of a superficial venous system at the level of the subdermal plexus arranged in a polygonal configuration, and through which the venae comitantes of the perforators were perfused. The axiality of the arterial and venous vascular territories were found to be inferomedial, suggesting that both arterial and venous perfusion can be optimized by orientating the flap paddle in this oblique orientation about the perforator.

This study found that a perforator with an internal diameter of 0.5mm or more originated from the descending branch of the thoracodorsal artery in all 25 specimens and a mean of 3.6 musculocutaneous perforators were found per flap. In all flaps the most proximal perforator was the largest from the descending branch, with the thickest smooth muscle wall. This perforator was found within 3cm of the lateral edge of the latissimus muscle from 6.6 to 15.4cm caudal to the posterior axillary fold. All flaps studied had a perforator >0.5mm, which is of sufficient caliber to support a flap, within a 5.9 x 4.3cm

area located between 9.5 and 15.4cm from the posterior axillary fold within 4.3cm of the lateral border of the latissimus muscle. The most proximal perforator from the descending branch has been shown to have the largest diameter, becoming sequentially smaller distally. The most proximal perforator was included within this area in 53% of flaps, and the second perforator was found in the remainder. The skin paddle should therefore be positioned over this region to ensure inclusion of a perforator (Barton *et al.*, 1983), particularly as the use of unidirectional Doppler ultrasound has been associated with a high range of false positive results for identifying TAP flap perforators (Angrigiani *et al.*, 1995).

Regarding the location of the descending branch of the thoracodorsal artery with respect to the lateral edge of the latissimus dorsi muscle, at 5cm from the posterior axillary fold the descending branch was found at a mean of 2.0cm (range 1.4 to 2.5cm) from the lateral edge of the latissimus dorsi muscle, at 10cm at a mean of 2.4cm (1.3 to 3.3cm), and at 15cm at a mean of 2.9cm (range 2.0 to 3.8cm). This may also be confirmed intraoperatively by using an intraoperative Doppler on the surface of the muscle, or by direct inspection of the underside of the flap. To protect the perforators and the pedicle some authors advocate harvest of a cuff of muscle (Hamdi *et al.*, 2004 and 2006). When used as a pedicled flap for reconstruction of defects of the breast, chest, neck, or upper arm, two pivot points exist: one pivot point at the muscle-skin paddle juncture and the second located at the bifurcation point. This allows greater degrees of freedom than is achievable with the parent musculocutaneous flap, and allows the flap to reach the anterior midline.

Chapter 5

Deep Inferior Epigastric Artery Perforator (DIEAP) Flap

The aim of this chapter is to describe the methodology, and to report and discuss the results of 3D and 4D analysis of the arterial and venous anatomies and perfusion of the DIEAP flap.

5.1 MATERIALS AND METHODS

5.1.1 Flap harvest and preparation

Twelve flaps were included in the study: ten flaps were harvested from fresh adult cadavers, and two abdominoplasty specimens were obtained following patient consent.

In the cadaveric specimens dissection was performed under loupe magnification. Injection of a dilute methylene blue solution through the DIEAs enabled all of the perforators to be identified and preserved, and their position to be measured with respect to the umbilicus. The largest medial and lateral row perforators and their accompanying venae commitantes were then cannulated and the flaps prepared as above. The SIEAs and SIEVs were also cannulated bilaterally and prepared as above.

5.1.2 Computed tomography imaging

Omnipaque was heated to 37°C to reduce the viscosity and improve vascular filling, and placed in a syringe loaded into a Harvard precision infusion pump. Adequate filling of the vascular territory was achieved with 3ml of contrast at an optimal rate of

injection of 0.25ml/min to gain a detailed appreciation of the development of the microvascularity over time. A volume of 5ml of Omnipaque was required to provide adequate filling of the venous system.

Helical scans were acquired as above, and the flaps were then irrigated with warmed normal saline to remove the contrast medium, and the next perforator was injected using the same protocol. The order of injection between the medial and lateral rows was alternated for sequential flaps in order to prevent injection order bias. Following injection studies the vascular territories of the medial and lateral row perforators were confirmed using 20ml aliquots of aqueous eosin red and methylene blue injections. Static images were also acquired.

5.1.3 Dye injection studies

The two abdominoplasty specimens were utilized in this part of the study. In one flap the largest medial row perforator was cannulated, and in the other the largest lateral row perforator was cannulated immediately following harvest. To examine the difference in perfusion characteristics *ex vivo* in the fresh specimen compared with the cadaveric specimen, injection of each perforator was performed with red dye within one hour of flap harvest. Once the cutaneous staining pattern was evident the vessels were copiously irrigated with warmed herparinised saline until the effluent was clear. The boundary of the skin staining was marked and the flaps were refrigerated at 4°C for 72 hours. Following this the same perforators were injected with methylene blue and the specimen was photographed.

5.1.4 Histology

Haematoxylin and eosin and Hart's elastin stains were performed for all of the

perforators ≥0.5mm in diameter from two of the flaps. Paraffin processing, embedding, sectioning and histological stains were performed by standard procedures. The perforator locations were recorded and the thickness of the smooth muscle in the tunica media was measured using microscopy and the presence of nerves was noted.

5.2 RESULTS

5.2.1 Arterial system

The arterial system of the DIEAP flap was arranged into distinct lateral and medial rows of perforators. Perfusion of the flap through these perforator complexes occurred in a stereotyped pattern dependent on the perforator location within the flap. Perfusion predominantly occurred via recurrent flow through the subdermal plexus, with smaller branches seen in most perforator complexes extending horizontally at the suprafascial level within each hemi-flap, and a variety of branching patterns seen within the subcutaneous adipose layer. There was considerable variation in the number of branches at the level of the subdermal plexus for both medial and lateral row perforators. Branching across the midline occurred predominatly at the level of the subdermal plexus, with small diameter vessels occasionally seen at the suprafascial level (**Figures 5.1 and 5.2**).

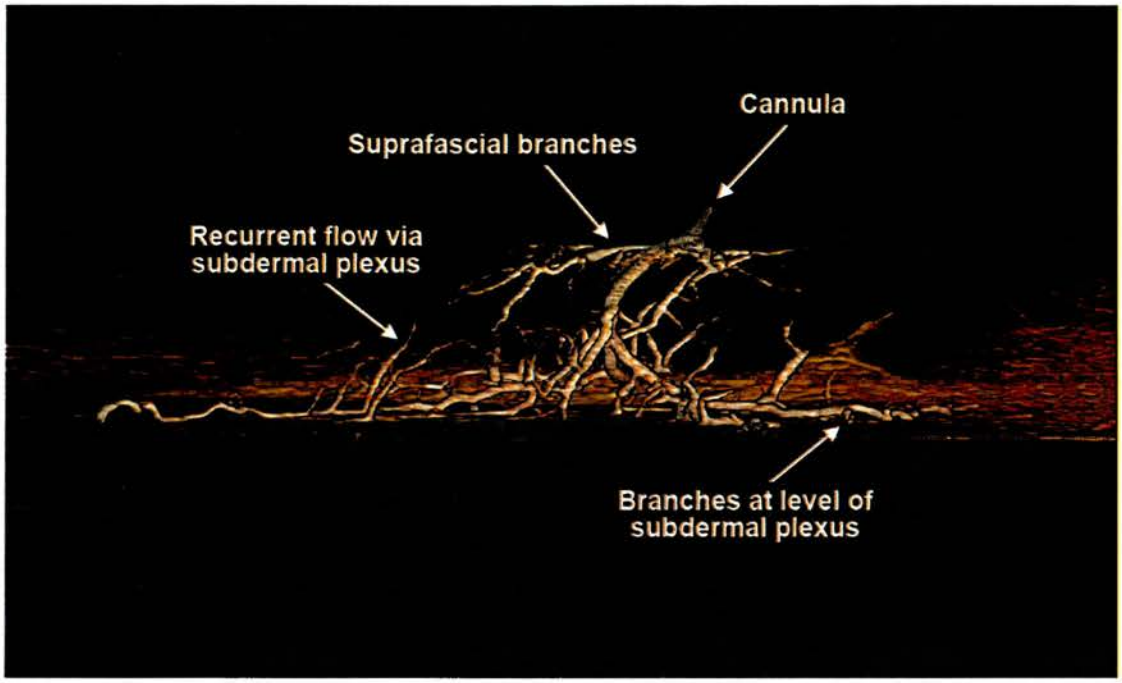

Figure 5.1 Lateral views of large lateral row perforator following injection with 0.2ml of contrast medium. The large diameter branches to the subdermal plexus were seen in all perforators, regardless of location, and varied from two to several. Branches at the suprafascial level by contrast are of much smaller diameter. Some perforator complexes did not have any branches at the suprafascial level. The suprafascial branches only coursed horizontally for a short distance before anastomosing with those of adjacent perforators, and were never seen to cross the midline. A variety of branching patterns could be seen within the subcutaneous adipose layer, although flow was seen to predominantly occur through the branches at the level of the subdermal plexus. Recurrent vessels to the adipose layer, filled via flow through the subdermal plexus, can be clearly seen. This phenomenon was first noted in the abdominal flap occurring across the midline by Moon and Taylor.

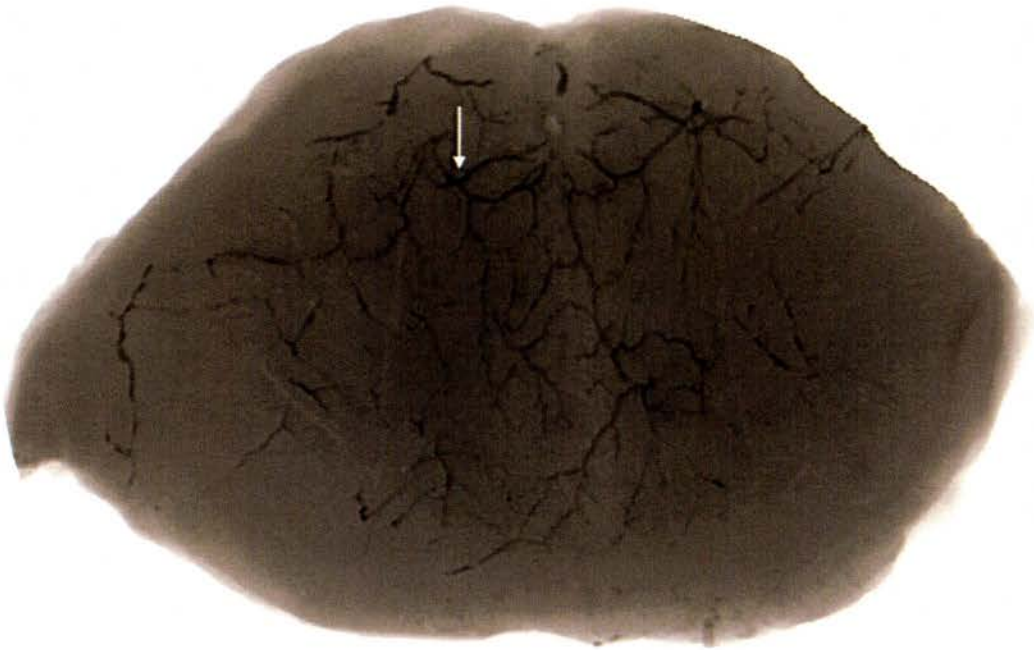

Figure 5.2 Anteroposterior view of static CT of flap following injection of a single medial row DIEA perforator (see white arrow) with a barium sulphate/gelatin mixture. Note the lattice of large diameter linking vessels across the midline connecting adjacent medial row perforators. The injection pattern resembles a centrally perfused ellipse with declined perfusion at the edges. This study was performed in a cadaveric flap, and thus is an underestimate of the vascular territory.

5.2.2 Medial row perforator

Branches of the medial row perforators were seen to be directed towards the midline where a lattice of large diameter vessels connected the medial row perforators across the midline at the level of the subdermal plexus (**Figure 5.2**). Injection of a single medial row perforator revealed immediate flow across the midline with perfusion of

medial row perforators on both sides of the midline. Further injection was seen to perfuse lateral row perforators bilaterally, and branches were seen to extend to zone IV (**Figure 5.3**). The perfusion pattern therefore resembled a centrally perfused ellipse with declining perfusion at the edges, and these findings were confirmed by dye injection.

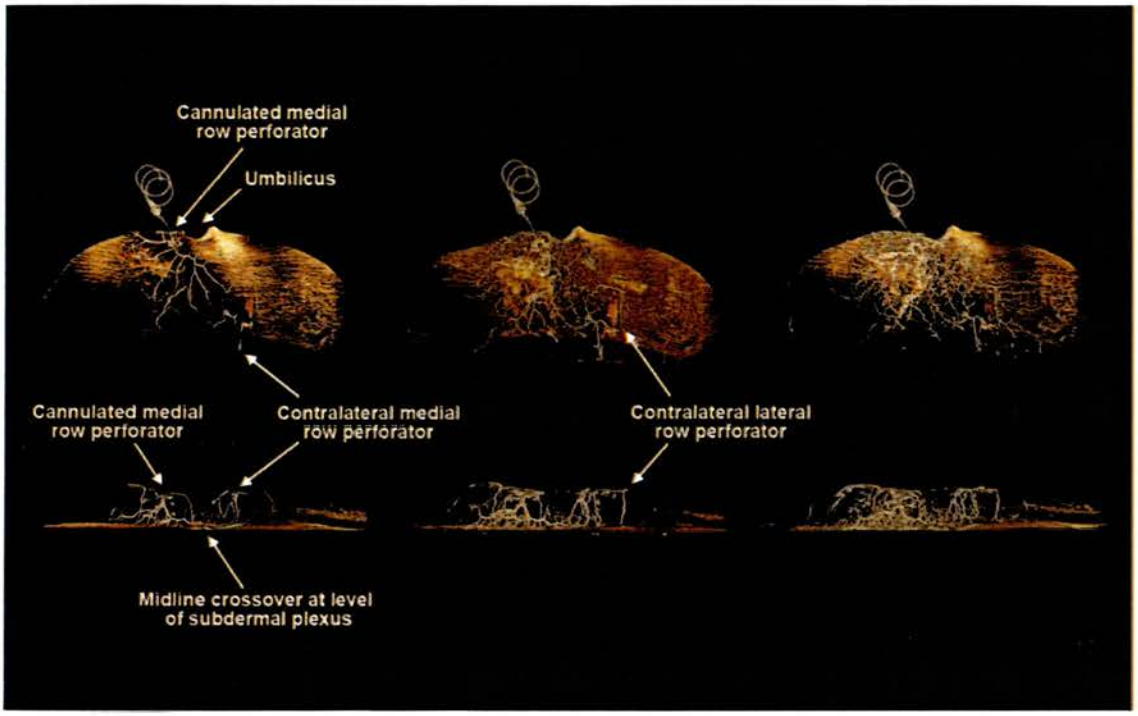

Figure 5.3 Anteroposterior and lateral views of dynamic CTA of a left medial row perforator, with images acquired at 0.5ml fill intervals. During early filling recurrent flow was seen to perfuse the adjacent medial row perforator and ipsilateral lateral row perforators, as well the contralateral medial row perforators via a lattice of large diameter vessels across the midline at the level of the subdermal plexus. Further injection was seen to perfuse the contralateral lateral row perforators, with branches extending to zone IV. Perfusion of a medial row perforator revealed a pattern of a centrally perfused ellipse with declining perfusion at the edges.

5.2.3 Lateral row perforator

Branches of the lateral row perforators at the level of the subdermal plexus were directed predominantly laterally. Injection of a single perforator from the lateral row revealed perfusion of the ipsilateral lateral aspect of the flap and adjacent lateral row perforators, as well as perfusing the ipsilateral medial row perforators via recurrent flow through the subdermal plexus. As the fill volume increased perfusion of the branches across the midline could be seen in some cases, with filling of the contralateral medial row perforators. Perfusion did not reach the contralateral lateral row perforators, regardless of the fill volume (**Figures 5.4 and 5.5**). Dye injection revealed that dye staining did not cross the midline.

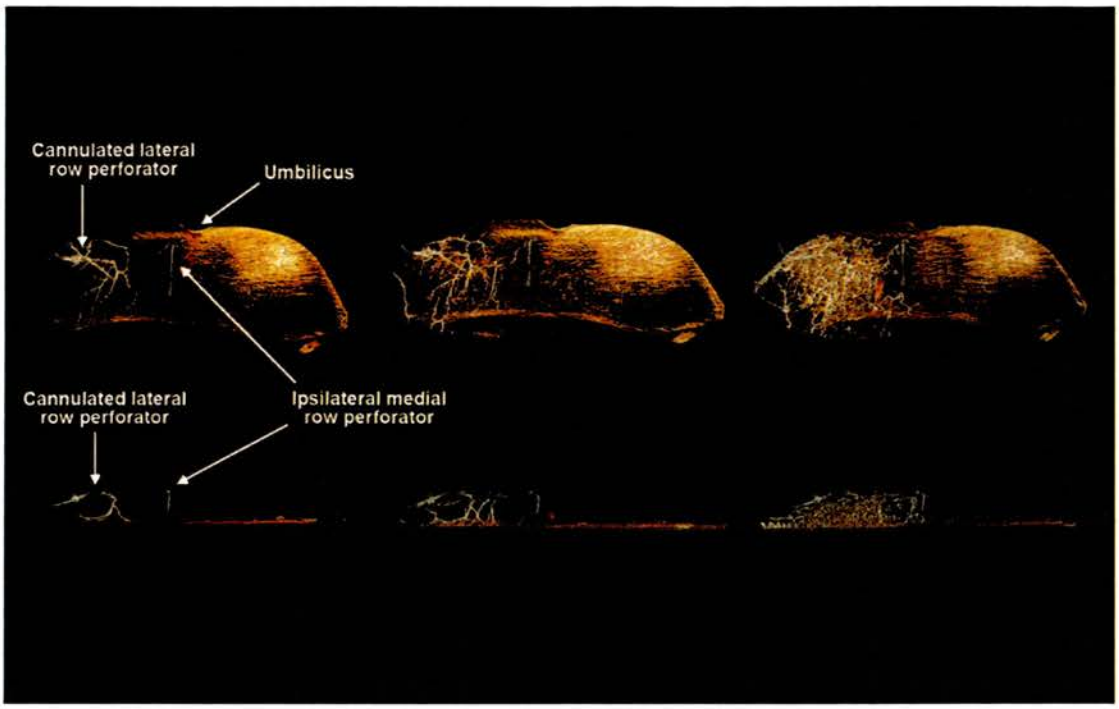

Figure 5.4 Anteroposterior and lateral views of dynamic CTA of a left lateral row perforator. Images are acquired at 0.5ml fill intervals. Predominantly lateral filling can be seen occur at the first interval, with early filling of the ipsilateral medial row perforator via recurrent flow through the subdermal plexus. Only a few branches can be seen to cross the midline, and perfusion of contralateral perforators has not occurred. This pattern was stereotyped for lateral row perforators, irrespective of the injection volume.

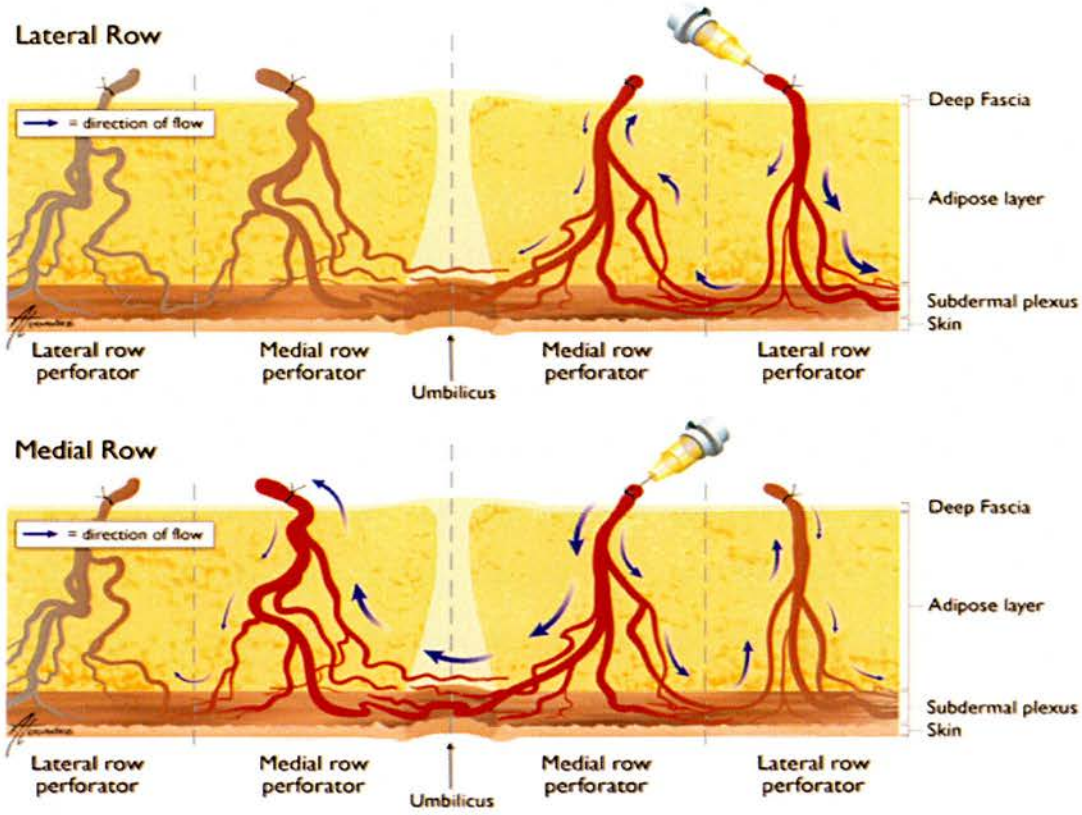

Figure 5.5 Illustration comparing flow within the flap following cannulation and injection of a medial versus lateral row perforator (lateral view). Note that in the lateral row perforator flow predominantly occured laterally, with perfusion not seen to extend beyond the contralateral medial row perforator after passing through the subdermal plexus twice. The medial row perforators were connected across the midline by large diameter linking vessels, with flap perfusion up to the contralateral lateral row perforators.

Dye injection of the abdominoplasty specimen immediately following harvest revealed staining of the zone contralateral to the midline, without staining of zone IV. Later injection of blue dye revealed that the dye did not cross the midline, suggesting that

although cadaveric injection studies are an underestimate of that seen *ex vivo* in fresh specimens, zone IV is not perfused by injection of a lateral row perforator (**Figure 5.6**).

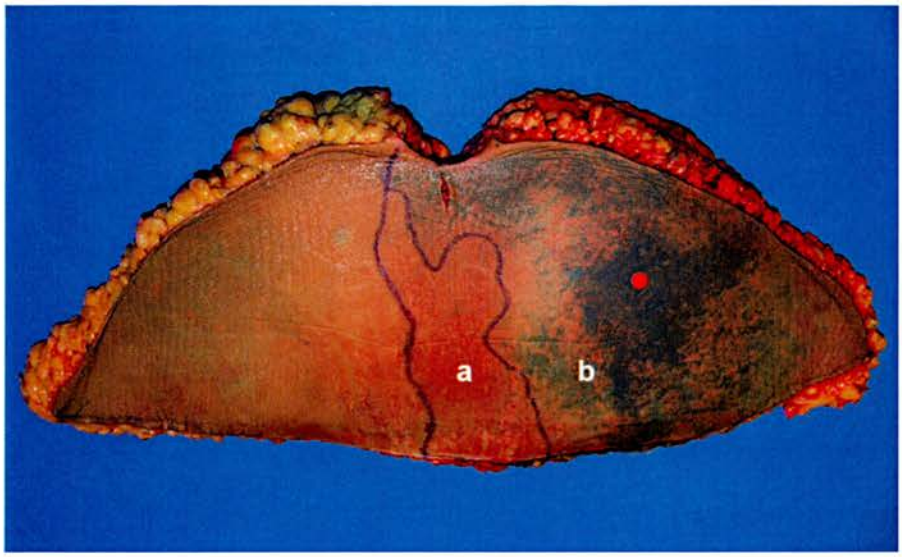

Figure 5.6 The largest lateral row perforator was cannulated immediately following harvest (position marked by red pin) and injection of 20ml red dye was performed within one hour of flap harvest. Once the cutaneous staining pattern was evident the vessels were copiously irrigated with warmed herparinised saline until the effluent was clear. The boundary of the skin staining was marked and the flap was refrigerated at 4°C for 72 hours. Following this the same perforator was injected with methylene blue and the specimen was photographed. Dye injection immediately following harvest revealed staining of the zone contralateral to the midline, without staining of zone IV (a). Later injection of blue dye revealed that the dye did not cross the midline (b), suggesting that although cadaveric injection studies are an underestimate of that seen *ex vivo* in the fresh specimen, zone IV is not perfused by injection of a lateral row perforator.

5.2.4 Superficial inferior epigastric artery

SIEAs were identified and cannulated in eight flaps. Injection of the SIEA revealed a perfusion pattern similar to that seen with a lateral row perforator. Branches coursed to the subdermal plexus, followed by filling of ipsilateral lateral and medial row perforators via recurrent flow through the subdermal plexus (**Figure 5.7**). Perfusion contralateral to the midline was not seen in any of the injection studies.

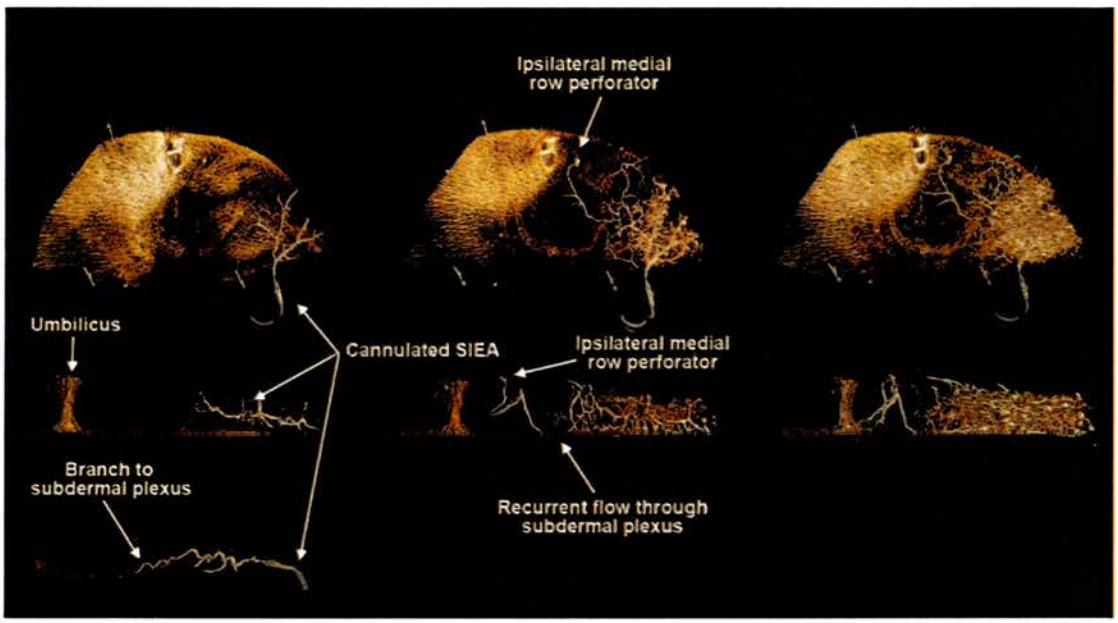

Figure 5.7 Anteroposterior, lateral, and side-on views of dynamic CTA of the right superficial inferior epigastric artery. Images were acquired at 0.5ml fill intervals. Injection of the SIEA revealed that terminal branches coursed to the subdermal plexus, followed by filling of ipsilateral lateral and medial row perforators via recurrent flow through the subdermal plexus. The perfusion pattern was therefore very similar to that seen with a lateral row perforator. Perfusion contralateral to the midline was not seen in any of the injection studies.

5.2.5 Venous system

The superficial and deep venous drainage systems consisted of the superficial and deep inferior epigastric veins, connected by the venae comitantes of the perforators of the DIEA (**Figure 5.8**). Injection of either the venae comitantes or the superficial epigastric veins revealed the same venous filling pattern, with filling of all of the adjacent venae comitantes. Filling of the adjacent superficial epigastric vein across the midline occurred through vessels crossing the midline at the level of the subdermal plexus (**Figures 5.9 and 5.10**). A variety of venous morphological patterns were seen: in one flap no midline crossover was seen, with a linking vein seen coursing cepahalad to the umbilicus; in another flap the linking vein was seen to course cephalad to the umbilicus to connect with the contralateral SIEV (**Figure 5.11**)

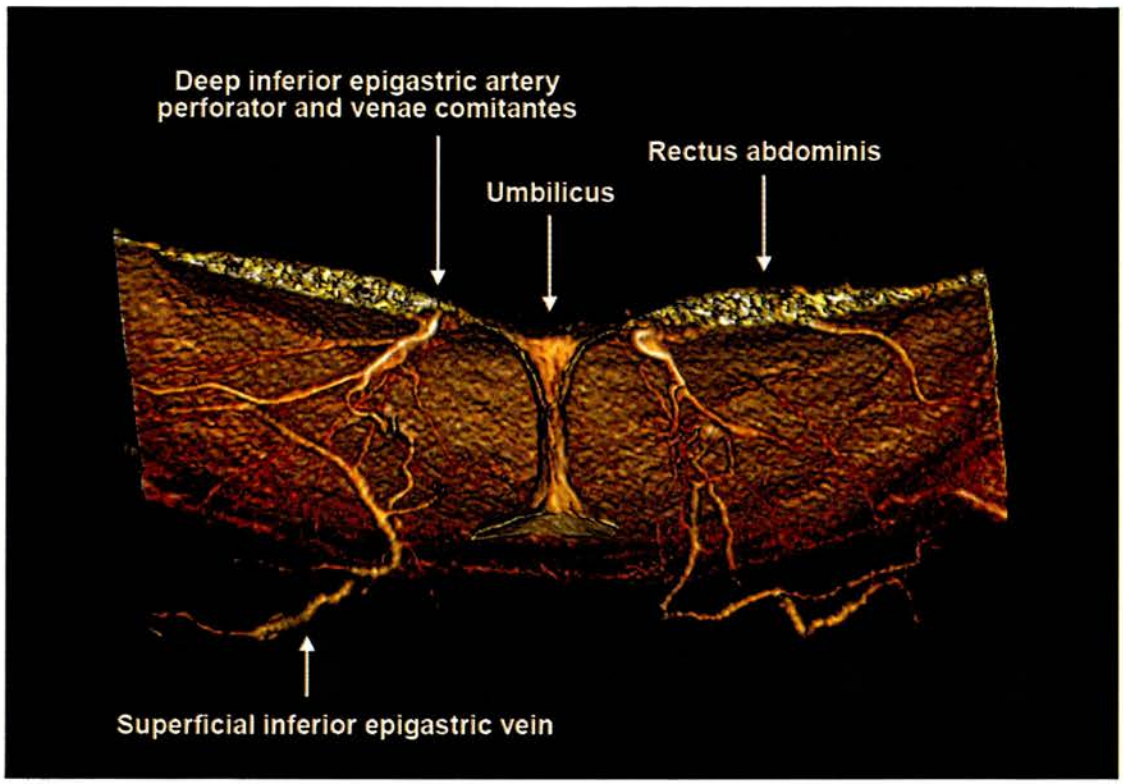

Figure 5.8 *In vivo* CTA demonstrating the relationship between the DIEA paraumbilical perforators and the SIEVs. Note that *in vivo* the SIEVs are larger than the DIEVs, suggesting that they represent the dominant source of venous drainage for the abdomen.

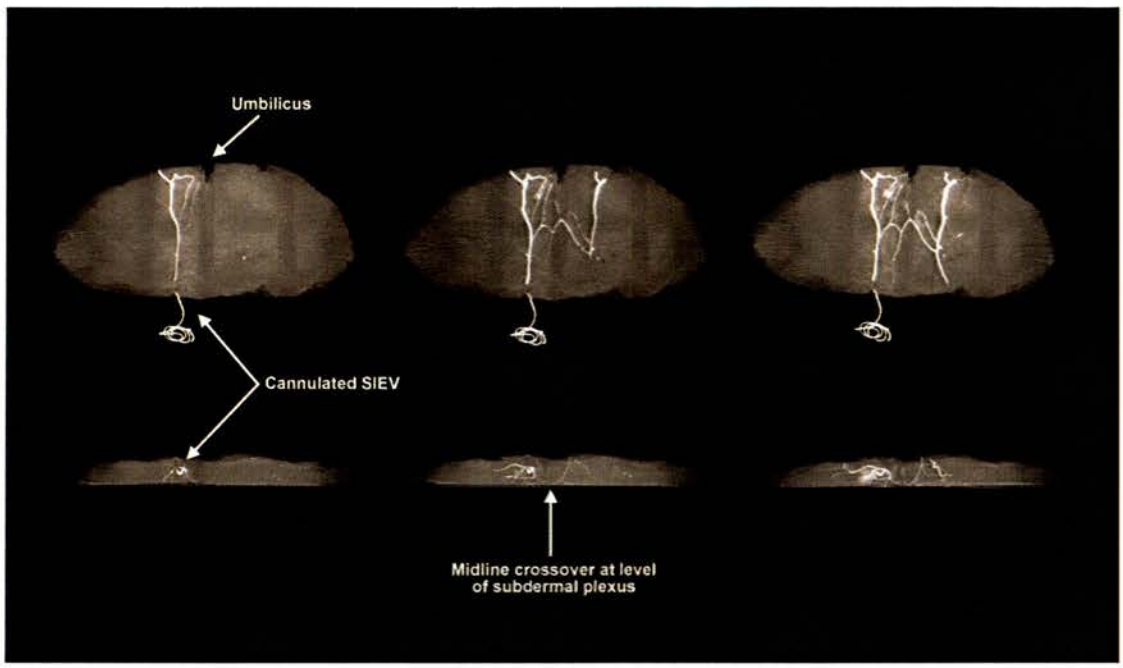

Figure 5.9 Anteroposterior and lateral views of dynamic CTV of the left SIEV. Images are acquired at 1ml fill increments. The superficial and deep venous drainage systems were found to consist of the superficial and deep inferior epigastric veins, connected by the venae comitantes of the perforators of the DIEA. Injection of either the venae comitantes or the superficial epigastric veins revealed the same venous filling pattern, with filling of all of the adjacent venae comitantes. Filling of the adjacent superficial epigastric vein across the midline occurred through vessels crossing the midline at the level of the subdermal plexus, and drainage vessels from the subdermal plexus were seen to return to the SIEVs.

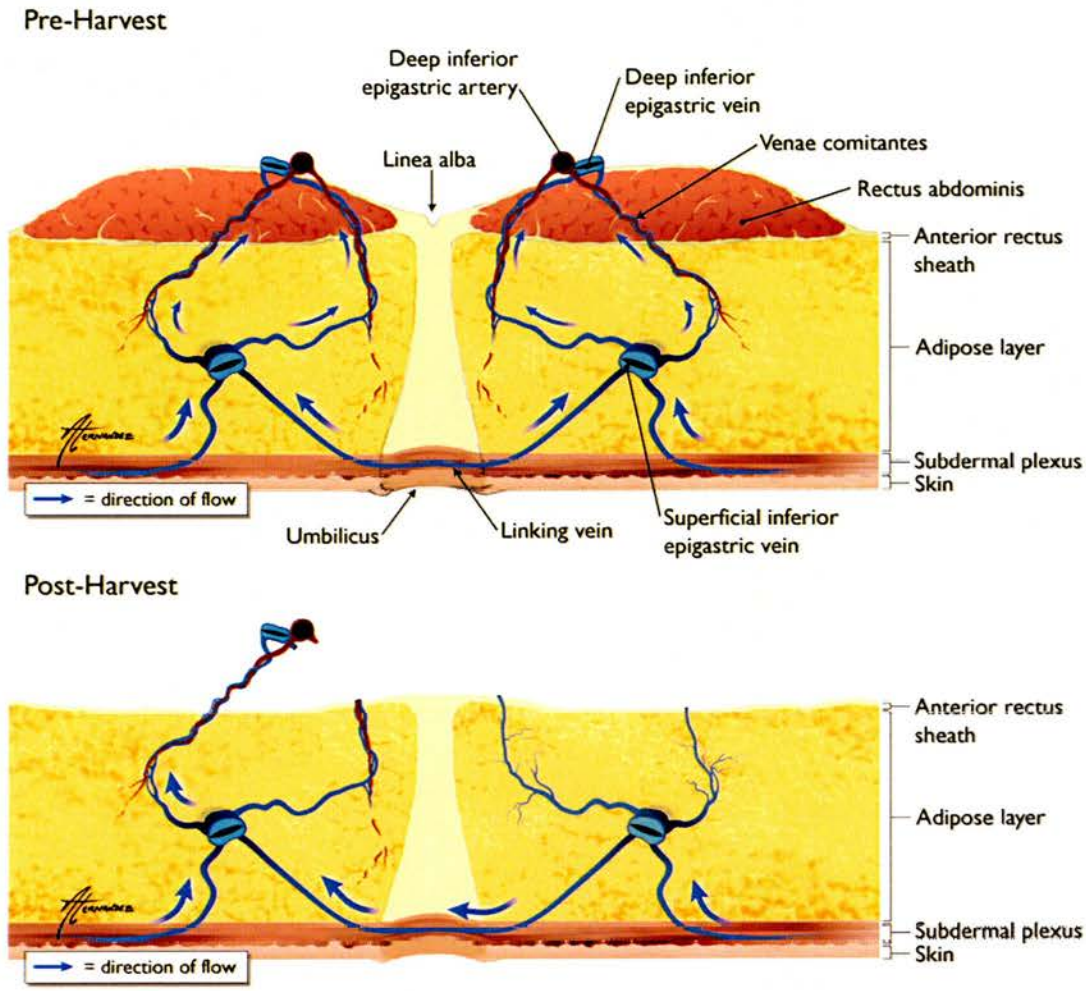

Figure 5.10 Illustrations of flap venous drainage pre- and post- flap harvest. In the normal physiological state venous drainage predominantly occurs via the SIEVs with some contribution through the venae comitantes of the DIEA. Following harvest all venous drainage is diverted into the venae comitantes of a single perforator. Absence of midline linking vessels may therefore lead to diffuse venous congestion.

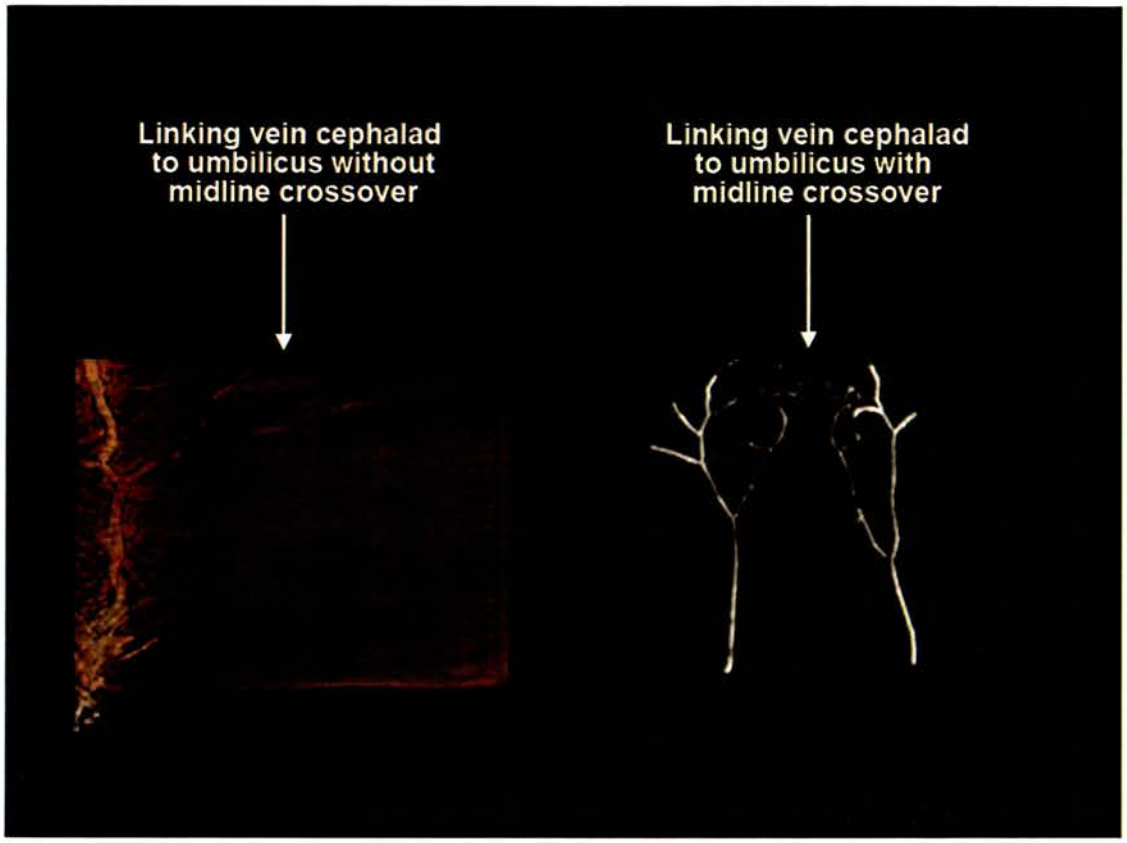

Figure 5.11 Anteroposterior static images of the venous system following cannulation of the left SIEV (by convention) and injection of a barium sulphate/gelatin mixture. A variety of venous morphological patterns were seen: in one flap no midline crossover was seen, with a linking vein seen coursing cepahalad to the umbilicus (*left*); in another flap the linking vein was seen to course cephalad to the umbilicus to connect with the contralateral SIEV *(right)*.

5.2.6 Histology

Histology revealed no significant differences in vessel diameter or smooth muscle wall thickness for perforators from the medial or lateral row (**Figure 5.12**). The largest perforators were found in the paraumbilical region.

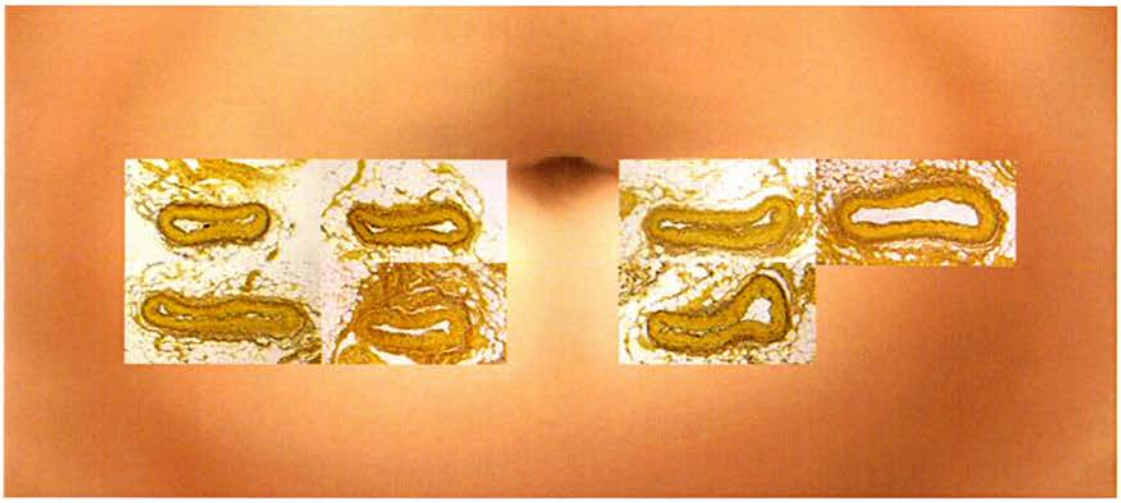

Figure 5.12 Hart's elastin histology of cross-section of all of the DIEA perforators ≥ 0.5mm in diameter from a single flap. Note that there are no significant differences in vessel diameter or smooth muscle wall thickness for perforators from the medial or lateral row. In general the largest perforators were found in the paraumbilical region.

5.2.7 Perforator mapping

All perforators were found within a 10cm radius of the umbilicus (**Figure 5.13**). There were a mean of 5.3 perforators (range 2 to 8) perforators ≥ 0.5mm in diameter per specimen.

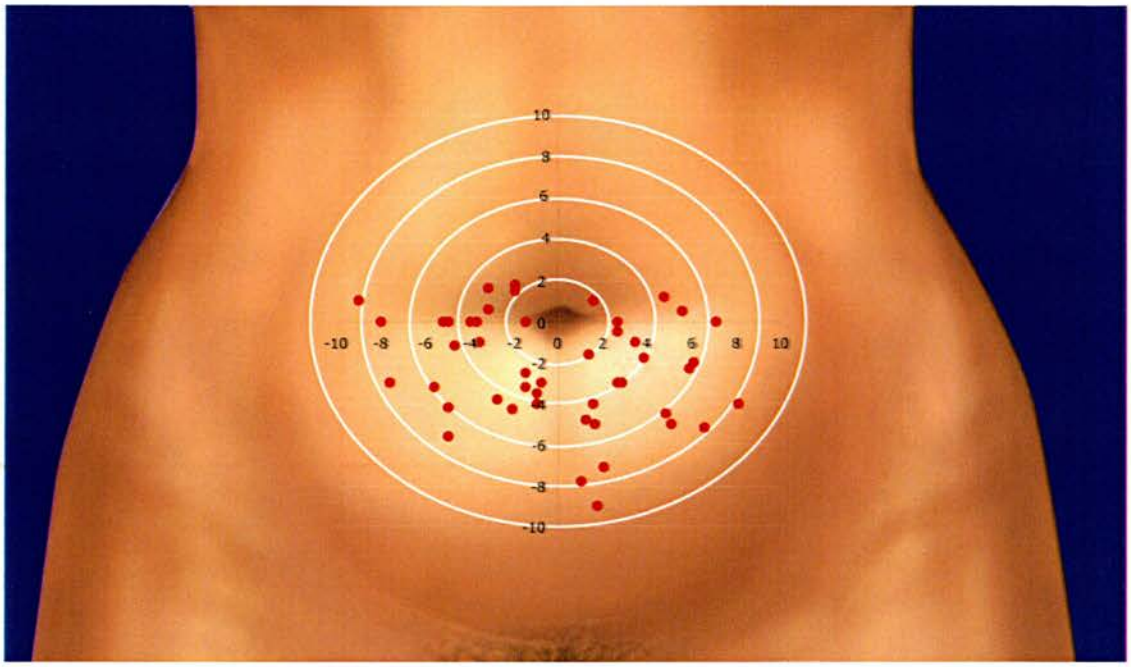

Figure 5.13 Illustration of the location of all of the perforators ≥ 0.5mm in diameter originating from the DIEA in ten flaps. All perforators were found within a 10cm radius of the umbilicus, and a mean of 5.3 perforators (range 2 to 8) perforators were found per specimen.

5.3 SUMMARY

5.3.1 Deep inferior epigastric artery perforator flap

This study found stereotyped patterns of perfusion following injection of medial or lateral row perforators. Injection of a medial row perforator revealed consistent perfusion of the ipsilateral territory as well as of the zone contralateral to the midline, whereas injection of a lateral row perforator revealed predominantly ipsilateral perfusion. This was due to large diameter linking vessels across the midline between the medial row perforators, whereas perfusion of lateral row perforators was mainly seen to occur

laterally. The predominantly lateral orientation of the lateral row perforators, forming choke vessel anastomoses between the lower four posterior intercostal arteries, has been noted by previous authors (Moon and Taylor, 1988). Dye injection studies revealed the stereotyped pattern of perfusion of the perforators dependent on location within the flap to remain regardless of the volume injected, suggesting that the limit of perfusion is when flow has to pass through the subdermal plexus more that twice, which has been shown in experimental models of skin flap perfusion (Morris and Taylor, 1993). Although a suprafascial plexus exists, as well as a variety of connections within the subcutaneous layer, flap perfusion mainly occured at the level of the subdermal plexus. Midline crossover occured predominantly at the level of the subdermal plexus. Of note in zone IV perfusion appeared to be absent deep to Scarpa's fascia even if a medial row perforator was used, and therefore may be the predominant site of fat necrosis, a finding that has been noted by other authors (Moon and Taylor, 1988). The different perfusion patterns depending on whether a medial or lateral row perforator is used may explain the different patterns of perfusion of the lower transverse abdominal flap raised on the deep inferior epigastric arteries seen in different studies. The consistent perfusion of the flap zone contralateral to the midline with branches extending to zone IV in the cadaveric flap, as well as dye staining of zone IV in the abdominoplasty specimen immediately following harvest, support the observations of Blondeel that the use of a medial row perforator is imperative if inclusion of zone IV is desired (Gill *et al.*, 2004). These observations may also explain conflicting reports in the literature regarding the reliability of zone IV in the DIEAP flap (Cheng *et al.*, 2006; Blondeel *et al.*, 2000).

This study confirms the findings of the study by Blondeel *et al.* (2000) on the venous system of the DIEAP flap. In the normal physiological state the SIEVs are the main source of venous drainage for the lower abdomen (Carramenha e Costa *et al.*, 1987;

Imanishi *et al.*, 2003), and this can clearly be seen using *in vivo* CTA for DIEAP flap presurgical imaging. The deep venous system also has anastomoses in the middle third of the rectus muscles, just above the umbilicus. When a DIEAP flap is harvested, venous drainage across the midline occurs through direct communicating veins between the SIEVs, and then through the venae comitantes of the perforator. A TRAM flap has multiple deep venous drainage points through the venae comitantes of several perforators, and this may explain why venous congestion is seen less frequently in the clinical setting. Blondeel *et al.* (2000) found no venous branches crossing the midline in 36 percent of transverse lower abdominal flap specimens. This study found no venous branching across the midline in one specimen, with the trajectory suggesting that it would cross the midline cephalad to the umbilicus. Although this observation may explain diffuse venous congestion seen clinically, these anatomical studies suggest that it should occur with greater frequency than is seen clinically. In one specimen venous branches were found to course cephalad to the umbilicus before connecting with the contralateral SIEV, suggesting that incorporation of tissue cephalad to the umbilicus in the flap would increase the chances of preserving these vessels.

Histologically we could find no differences between medial and lateral row perforators, with similar diameters and thickness of the tunica media, although the largest flap perforators were generally found in the paraumbilical area, as has been reported by other authors (Boyd *et al.*, 1984; Moon and Taylor, 1988; Heitmann *et al.*, 2000; El Mrakby and Milner, 2002; Munhoz *et al.*, 2004).

This study has also confirmed for the first time that injection studies in cadaveric specimens are an underestimate of that seen *ex vivo* in fresh specimens. This may be due to collapse of the precapillary smooth muscle sphincter cells in the cadaveric specimen (Braverman, personal communication October 2006; Braverman, 2000, 1996, and 1989).

Despite this underestimate, injection of a lateral row perforator was still found to be unable to perfuse zone IV of the flap.

5.3.2 Superficial inferior epigastric artery flap

Injection of the SIEA demonstrated that flow up to the abdominal midline was mediated through communications with the perforators of the DIEA via recurrent flow through the subdermal plexus. Due to the lateral position of the vessels within the flap, the flow pattern resembled that of a lateral row perforator, and perfusion contralateral to the midline was not seen in any specimens. This experimental data supports clinical observations that flap necrosis may be seen if the flap is extended across the midline. Venous drainage was via the ipsilateral SIEV.

Chapter 6

DISCUSSION

6.1 Background

Perforator flaps represent a paradigm shift in how flaps may be designed and much more research is required not only to determine the vascular territories of individual perforator flaps but also to understand the vascular systems within the specific circulatory region. The perforator flap concept, introduced by Kroll and Rosenfield in 1988, developed from a realization that the underlying muscle is a passive carrier that is not essential for flap survival, enabling preservation of form and function at the donor site. The merits and reliability of these flaps for extremity, head and neck, breast, abdominal and trunk reconstruction have been well described. Their popularity is in large part due to their ability to reliably support a large skin territory on a single perforator. The pedicle is also longer than is achievable with the parent musculocutaneous flap and is unconstrained by orientation. Perforator flaps can be tailored to reconstruct a wide spectrum of deficits, from the resurfacing of shallow defects without the bulk associated with musculocutaneous flaps, to the harvest of several different tissue components based on individual perforators from a single source artery. The arterial and venous anatomies and physiology of perforator flaps, however, is poorly understood, particularly regarding the ability of a single perforator to support a relatively large adipocutaneous vascular territory.

The majority of anatomical vascular studies of surgical flaps in the past have utilized lead oxide injections followed by 2D radiography to analyse the vascular

anatomies (Bergeron *et al.*, 2006). Although this methodology provides excellent images, there are many limitations of 2D appraisal of 3D anatomy. Nakajima *et al.* (1998) realized that the future development of perforator flaps hinged on our ability to better understand the vascular anatomy superficial to the deep fascia, and in response to this 3D computer graphical representation of 2D lead oxide radiographs was performed. This enabled classification of the components of the vascular plexus of each source artery in 3D, resulting in the development of new flaps.

3D and 4D radiography have distinct advantages over traditional 2D radiographic techniques, enabling a more detailed evaluation of surgical flap vascular anatomy. Qualitative data on vascular anatomy is obtained, as well as information on the direction and location of blood flow within each layer of a flap. The use of CT eliminates the superimposition of images of structures outside the area of interest, has an inherently high-contrast resolution, and images acquired can be viewed in 3D. The image can also be processed using various volume-rendering functions, with the ability to select and hide desired regions of the image, enabling detailed evaluation of the region of interest in 3D. The high spatial contrast of CT enables detailed evaluation of the 3D relationship of vessels with respect to each other and the soft tissues. The use of CT also enables images of high contrast resolution to be obtained following intravascular injection of barium sulphate, rather than lead oxide, due to the hardening artefacts seen when lead oxide was used. The use of barium sulphate also avoids the hazards to researchers that are encountered when preparing lead-based solutions.

In particular 4D CTA and CTV, which are possible due to the ability of MDCT to perform high-speed scans of anatomy (Wolbarst, 2004), have enabled evaluation of the dynamic filling patterns of the perforator superficial to the deep fascia including the subdermal plexus, the angiosome of the perforator, and the recruitment of adjacent

angiosomes in 3D. The venous drainage can also be evaluated dynamically using this method. The contrast agent flows through the vena comitans in the direction of the valves, enabling accurate appreciation of the venous territory of the flap. This may have important implications in the design of certain perforator flaps, where inadequate venous drainage and subsequent flap venous congestion may occur clinically. This methodology also enables this process to be evaluated for the simultaneous or sequential investigation of adjacent vascular territories. Unlike mixtures based on heavy metal compounds (lead oxide; barium sulphate), iodinated contrast medium can be washed out of the vasculature, to enable multiple investigations of each perforator within the flap. Iodinated CT contrast medium also has a viscosity comparable to that of blood and therefore detailed imaging at the level of subdermal plexus can be obtained, which is not achievable with conventional lead-oxide radiology (Imanishi *et al.*, 2000). Static 3D and dynamic 4D CTA and CTV, therefore, may become important tools for the investigation of the vascular anatomies of surgical flaps.

To date, no studies have examined the 3D and 4D arterial and venous anatomies of the commonly used perforator flaps, such as the LCFAP-*vl*, TAP and DIEAP flaps. This study described the methodology and results of the use of volume-rendered 3D and 4D CTA and CTV to evaluate the arterial and venous anatomies of the anatomical regions of these workhorse perforator flaps.

6.2 Summary

These studies have demonstrated for the first time the vast potential of these novel 3D and 4D imaging modalities for the investigation of microvascular anatomy and perfusion of surgical flaps. Refinement of perforator flap harvest has hinged on our

ability to better understand the vascular anatomy superficial to the deep fascia, and this technique has enabled this to be accomplished.

Limitations of the studies in cavaveric flaps are well known, and this is the first study to demonstrate that experiments in cadaveric flaps result in an inherent underappreciation of the vascular territory seen *ex vivo* in fresh specimens. The factors behind this were not explored in detail in this study, but may relate to the state of the contractile cells surrounding the vessel walls in the microvasculature. The cutaneous microvasculature is known to be organized into upper and lower horizontal plexuses, and sphincter-like smooth muscle cells occur at the point where the ascending arterioles divide to form the arteriolar component of the upper horizontal plexus (Braverman, 1989, 1997 and 2000; Braverman and Sibley, 1990). In cadaveric flaps it is hypothesized that the smooth muscle cells may be collapsed, narrowing the flow into the capillary beds, and therefore increasing the vascular resistance and reducing the vascularity territory that would be perfused by injection of the source artery (Braverman, personal communication October 2006).

The most significant finding was the dynamic visualization of the phenomenon of recurrent flow through the subdermal plexus for the first time. This appears to be a major mechanism for perfusion of the integument in general. Harvest of an adipofascial flap prevented recurrent flow, demonstrating the pivotal role of the subdermal plexus in mediating the phenomenon. This has clinical relevanace to flap deepithelialisation, commonly performed for parts of flaps and breast reduction pedicles that are subcutaneous, where the subdermal plexus layer needs to be meticulously preserved in order not to affect flap perfusion.

6.2.1 Anterolateral thigh perforator (LCFAP-*vl*) flap

For the LCFAP-*vl* flap this study has found that large diameter linking vessels at the suprafascial level enabled perfusion of adjacent vascular territories, as well as perfusion of the subdermal plexus between angiotomes. A reduction in vascular territory occurred in the LCFAP-*vl* flap following thinning and was due to ligation of vessels within the suprafascial plexus that were associated with the lateral femoral cutaneous nerve along the axis of the falp between the ASIS and superolateral aspect of the patella. Flap thinning may be performed under magnification with preservation of these large diameter linking vessels where a large flap is required, or the flap can be thinned secondarily. Three distinct perforator complex patterns were found with direct consequences for the effect of thinning on the flap, and the more significant the component at the suprafascial plexus, which can be visualized directly during thinning, the greater the reduction in potential flap vascular territory as a result of thinning.

There was a superficial venous system, arranged in a polygonal pattern on the subdermal plexus, which perfused the venae commitantes of the descending branch of the lateral femoral circumflex artery, as well as the long saphenous vein. Venous drainage occurred medially, and therefore flap extension should be lateral with respect to the entry point of the perforator to minimize the risk of venous complications. Where a very large flap is required, it seems that inclusion of the long saphenous vein by additional microvascular anatomosis may aid in venous superdrainage of the flap where venous drainage becomes compromised. Inclusion of the long saphenous vein in normal flap harvest would result in unnecessary morbidity.

6.2.2 Thoracodorsal artery perforator (TAP) flap

In the TAP flap a very large vascular territory and inherent thinness of the flap were found. The large potential flap vascular territory was due to large diameter anastomotic connections between the thoracodorsal and dorsal intercostal angiosomes found superficial to the superficial fascia. Preservation of this fascia with the flap harvest whilst excising the deep adipose layer did not change the flap vascular territory. The flap was found to have a mean thickness of 1.3cm (compared with the mean thickness of the LCFAP-*vl* flap which was found to be 2.0cm), and thinning between the superficial and deep adipose layers was found to safely reduce the mean thickness by a further 27 percent. This finding may have wider clinical application, supporting the need to preserve the superficial fascia with the skin flaps when raising an extended latissimus dorsi flap. Failure to do so may lead to skin flap necrosis at the donor site.

Venous drainage occurred inferomedially towards the midline, and superolaterally towards the axilla, and therefore the axiality of both the arterial and venous systems suggested that the skin paddle should be orientated obliquely in an inferomedial direction about the perforator. This may explain the high rates of flap complications seen in a series where a vertical skin paddle was harvested (Schwabegger *et al.*, 2002).

Two distinct perforator complex types were found and differed in the presence or absence of branches at the suprafascial level. These branches can easily be identified directly under magnification and avoided when performing flap thinning. If this is not possible then a radius of at least 4.1cm should be preserved about the perforator to avoid injury to these vessels.

Perforators from the descending branch of the thoracodorsal artery were found in reliable locations. A perforator with an internal diameter of 0.5mm or more originated from the descending branch of the thoracodorsal artery in all 25 specimens and a mean of

3.6 musculocutaneous perforators were found per flap. In all flaps the most proximal perforator was the largest from the descending branch, with the thickest smooth muscle wall. This perforator was found within 3cm of the lateral edge of the latissimus muscle from 6.6 to 15.4cm caudal to the posterior axillary fold. All flaps studied had a perforator >0.5mm, which is of sufficient caliber to support a flap, within a 5.9 x 4.3cm area located between 9.5 and 15.4cm from the posterior axillary fold within 4.3cm of the lateral border of the latissimus muscle. Inclusion of this segment of the muscle with flap, with preservation of the motor nerve, would therefore allow flap harvest without potential damage to the perforators during intramuscular dissection (Hamdi *et al.*, 2004 and 2006). It should be noted that the distance between the anterior edge of the muscle and the descending branch increases with increasing distance from the neurovascular hilus. This can be confirmed intraoperatively by using an intraoperative Doppler on the surface of the muscle, or by direct inspection of the underside of the flap where a septum is often visualised. When used as a pedicled flap for reconstruction of defects of the breast, chest, neck, or upper arm, two pivot points exist: one pivot point at the muscle-skin paddle juncture and the second located at the bifurcation point. This allows greater degrees of freedom than is achievable with the parent musculocutaneous flap, and allows the flap to reach the anterior midline.

6.2.3 Deep inferior epigastric artery perforator (DIEAP) and superficial inferior epigastric artery (SIEA) flaps

Regarding the DIEAP flap, differences in perfusion patterns for medial and lateral row perforators were seen, with flow through medial and lateral row perforators occurring in physiologically stereotyped patterns. Zone IV was not perfused following

injection of a lateral row perforator, whereas injection of a medial row perforator consistently resulted in perfusion of zone IV. Image analysis revealed the presence of large diameter linking vessels at the level of the subdermal plexus between the perforators of the medial row, whereas lateral row perforators predominantly perfused the lateral aspect of the flap and perfused the medial row perforators via recurrent flow through the subdermal plexus. Injection of a medial row perforator perfused the flap in a central elliptical pattern, with declining perfusion at the edges, whereas injection of a lateral row perforator predominantly perfused the ipsilateral portion of flap. The different stereotyped perfusion patterns between medial and lateral row perforators may explain the differing pattern of perfusion reported clinically, and support the selection of a medial row perforator when a large flap is required (Gill *et al.*, 2004). The findings were due to large diameter linking vessels across the midline between the medial row perforators, whereas perfusion of lateral row perforators was mainly seen to occur laterally. The limit of perfusion appeared to be when contrast flow had to pass through the subdermal plexus more that twice, which has been shown in experimental models of skin flap perfusion (Morris and Taylor, 1993). Perfusion of zone IV deep to Scarpa's fascia was not seen even if a medial row perforator was used, and therefore this may be a predominant site of fat necrosis seen clinically, a finding that has been suggested by other authors (Moon and Taylor, 1988). The different perfusion patterns depending on whether a medial or lateral row perforator is used may explain the different patterns of perfusion of the lower transverse abdominal flap raised on the deep inferior epigastric arteries seen in different studies and conflicting reports in the literature regarding the reliability of zone IV in the DIEAP flap (Cheng *et al.*, 2006; Blondeel *et al.*, 2000). Histologically no differences were found between medial and lateral row perforators, with similar diameters and thickness of the tunica media, although the largest flap perforators were generally found

in the paraumbilical area, as has been reported by other authors (Boyd *et al.*, 1984; Moon and Taylor, 1988; Heitmann *et al.*, 2000; El Mrakby and Milner, 2002; Munhoz *et al.*, 2004). The SIEA vessel branches were seen to course to the subdermal plexus, and then to perfuse ipsilateral perforators through the subdermal plexus in a similar pattern to that visualized for a lateral row perforator. No midline crossover was seen in any of the SIEA flap studies, providing experimental evidence to confirm clinical observations that the SIEA does not provide reliable perfusion across the midline.

Venous drainage occurred via the SIEVs and the venae comitantes of the perforators, and valveless branches across the midline were seen to connect the SIEVs. This study confirms the findings of the study by Blondeel *et al.* (2000) on the venous system of the DIEAP flap, whereby no venous branches crossing the midline was seen in one specimen. In another the linking branches were seen cephalad to the umbilicus, supporting the inclusion of a cuff of tissue cepahlad to the umbilicus during flap harvest. Although this observation may explain diffuse venous congestion seen clinically, it would suggest that it should occur with greater frequency than is seen clinically. It is therefore theorized that arteriovenous blood flow must occur through shunts to allow venous drainage of the flap contralateral to the midline. It was also noted that the venous connections of the venae comitantes of the perforators varied in their caliber. It is possible that when single perfortaor DIEAP flaps are raised, in some instances the venae comitantes provide insufficient venous outflow, and hence a second anastomosis to the SIEV has been shown to be beneficial in this clinical scenario. This would also support the finding of venous congestion seen less frequently in the clinical setting where a TRAM flap has been harvested, where there are multiple venous drainage points through the venae comitantes of several perforators (Blondeel *et al.*, 2000).

6.3 Discussion

The new techniques presented for the first time in this thesis may help expand our knowledge of the vascular anatomy and perfusion of the integument in general. The perfusion within the regions studied in this thesis was dependent upon the vascularity at the level of the suprafascial plexus, and via recurrent flow through the subdermal plexus. For example in the LCFAP-*vl* flap the large diameter linking vessels occurred at the suprafascial level where the fascia is thick and well developed. This deep fascial layer provides stability and protection for these vessels, and may be the reason for their development. By contrast in the TAP flap region the deep fascia is very thin, and the suprafascial plexus is virtually absent. The vascular territory in this region is large with large diameter vessels coursing to the subdermal plexus, enabling perfusion of large flaps via recurrent flow. It may be hypothesised that regions where the deep fascia are thicker may have greater reliance on perfusion through the suprafascial plexus and reduced tolerance to flap thinning, for example in the lower limb. Studies of other vascular regions may demonstrate whether this finding can be generalised.

This thesis has imaged recurrent flow for the first time, and has also demonstrated that the subdermal plexus is essential for this phenomenon. Interestingly the large diameter linking vessels seen in the anterolateral thigh were seen to fill via recurrent flow, and then to provide branches to the subdermal plexus to perfuse the regions between adjacent vascular territories, increasing our understanding of the vascular anatomy of the integument in general. The finding of recurrent flow in all regions explored suggest that it is a dominant mechanism of perfusion of the integument, and studies of other vascular regions may further our understanding of this phenomenon and its application in flap harvest.

Although not the focus of this thesis, in addition the methods used in this study can provide high contrast resolution 3D images of the vascular anatomy of perforators and their source arteries in gross specimens (**Figures 1.5 to 1.8**), enabling new perforator flaps options to be explored. The technique of displaying the integument over a radiolucent cast to allow high contrast resolution imaging of the vascular anatomy in its accurate 3D anatomical position avoids the conceptual limitations of representation of the integument in 2D, and allows the perforator complexes to be evaluated *in situ* (**Figure 1.9**). This is a vast improvement over current methods of representation of the 3D integument in a 2D sheet, which does not easily allow appreciation of the anatomy in 3D.

The novel dynamic imaging modality described in this thesis has allowed closer modeling of *in vivo* physiology than has been achievable previously, with the viscosity of the warmed contrast agent similar to that of blood. The precision pump, however, typically injected contrast at a rate of 0.5ml/min. Experimental studies using *ex vivo* flaps have found that the flow rate required to achieve a stable baseline perfusion pressure (approximately 50 mmHg) is approximately 2ml/min (Black *et al.*, 2001; Kreidstein *et al.*, 1991). The low injection rates allowed dynamic appreciation of the early perforator complex filling, and therefore the branching pattern and pattern of perfusion within each vascular territory to be evaluated, without causing flow through the venous system, which was found to obscure the images and limit interpretation. Careful image scrutiny confirmed that venous filling was not seen in any of the studies using the lower injection rates. The dynamic 3D imaging method employed in this study, however, more closely models *in vivo* effects than has been achievable previously with contrast studies.

The limitations of this study are those of any anatomical study in cadaveric specimens. The main weakness of this study relates to the experimental design using cadaveric flaps, and the vascular territories are likely to be an underestimate of that which

occurs *in vivo*. This has been suggested in the DIEAP flap study, where dye injection of the abdominoplasty specimen immediately following harvest revealed staining of the zone contralateral to the midline, without staining of zone IV, whereas later injection of dye revealed that the vascular territory perfused did not cross the midline.

Irrigation of the flap with warmed normal saline to remove the contrast between scans was shown not to cause opening of linking vessels, and therefore this is unlikely to be a source of study error. Repeated scanning sequences followed by large volume washouts were performed in control flaps followed by vascular territory measurement using the CT workstation prior to the start of the study, and revealed that the area of the vascular territory was unchanged following repeated washouts, and that the diameter of the large linking vessels remained unchanged. This indicated that the vessel walls were elastic, and that vasodilatory mechanisms seen *in vivo* did not occur in the cadaveric flaps, as expected.

6.4 Future directions

The cadaveric flap model used in this study has provided closer modeling of *in vivo* flap perfusion than has been achievable previously using an experimental setup for the cadaveric specimen. Closer *in vivo* modeling may be achieved by steady-state injection rates in *ex vivo* fresh specimens and would be a valuable future area of study. This would optimally use human tissue discarded from theatre whilst the cells in the specimen are still alive. The ideal specimen, as was used in this study, is the abdominoplasty specimen as a model for the DIEAP flap. Unfortunately none of the other workhorse flaps lie in flap regions routinely discarded during excision surgery. An experimental set up devised by Kreidstein *et al.* (1991) used the excised abdominoplasty specimen cannulated within 3 hours of harvest and perfused using a gassed 37°C Krebs-

Henseleit buffer containing albumin. The study showed that the specimen could remain perfused for a four-hour period whilst remaining metabolically active with functionally intact endothelium. The flow rate required to achieve a stable baseline perfusion pressure (approximately 50 mmHg) was found to be approximately 2ml/min. Such a model would allow better *in vivo* modeling for the DIEAP flap, in particular with regards to perfusion of zone IV of the flap and venous drainage across the midline. Limitations of such a study are the time limitations on collection and cannulation of the specimen, as well as cost and availability of the equipment.

In vivo angiography would allow the most accurate appraisal of the perfusion of perforator flaps. The studies within this thesis have confirmed the individual patterns of perfusion within the same vascular regions, and suggest that individual scans in theatre would allow harvest of the flap according to the vascular anatomy of the individual, the ultimate goal of flap vascular imaging. Ohjimi *et al.* (2005) have performed a series of experiments using 2D radiography on TRAM flaps immediately following harvest and have demonstrated the success of such techniques without adverse affects on the flap. Using CTA would increase the amount of useful information obtained from such experiments and would allow experimentation in any flap harvested. Limitations of such a study would include concerns regarding potential damage to the microvascularity of the pedicle vessel from the cannulation or CT contrast medium, possibly increasing the risk of flap failure. The venous system could not be evaluated by cannulation of the pedicle vein due to presence of valves, although flow through the arterial system and into the venous system may allow appreciation of the venous drainage of such flaps. Such studies would be very valuable, however, as the pedicle is cannulated, as opposed to generalized perfusion studies achieved by CTA and magnetic resonance angiography (MRA) presurgical imaging.

CTA and MRA presurgical imaging are undoubtedly becoming the standard of care for DIEAP flap harvest in order to evaluate the specific donor site anatomy, reduce the operation length, and decrease the risk complications due to adverse anatomy. These modalities have been described for DIEAP, TAP, and LCFA-vl flap presurgical imaging (Smit *et al.*, 2009; Rozen *et al.*, 2008a and b; Neil-Dwyer *et al.*, 2008; Mun *et al.*, 2008; Ribuffo *et al.*, 2009) and have proven valuable at evaluating the course and caliber of the perforator and pedicle, allowing greater preoperative planning. For the DIEAP flap these modalities can also evaluate the venous system, which may allow perforator selection based on adequate venous outflow as well as adequate inflow. Both techniques will benefit from the continually increasing contrast resolutions of both technologies, and there is a very real chance that the microvascular anatomy of flaps may be able to be evaluated using these techniques. The major limitation will still remain that the flap cannot be evaluated isolated on the flap pedicle, even if angiography is performed directly into the vessel of interest.

6.5 Conclusions

The 3D and 4D CTA and CTV imaging methods described within this thesis have resulted in a much greater understanding of the vascular anatomy and perfusion of the workhorse perforator flaps, including the LCFAP-*vl*, TAP, and DIEAP flaps, as well as the SIEA flap, than has been achievable previously. Limitations of vascular perfusion studies in cadaveric flaps are well known, and validation *in vivo* is required. The new techniques presented for the first time in this thesis allow detailed evaluation of the microvascular anatomy of perforator flaps in 3D, as well as of the skin in general, overcoming the conceptual limitations of 2D radiography. This will better our understanding of the vascular anatomy and perfusion of surgical flaps and the

integument, as well as improving our knowledge of vascular anatomy in general, and may aid in the design of new flaps.

Chapter 7

REFERENCES

Adams, W. P. Jr, Lipschitz, A. H., Ansari, M., Kenkel, J. M., Rohrich, R. J. (2004). Functional donor site morbidity following latissimus dorsi muscle flap transfer. *Ann. Plast. Surg.* 53: 6-11.

Adani, R., Tarallo, L., Marcoccio, I., Cipriani, R., Gelati, C., and Innocenti, M. (2005). Hand reconstruction using the thin anterolateral thigh flap. *Plast. Reconstr. Surg.* 116: 467-7.

Alkureishi, L. W., Shaw-Dunn, J., and Ross, G. L. (2003). Effects of thinning the anterolateral thigh flap on the blood supply to the skin. *Br. J. Plast. Surg.* 56: 401-8.

Allen, R. J., and Treece, P. (1994). Deep inferior epigastric perforator flap for breast reconstruction. *Ann. Plast. Surg.* 32: 32-8.

Alonso-Burgos, A., García-Tutor, E., Bastarrika, G., Cano, D., Martínez-Cuesta, A., and Pina, L. J. (2006). Preoperative planning of deep inferior epigastric artery perforator flap reconstruction with multislice-CT angiography: imaging findings and initial experience. *J. Plast. Reconst. Aesthet. Surg.* 59: 585-93.

Alvarez-Linera, J., Benito-León, J., Escribano, J., Campollo, J., and Gesto, R. (2003). Prospective evaluation of carotid artery stenosis: elliptic centric contrast enhanced MR angiography and spiral CT angiography compared with digital subtraction angiography. *American Jouranl of Neuroradiology*. 24: 1012-1019.

Angrigiani, C., Grilli, D., and Siebert, J. (1995). Latissimus dorsi musculocutaneous flap without muscle. *Plast. Reconstr. Surg*. 96: 1608-14.

Apffelstaedt, J. (2002). Indications and complications of latissimus dorsi myocutaneous flaps in oncologic breast surgery. *World. J. Surg*. 26: 1088-93.

Banbury, J., Siemionow, M., Porvasnik, S., Petras, S., and Zins, J. E. (1999) Muscle flaps' triphasic microcirculatory response to sympathectomy and denervation. *Plast. Reconstr. Surg*. 104: 730-7.

Barclay, T. L., Cardoso, E., Sharpe, D. T., and Crockett, D. J. (1982). Repair of lower leg injuries with fascio-cutaneous flaps. *Br. J. Plast. Surg*. 35: 127-32.

Bartlett, S. P., May, J. W. Jr., and Yaremchuk, M. J. (1981). The latissimus dorsi muscle: a fresh cadaver study of the primary neurovascular pedicle. *Plast. Reconstr. Surg*. 67: 631-6.

Barton, F. E., Spicer, T. E., and Byrd, H. S. (1983). Head and neck reconstruction with the latissimus dorsi myocutaneous flap. Anatomic observations and report of 60 cases. *Plast. Reconstr. Surg*. 71: 199–204.

Behan, F. C., and Wilson, I. (1975). The principle of the angiotome, a system of linked axial pattern flaps. In: *Trans. Vlth Int. Congr. Plast. Reconstr. Surg.* Paris.

Behan, F. C. (1992). The fasciocutaneous island flap: an extension of the angiotome concept. *Aust. NZ J. Surg.* 62: 874–86.

Beregi, J. P., Elkohen, M., Deklunder, G., Artaud, D., Coullet, J. M., and Wattinne, L. (1996). Helical CT angiography compared with arteriography in the detection of renal artery stenosis. *Am. J. Roentgenol.* 167: 495-501.

Bergeron, L., Tang, M., and Morris, S. F. (2006). A review of vascular injection techniques for the study of perforator flaps. *Plast. Reconstr. Surg.* 117: 2050-7.

Berry, E., Kelly, S., Hutton, J., Harris, K. M., Roderick, P., Boyce, J. C., Cullingworth, J., Gathercole, L., O'Connor, P. J., and Smith, M. A. (1999). A systematic literature review of spiral and electron beam computed tomography: with particular reference to clinical applications in hepatic lesions, pulmonary embolus and coronary artery disease. *Health Technology Assessment.* 3: 18.

Bhattacharya, V., Deshpande, S.B., Watts, R.K., Reddy, G.R., Singh, S.K. and Goyal, S. (2005). Measurement of perfusion pressure of perforators and its correlation with their internal diameter. *Br. J. Plast. Surg.* 58: 759-64.

Black, C. E., Huang, N., Neligan, P. C., Levine, R. H., Lipa, J. E., Lintlop, S., Forrest, C. R., and Pang, C. Y. (2001). Effect of nicotine on vasoconstrictor and vasodilator

responses in human skin vasculature. *Am. J. Physiol. Regul. Integr. Comp. Physiol.* 281: 1097-104.

Blondeel, P. N. (1999). One hundred free DIEP flap breast reconstructions: a personal experience. *Br. J. Plast. Surg.* 52: 104-11.

Blondeel, N., Vanderstraeten, G. G., Monstrey, S. J., Van Landuyt, K., Tonnard, P., Lysens, R., Boeckx, W. D., and Matton, G. (1997). The donor site morbidity of free DIEP flaps and free TRAM flaps for breast reconstruction. *Br. J. Plast. Surg.* 50: 322-30.

Blondeel, P. N., Beyens, G., Verhaeghe, R., Van Landuyt, K., Tonnard, P., Monstrey, S. J., and Matton, G. (1998). Doppler flowmetry in the planning of perforator flaps. *Br. J. Plast. Surg.* 51: 202-9.

Blondeel, P. N., Arnstein, M., Verstraete, K., Depuydt, K., Van Landuyt, K. H., Monstrey, S. J., Kroll, S. S. (2000). Venous congestion and blood flow in free transverse rectus abdominis myocutaneous and deep inferior epigastric perforator flaps. *Plast. Reconstr. Surg.* 106: 1295-9.

Blondeel, P. N., Van Landuyt, K. H., Monstrey, S. J., Hamdi, M., Matton, G. E., Allen, R. J., Dupin, C., Feller, A. M., Koshima, I., Kostakoglu, N., and Wei, F. C. (2003). The "Gent" consensus on perforator flap terminology: preliminary definitions. *Plast. Reconstr. Surg.* 112: 1378-83.

Blondeel, P. N., Morris, S. F., Hallock, G. G., and Neligan, P. C. (2006). Perforator

Flaps: Anatomy, Technique and Clinical Application. QMP St. Louis.

Bloomgarden, D. C., and Rosen, M. P. (2001). Newer diagnostic modalities for pulmonary embolism. Pulmonary angiography using CT and MR imaging compared with conventional angiography. *Emerg. Med. Clin. N. Am.* 19: 975-994.

Bostwick, J., Vasconez, L. O., and Jurkiewicz, M. J. (1978). Breast reconstruction after a radical mastectomy. *Plast. Reconstr. Surg.* 61: 682.

Boyd, J. B., Taylor, G. I., and Corlett, R. J. (1984). The vascular territory of the superior epigastric and the deep inferior epigastric arteries. *Plast. Reconstr. Surg.* 73: 1.

Braverman, I. M. October 2006. Personal communication.

Braverman, I. M. (2000). The cutaneous microcirculation. *J. Investig. Dermatol. Symp. Proc.* 5: 3-9.

Braverman, I. M. (1997). The cutaneous microcirculation: ultrastructure and microanatomical organization. *Microcirculation.* 4: 329-40.

Braverman, I. M. (1989)"! Ultrastructure and organization of the cutaneous microvasculature in normal and pathologic states. *J. Invest. Dermatol.* 93: 2-9.

Braverman, I. M. and Sibley, J. (1990). Ultrastructural and three-dimensional analysis of the contractile cells of the cutaneous microvasculature. *J. Invest. Dermatol.* 95: 90-6.

Brenner, D. J., and Hall, E. J. (2007). Computed Tomography - An Increasing Source of Radiation Exposure. *N. Engl. J. Med.* 357:2277-84.

Brumback, R. J., McBride, M. S., and Ortolani, N. C. (1992). Functional evaluation of the shoulder after transfer of the vascularized latissimus dorsi muscle. *J. Bone Joint Surg. Am.* 74: 377-82.

Budoff, M. J., Achenbach, S. and Duerinckx, A. (2003). Clinical utility of computed tomograhpy and magnetic resonance techniques for noninvasive coronary angiography. *JACC.* 42: 1867-1878.

Burrill, J., Dabbagh, Z., Gollub, F., and Hamady, M. (2007). Multidetector computed tomographic angiography of the cardiovascular system. *Postgrad. Med. J.* 83; 698-704.

Bushberg, J. T., Seibert, J. A., Leidhold, E. M. Jr., and Boone, J. M. (2002) The Essential Physics of Medical Imaging, 2nd ed, Lippincott Williams and Wilkins, Philadelphia, PA.

Carramenha e Costa, M. A., Carriquiry, C., Vasconez, L. O., Grotting, J. C., Herrera, R. H., and Windle, B. H. (1987). An anatomic study of the venous drainage of the transverse rectus abdominis musculocutaneous flap. *Plast. Reconstr. Surg.* 79: 208.

Celik, N., Wei, F. C., Lin, C. H., Cheng, M. H., Chen, H. C., Jeng, S. F., and Kuo, Y. R. (2002). Technique and strategy in anterolateral thigh perforator flap surgery, based on an analysis of 15 complete and partial failures in 439 cases. *Plast. Reconstr. Surg.* 109: 2211-6.

Chana, J. S., and Wei, F. C. (2004). A review of the advantages of the anterolateral thigh flap in head and neck reconstruction. *Br. J. Plast. Surg.* 57: 603-9.

Cheng, M. H., Robles, J. A., Ulusal, B. G., and Wei, F. C. (2006). Reliability of zone IV in the deep inferior epigastric perforator flap: a single center's experience with 74 cases. *Breast.* 15: 158-66.

Chevray, P. M. (2004). Breast reconstruction with superficial inferior epigastric artery flaps: a prospective comparison with TRAM and DIEP flaps. *Plast. Reconstr. Surg.* 114: 1077-83.

Chow, L. C., Napoli, A., Klein, M. B., Chang, J., Rubin, G. D. (2005). Vascular mapping of the leg with multi-detector row CT angiography prior to free-flap transplantation. *Radiology.* 237: 353-60.

Cochran, S. T., Krasny, R. M., and Danovitch, G. M. (1997). Helical CT angiography for examination of living renal donors. *American Jouranl of Radiology.* 168: 1569-1573.

Cormack, G. C., and Lamberty, B. G. (1984). Fasciocutaneous vessels. Their distribution on the trunk and limbs, and their clinical application in tissue transfer. *Anat. Clin.* 6: 121-31.

Davis, J. P., Nield, D. V., Garth, R. J., and Breach, N. M. (1992). The latissimus dorsi flap in head and neck reconstructive surgery: a review of 121 procedures. *Clin. Otolaryngol. Allied Sci.* 17: 487–490.

Delay, E., Gounot, N., Bouillot, A., Zlatoff, P., and Rivoire, M. (1998). Autologous latissimus breast reconstruction: a 3-year clinical experience with 100 patients. *Plast. Reconstr. Surg.* 102: 1461-78.

D'Este, S. (1912). La technique de l'amputation de la mamelle pour carcinome mammaire. *Rev. Chir.* 45: 194.

Dinner, M. I., Dowden, R. V., and Scheflan, M. (1983). Refinements in the use of the transverse abdominal island flap for postmastectomy reconstruction. *Ann. Plast. Surg.* 11: 362–372.

Dowden, R. V., and McCraw, J. B. (1980). The vastus lateralis muscle flap: technique and applications. *Ann. Plast. Surg.* 4: 396-404.

Drimmer, M. A., and Krasna, M. J. (1987). The vastus lateralis myocutaneous flap. *Plast. Reconstr. Surg.* 79: 560-6.

El-Mrakby, H. H., and Milner, R. H. (2002). The vascular anatomy of the lower anterior abdominal wall: a microdissection study on the deep inferior epigastric vessels and the perforator branches. *Plast. Reconstr. Surg.* 109: 539-43.

Figus, A., Mosahebi, A. and Ramakrishnan, V. (2006). Microcirculation in DIEP flaps: a study of the haemodynamics using laser Doppler flowmetry and lightguide reflectance spectrophotometry. *J. Plast. Reconstr. Aesthet. Surg*; 59: 604-12.

Fix, R. J. and Vasconez, L. O. (1991). Fasciocutaneous flaps in reconstruction of the lower extremity. *Clin. Plast. Surg.* 18: 571–582.

Fraulin, F. O., Louie, G., Zorrilla, L., and Tilley, W. (1995). Functional evaluation of the shoulder following latissimus dorsi muscle transfer. *Ann. Plast. Surg.* 35: 349-55.

Friedrich, W., Herberhold, C., and Lierse, W. (1988). Vascularization of the myocutaneous latissimus dorsi flap. Injection study on the thoracodorsal artery. *Acta. Anat. (Basel).* 131: 97-102.

Fuchs, T., Kachelrieß, M., and Kalender, W. A. (2000). Technical advances in multi-slice spiral CT. *European Journal of Radiology.* 36: 69–73.

Futter, C. M., Webster, M. H., Hagen, S., and Mitchell, S. L. (2000). A retrospective comparison of abdominal muscle strength following breast reconstruction with a free TRAM or DIEP flap. *Br. J. Plast. Surg.* 53: 578-83.

Garvey, C. J., and Hanlon, R. (2002). Computed tomography in clinical practice. *BMJ.* 324; 1077-80.

Gaylord, G. M. (2002). Computed tomographic and magnetic resonance coronary angiography: are you ready? *Radiol. Management.* 24: 16-20.

Geddes, C. R., Morris, S. F., and Neligan, P. C. (2003). Perforator Flaps, Evolution, Classification and Applications. *Ann. Plast. Surg.* 50: 90-9.

Gedebou, T. M., Wei, F. C., and Lin, C. H. (2002). Clinical experience of 1284 free anterolateral thigh flaps. *Handchir. Mikrochir. Plast. Chir.* 34: 239-44.

Ger, R. (1966). The operative treatment of the advanced stasis ulcer. A preliminary communication. *Am. J. Surg.* 111: 659-63.

Gill, P. S., Hunt, J. P., Guerra, A. B., Dellacroce, F. J., Sullivan, S. K., Boraski, J., Metzinger, S. E., Dupin, C. L., and Allen, R. J. (2004). A 10-year retrospective review of 758 DIEP flaps for breast reconstruction. *Plast. Reconstr. Surg.* 113: 1153-60.

Giunta, R. E., Geisweid, A., and Feller, A. M. (2000). The value of preoperative Doppler sonography for planning free perforator flaps. *Plast. Reconstr. Surg.* 105: 2381-6.

Goldman, L. W. (2007). Principles of CT and CT Technology. *J. Nucl. Med. Technol.* 35: 115–28.

Granzow, J. W., Levine, J. L., Chiu, E. S., and Allen, R. J. (2006). Breast reconstruction using perforator flaps. *J. Surg. Oncol.* 94: 441-54.

Gravvanis, A. I., Tsoutsos, D. A., Karakitsos, D., Panayotou, P., Iconomou, T., Zografos, G., Karabinis, A., Papadopoulos, O. (2006). Application of the pedicled anterolateral thigh flap to defects from the pelvis to the knee. *Microsurgery.* 26: 432-8.

Gravvanis, A., Tsoutsos, D., Karakitsos, D., Iconomou, T., Papadopoulos, O. (2007). Blood perfusion of the free anterolateral thigh perforator flap: its beneficial effect in the reconstruction of infected wounds in the lower extremity. *World J. Surg.* 31: 11-8.

Guerra, A. B., Metzinger, S. E., Lund, K. M., Cooper, M. M., Allen, R. J., and Dupin, C. L. (2004). The thoracodorsal artery perforator flap: clinical experience and anatomic study with emphasis on harvest techniques. *Plast. Reconstr. Surg.* 114: 32-41.

Haertsch, P. (1981). The surgical plane in the leg. *Br. J. Plast. Surg.* 34: 464-9.

Hallett, R. L., and Fleischmann, D. (2006). Tools of the Trade for CTA: MDCT Scanners and Contrast Medium Injection Protocols. *Tech. Vasc. Interventional. Rad.* 9: 134-42.

Hallock, G. G. (2001). Physiological studies using laser Doppler flowmetry to compare blood flow to the zones of the free TRAM flap. *Ann. Plast. Surg.* 47: 229.

Hallock, G. G. (2003). Direct and indirect perforator flaps: The history and the controversy. *Plast. Reconstr. Surg.* 111: 855-65.

Hallock, G. G. (2005). The proximal pedicled anterolateral thigh flap for lower limb coverage. *Ann. Plast. Surg.* 55: 466-9.

Hamdi, M,, and Rebecca, A. (2006). The Deep Inferior Epigastric Artery Perforator Flap (DIEAP) in Breast Reconstruction. *Semin. Plast. Surg.* 20: 95-102.

Hamdi, M., Van Landuyt, K., Monstrey, S., Blondeel, P. (2004). Pedicled perforator flaps in breast reconstruction: a new concept. *Br. J. Plast. Surg.* 57: 531-9.

Hamdi, M. and De Frene, B. (2006). Pedicled Perforator Flaps in Breast Reconstruction. *Semin. Plast. Surg.* 20: 73-78.

Hartrampf, C. R., Scheflan, M., and Black, P. W. (1982). Breast reconstruction with a transverse abdominal island flap. *Plast. Reconstr. Surg.* 69: 216.

Haschek, E., and Lindenthal, O. A. (1896). Contribution to the Practical Use of Photography According to Röntgen. *Wien. Chir. Wochenschr.* 9: 63.

Haughey, B. V., and Fredrickson, J. M. (1991). The latissimus dorsi donor site—Current use in head and neck reconstruction. *Arch. Otolaryngol. Head Neck Surg.* 117: 1129–1134.

Heitland, A. S., Markowicz, M., Koellensperger, E., Schoth, F., Feller, A. M., and Pallua, N. (2005) Duplex ultrasound imaging in free transverse rectus abdominis muscle, deep inferior epigastric artery perforator, and superior gluteal artery perforator flaps: early and long-term comparison of perfusion changes in free flaps following breast reconstruction. *Ann. Plast. Surg.* 55: 117-21.

Heitmann, C., Guerra, A., Metzinger, S. W., Levin, L. S., and Allen, R. J. (2003). The thoracodorsal artery perforator flap: anatomic basis and clinical application. *Ann. Plast. Surg.* 51: 23-9.

Herter, F., Ninkovic, M., and Ninkovic, M. (2007). Rational flap selection and timing for coverage of complex upper extremity trauma. *J. Plast. Reconstr. Aesthet. Surg.* 60: 760-8.

Hester, T. R. Jr., Nahai, F., Beegle, P. E., and Bostwick, J. 3rd. (1984). Blood supply of the abdomen revisited, with emphasis on the superficial inferior epigastric artery. *Plast. Reconstr. Surg.* 74: 657-70.

Holm, C., Mayr, M., Hofter, E., and Ninkovic, M. (2006). Perfusion zones of the DIEP flap revisited: a clinical study. *Plast. Reconstr. Surg.* 117: 37-43.

Holmström, H. (1979). The free abdominoplasty flap and its use in breast reconstruction. An experimental study and clinical case report. *Scand. J. Plast. Reconstr. Surg.* 13: 423-27.

Hsieh, C. H., Yang, C. C., Kuo, Y. R., Tsai, H. H., and Jeng, S. F. (2003). Free anterolateral thigh adipofascial perforator flap. *Plast. Reconstr. Surg.* 112: 976-82.

Imanishi, N., Nakajima, H., Minabe, T., and Aiso, S. (2000). Angiographic study of the subdermal plexus: a preliminary report. *Scand. J. Plast. Reconstr. Surg. Hand Surg.* 34: 113-6.

Imanishi, N., Nakajima, H., Minabe, T., Chang, H., and Aiso, S. (2003). Anatomical relationship between arteries and veins in the paraumbilical region. *Br. J. Plast. Surg.* 56: 552-6.

Javaid, M., and Cormack, G. C. (2003). Anterolateral thigh free flap for complex soft tissue hand reconstructions. *J. Hand Surg. [Br].* 28: 21-7.

Josephson, S. A., Bryant, S. O., Mak, H. K., Johnston, S. C., Dillon, W. P., and Smith, W. S. (2004). Evaluation of carotid stenosis using CT angiography in the initial evaluation of stroke and TIA. *Neurology.* 63: 457-460.

Kaatee, R., Beek, F. J. A., de Lange, E., van Leeuwen, M. S., Smits H. F., van der Ven P. J., Beutler, J. J., Mali, W. P. (1997). Renal artery stenosis: detection and quantification with spiral CT angiography versus optimized digital subtraction angiography. *Radiology.* 205: 121-127.

Kalender, W. A. (2005). CT: the unexpected evolution of an imaging modality. *Eur. Radiol.* 15: 21-4.

Kalender, W. A. (2006). X-ray computed tomography. *Phys. Med. Biol.* 51: 29-43.

Kawai, K., Imanishi, N., Nakajima, H., Aiso, S., Kakibuchi, M., and Hosokawa, K. (2004). Vascular anatomy of the anterolateral thigh flap. *Plast. Reconstr. Surg.* 114: 1108-17.

Keller, A. (2006). Perfusion zones of the DIEP flap revisited: a clinical study. *Plast. Reconstr. Surg.* 118: 1076-7.

Kim, J. T. Latissimus dorsi perforator flap. (2003). *Clin. Plast. Surg.* 30: 403-31.

Kim, J. T. (2005). Two options for perforator flaps in the flank donor site: latissimus dorsi and thoracodorsal perforator flaps. *Plast. Reconstr. Surg.* 115: 755-63.

Kim, J. T., Koo, B. S., and Kim, S. K. (2001). The thin latissimus dorsi perforator-based free flap for resurfacing. *Plast. Reconstr. Surg.* 107: 374-82.

Kim, D. Y., Jeong, E. C., Kim, K. S., Lee, S. Y., and Cho, B. H. (2002). Thinning of the thoracodorsal perforator-based cutaneous flap for axillary burn scar contracture. *Plast. Reconstr. Surg.* 109: 1372-7.

Kim, J. T., and Kim, S. K. (2003). Hand resurfacing with the superthin latissimus dorsi perforator-based free flap. *Plast. Reconstr. Surg.* 111: 366-70.

Kimata, Y., Uchiyama, K., Ebihara, S., Nakatsuka, T., and Harii, K. (1998). Anatomic variations and technical problems of the anterolateral thigh flap: a report of 74 cases. *Plast. Reconstr. Surg.* 102: 1517-23.

Kimata, Y., Uchiyama, K., Ebihara, S., Sakuraba, M., Iida, H., Nakatsuka, T., and Harii, K. (2000). Anterolateral thigh flap donor-site complications and morbidity. *Plast. Reconstr. Surg.* 106: 584-9.

Kimura, N., and Satoh, K. (1996). Consideration of a thin flap as an entity and clinical applications of the thin anterolateral thigh flap. *Plast. Reconstr. Surg.* 97: 985-92.

Kimura, N., Satoh, K., Hasumi, T., and Ostuka, T. (2001). Clinical application of the free

thin anterolateral thigh flap in 31 consecutive patients. *Plast. Reconstr. Surg.* 108: 1197-208.

Kimura, N., Saito, M., Itoh, Y., and Sumiya, N. (2006). Giant combined microdissected thin thigh perforator flap. *J. Plast. Reconstr. Aesthet. Surg.* 59: 1325-9.

Koshima, I. (2000). Free anterolateral thigh flap for reconstruction of head and neck defects following cancer ablation (Discussion). *Plast. Reconstr. Surg.* 105: 2358.

Koshima, I,, and Soeda, S. (1989). Inferior epigastric artery skin flaps without rectus abdominis muscle. *Br. J. Plast. Surg.* 42: 645-8.

Koshima I. (2001). A new classification of free combined or connected tissue transfers: introduction to the concept of bridge, siamese, chimeric, mosaic, and chain-circle flaps. *Acta. Med. Okayama.* 55: 329-32.

Koshima, I., Moriguchi, T., and Soeda, S. (1992). Free thin paraumbilical perforator-based flaps. *Ann. Plast. Surg.* 29: 12-7.

Koshima, I., Fukuda, H., Yamamoto, H., Moriguchi, T., Soeda, S., and Ohta, S. (1993). Free anterolateral thigh flaps for reconstruction of head and neck defects. *Plast. Reconstr. Surg.* 92: 421-8.

Koshima, I., Yamamoto, H., Hosoda, M., Moriguchi, T., Orita, Y., and Nagayama, H. (1993). Free combined composite flaps using the lateral circumflex femoral system for

repair of massive defects of the head and neck regions: an introduction to the chimeric flap principle. *Plast. Reconstr. Surg.* 92: 411-20.

Koshima, I., Yamamoto, H., Moriguchi, T., and Orita, Y. (1994). Extended anterior thigh flaps for repair of massive cervical defects involving pharyngoesophagus and skin: an introduction to the "mosaic" flap principle. *Ann. Plast. Surg.* 32: 321-7.

Koshima, I., Kawada, S., Etoh, H., Kawamura, S., Moriguchi, T., and Sonoh, H. (1995). Flow-through anterior thigh flaps for one-stage reconstruction of soft-tissue defects and revascularization of ischemic extremities. *Plast. Reconstr. Surg.* 95: 252-60.

Koshima, I., Hosoda, S., Inagawa, K., Urushibara, K., and Moriguchi, T. (1998). Free combined anterolateral thigh flap and vascularized fibula for wide, through-and-through oromandibular defects. *J. Reconstr. Microsurg.* 14: 529-34.

Koshima, I., Saisho, H., Kawada, S., Hamanaka, T., Umeda, N., and Moriguchi, T. (1999). Flow-through thin latissimus dorsi perforator flap for repair of soft-tissue defects in the legs. *Plast. Reconstr. Surg.* 103: 1483.

Kreidstein, M. L., Pang, C. Y., Levine, R. H., and Knowlton, R. J. (1991). The isolated perfused human skin flap: design, perfusion technique, metabolism, and vascular reactivity. *Plast. Reconstr. Surg.* 87: 741-9.

Kroll, S. S., and Rosenfield, L. (1988). Perforator-based flaps for low posterior midline defects. *Plast. Reconstr. Surg.* 81: 561–566.

Kuo, Y. R., Jeng, S. F., Kuo, M. H., Huang, M. N., Liu, Y. T., Chiang, Y. C., Yeh, M. C., and Wei, F. C. (2001). Free anterolateral thigh flap for extremity reconstruction: clinical experience and functional assessment of donor site. *Plast. Reconstr. Surg.* 107: 1766-71.

Kuo, Y. R., Seng-Feng, J., Kuo, F. M., Liu, Y. T., and Lai, P. W. (2002). Versatility of the free ALT flap for reconstruction of soft tissue defects: review of 140 cases. *Ann. Plast. Surg.* 48: 161-6.

Laitung, J. K., Peck, F. (1985). Shoulder function following the loss of the latissimus dorsi muscle. *Br. J. Plast. Surg.* 38: 375-9.

Lamberty, B. G. H., and Cormack, G. C. (1986). The arterial anatomy of skin flaps. Churchill Livingstone.

Lin, C. T., Huang, J. S., Yang, K. C., Hsu, K. C., Chen, J. S., and Chen, L. W. (2006). Reliability of anatomical landmarks for skin perforators of the thoracodorsal artery perforator flap. *Plast. Reconstr. Surg.* 118: 1376-86.

Lin, Y. T., Lin, C. H., and Wei, F. C. (2006). More degrees of freedom by using chimeric concept in the applications of anterolateral thigh flap. *J. Plast. Reconstr. Aesthet. Surg.* 59: 622-7.

Lin, C. H., Wei, F. C., Lin, Y. T., Yeh, J. T., Rodriguez Ede, J., and Chen, C. T. (2006). Lateral circumflex femoral artery system: warehouse for functional composite free-tissue reconstruction of the lower leg. *J. Trauma.* 60: 1032-6.

Lipa, J. E., Novak, C. B., and Binhammer, P. A. (2005). Patient-reported donor-site morbidity following anterolateral thigh free flaps. *J. Reconstr. Microsurg.* 21: 365-70.

Manchot, C. (1889). Die Hautarterien des Menschlichen Korpers. Leipzig: FCW Vogel.

Manchot, C. (1983). The Cutaneous Arteries of the Human Body. New York: Springer-Verlag.

Masia, J., Clavero, J. A., Larrañaga, J. R., Alomar, X., Pons, G., and Serret, P. (2006). Multidetector-row computed tomography in the planning of abdominal perforator flaps. *J. Plast. Reconstr. Aesthet. Surg.* 59: 594-9.

Mathes, S. J., and Nahai, F. (1981). Classification of the vascular anatomy of muscles: experimental and clinical correlation. *Plast. Reconstr. Surg.* 67: 177-87.

Mathes, S. J., and Nahai, F. (1997). General principles. Reconstructive surgery: Principles, anatomy & technique. New York: Quality Medical Publishing and Churchill Livingston. 3–253.

Maxwell, G. P. (1980). Iginio Tansini and the origin of the latissimus dorsi musculocutaneous flap. *Plast. Reconstr. Surg.* 65: 686-92.

McCraw, J. B., Dibbell, D. G., and Carraway, J. H. (1977). Clinical definition of independent myocutaneous vascular territories. *Plast. Reconstr. Surg.* 60: 341.

McGregor, A. D. (1992). The angiosome--an *in vivo* study by fluorescein angiography. *Br. J. Plast. Surg.* 45: 219-21.

McGregor, I. A., and Jackson, I. T. (1972). The groin flap. *Br. J. Plast. Surg.* 25: 3-16.

McGregor, I. A., and Morgan, G. (1973). Axial and random pattern flaps. *Br. J. Plast. Surg.* 26: 202.

Mehrara, B. J. (2007). Presented ASRM meeting.

Milton, S. H. (1970). Pedicled skin-flaps: the fallacy of the length:width ratio. *Br. J. Surg.* 57: 502–508.

Momeni, A., Krischak, S., and Bannasch, H: (2006). The thoracodorsal artery perforator flap with a vascularized scapular segment for reconstruction of a composite lower extremity defect. *Microsurgery.* 26: 515-8.

Moon, H. K., and Taylor, G. I. (1988). The vascular anatomy of rectus abdominis musculocutaneous flaps based on the deep superior epigastric system. *Plast. Reconstr. Surg.* 82: 815-32.

Morris, S. F., and Taylor, G. I. (1993). Predicting the survival of experimental skin flaps with a knowledge of the vascular architecture. *Plast. Reconstr. Surg.* 92: 1352-61.

Millard, D. R. Jr. (1981). Variations in the design of the latissimus dorsi flap in breast reconstruction. *Ann. Plast. Surg.* 7: 269-71.

Morain, W. D. (1985). Carl Manchot, plastic surgery's missed opportunity. *Med. Herit.* 1: 174-80.

Muhlbauer, W., and Olbrisch, R. (1977). The latissimus dorsi myocutaneous flap for breast reconstruction. *Chir. Plast. (Berlin).* 4: 27.

Mun, G. H., Kim, H. J., Cha, M. K., Kim, W. Y. (2008) Impact of perforator mapping using multidetector-row computed tomographic angiography on free thoracodorsal artery perforator flap transfer. *Plast. Reconstr. Surg.* 122: 1079-88.

Munhoz, A. M., Ishida, L. H., Sturtz, G. P., Cunha, M. S., Montag, E., Saito, F. L., Gemperli, R., and Ferreira, M. C. (2004). Importance of lateral row perforator vessels in deep inferior epigastric perforator flap harvesting. *Plast. Reconstr. Surg.* 113: 517-24.

Mureau, M. A., Posch, N. A., Meeuwis, C. A., and Hofer, S. O. (2005). Anterolateral thigh flap reconstruction of large external facial skin defects: a follow-up study on functional and aesthetic recipient- and donor-site outcome. *Plast. Reconstr. Surg.* 115: 1077-86.

Nagler, R. M., Braun, J., Daitzman, M., and Laufer, D. (1997). Spiral CT angiography: an alternative vascular evaluation technique for head and neck microvascular reconstruction. *Plast. Reconstr. Surg.* 100: 1697-702.

Nakajima, H., Minabe, T., and Imanishi, N. (1998). Three-dimensional analysis and classification of arteries in the skin and subcutaneous adipofascial tissue by computer graphics imaging. *Plast. Reconstr. Surg.* 102: 748-60.

Nakayama, B., Hyodo, I., Hasegawa, Y., Fujimoto, Y., Matsuura, H., Yatsuya, H., and Torii, S. (2002). Role of the anterolateral thigh flap in head and neck reconstruction: advantages of moderate skin and subcutaneous thickness. *J. Reconstr. Microsurg.* 18: 141-6.

Neil-Dwyer, J. G., Ludman, C. N., Schaverien, M., McCulley, S. J., Perks, A. G. (2008). Magnetic resonance angiography in preoperative planning of deep inferior epigastric artery perforator flaps. *J. Plast. Reconstr. Aesthet. Surg.* In Press.

Neligan, P. C., and Lipa, J. E. (2006). Perforator Flaps in Head and Neck Reconstruction. *Semin. Plast. Surg.* 20: 56-63.

Nojima, K., Brown, S. A., Acikel, C., Arbique, G., Ozturk, S., Chao, J., Kurihara, K., and Rohrich, R. J. (2005). Defining vascular supply and territory of thinned perforator flaps: part I. Anterolateral thigh perforator flap. *Plast. Reconstr. Surg.* 116: 182-93.

Offman, S. L., Geddes, C. R., Tang, M., and Morris, S. F. (2005). The vascular basis of perforator flaps based on the source arteries of the lateral lumbar region. *Plast. Reconstr. Surg.* 115: 1651-9.

Ohjimi, H., Era, K., Fujita, T., Tanaka, T., and Yabuuchi, R. (2005). Analyzing the vascular architecture of the free TRAM flap using intraoperative ex vivo angiography. *Plast. Reconstr. Surg.* 116: 106-13.

Olivari, N. (1976). The latissimus flap. *Br. J. Plast. Surg.* 29: 126-8.

Orticochea, M. (1972). The musculo-cutaneous flap method: an immediate and heroic substitute for the method of delay. *Br. J. Plast. Surg.* 25: 106–10.

Pan, S. C., Yu, J. C., Shieh, S. J., Lee, J. W., Huang, B. M., and Chiu, H. Y. (2004). Distally based anterolateral thigh flap: an anatomic and clinical study. *Plast. Reconstr. Surg.* 114: 1768-75.

Phillips, C. D., and Bubash, L. A. (2002). CT angiography and MR angiography in the evaluation of extracranial carotid vascular disease. *Radiol. Clin. N. Am.* 40: 783-798.

Pinsolle, V., Grinfeder, C., Mathoulin-Pelissier, S., and Faucher, A. (2006). Complications analysis of 266 immediate breast reconstructions. *J. Plast. Reconstr. Aesthet. Surg.* 59: 1017-24.

Pontén, B. (1981). The fasciocutaneous flap: its use in soft tissue defects of the lower leg. *Br. J. Plast. Surg.* 34: 215–20.

Reardon, C. M., O'Ceallaigh, S., and O'Sullivan, S. T. (2004). An anatomical study of the superficial inferior epigastric vessels in humans. *Br. J. Plast. Surg.* 57: 515-9.

Ribuffo, D., Cigna, E., Gargano, F., Spalvieri, C., and Scuderi, N. (2005). The innervated anterolateral thigh flap: anatomical study and clinical implications. *Plast. Reconstr. Surg.* 115: 464-70.

Ribuffo, D., Atzeni, M., Saba, L., Milia, A., Guerra, M., Mallarini, G. (2009). Angio computed tomography preoperative evaluation for anterolateral thigh flap harvesting. *Ann. Plast. Surg.* 62: 368-71.

Rickard, R. (2001). TRAM and DIEP flap zones. *Br. J. Plast. Surg.* 54: 272.

Röntgen, W. (1895). Über eine neue Art von Strahlen. *Sitzungsberichte der physikalisch medizinischen Gesellschaft zu Würzburg.* 9: 132-141.

Ross, G. L., Dunn, R., Kirkpatrick, J., Koshy, C. E., Alkureishi, L. W., Bennett, N., Soutar, D. S., and Camilleri, I. G. (2003). To thin or not to thin: The use of the anterolateral thigh flap in the reconstruction of intraoral defects. *Br. J. Plast. Surg.* 56: 409.

Roy, M. K., Shrotia, S., Holcombe, C., Webster, D. J., Hughes, L. E., and Mansel, R. E. (1998). Complications of latissimus dorsi myocutaneous flap breast reconstruction. *Eur. J. Surg. Oncol.* 24: 162-5.

Rozen, W. M., Ashton, M. W., Grinsell, D., Stella, D. L., Phillips, T. J., Taylor, G. I. (2008a). Establishing the case for CT angiography in the preoperative imaging of abdominal wall perforators. *Microsurgery.* 28: 306-13.

Rozen, W. M., Garcia-Tutor, E., Alonso-Burgos, A., Acosta, R., Stillaert, F., Zubieta, J. L., Hamdi, M., Whitaker, I. S., Ashton, M. W. (2008b). Planning and optimising DIEP flaps with virtual surgery: the Navarra experience. J. Plast. Reconstr. Aesthet. Surg. In Press.

Rubin, G. D., Alfrey, E. J., Dake, M. D., Semba, C. P., Sommer, F. G., Kuo, P. C., Dafoe, D. C., Waskerwitz, J. A., Bloch, D. A., and Jeffrey, R. B. (1995). Spiral CT for the assessment of living renal donors. *Radiology*. 195: 457-462.

Rubin, G. D., Schmidt, A. J., Logan, L. J., and Sofilos, M.C. (2001). Multi-detector row CT angiography of lower extremity arterial inflow and runoff: initial experience. *Radiology*.221: 146-158.

Rubino, C., Coscia, V., Cavazzuti, A. M., and Canu, V. (2006). Haemodynamic enhancement in perforator flaps: The inversion phenomenon and its clinical significance. A study of the relation of blood velocity and flow between pedicle and perforator vessels in perforator flaps. *J. Plast. Reconstr. Aesthet. Surg*. 59: 636-43.

Ruetschi, M. S., LeWinn, L. R., and Chaglassian, T. A. (1981). Variation of latissimus dorsi skin island design for postmastectomy reconstruction. *Ann. Plast. Surg*. 6: 171-8.

Russell, R. C., Pribaz, J., Zook, E. G.,. Leighton, W. D., Eriksson, E., and Smith, C. J. (1986). Functional evaluation of latissimus dorsi donor site. *Plast. Reconstr. Surg*. 78: 336-44.

Saint-Cyr, M. and Gupta, A. (2007). Indications and selection of free flaps for soft tissue coverage of the upper extremity. *Hand Clin.* 23: 37-48.

Salmon, M. (1936). Arteres de la Peau. Paris: Masson et Cie.

Salmon, M. (1988). Arteries of the Skin (edited by G. I. Taylor and M. Tempest). London: Churchill Livingstone.

Scheflan, M., and Dinner, M. I. (1983). The transverse abdominal island flap: Part I. Indications, contraindications, results, and complications. *Ann. Plast. Surg.* 10: 24.

Scheflan, M., and Dinner, M. I. (1983). The transverse abdominal island flap: Part II. Surgical technique. *Ann. Plast. Surg.* 10: 120.

Schneider, W. J., Hill, H. L., and Brown, R. G. (1977). Latissimus dorsi myocutaneous flap for breast reconstruction. *Br. J. Plast. Surg.* 30: 277.

Schwabegger, A. H., Bodner, G., Ninkovic, M., and Piza-Katzer, H. (2002). Thoracodorsal artery perforator (TAP) flap: report of our experience and review of the literature. *Br. J. Plast. Surg.* 55: 390-5.

Schwabegger, A. H., Harpf, C., and Rainer, C. (2003). Muscle-sparing latissimus dorsi myocutaneous flap with maintenance of muscle innervation, function, and aesthetic appearance of the donor site. *Plast. Reconstr. Surg.* 111: 1407-11.

Shehan, D. C., and Hrapchak, B. B. (1980). Theory and Practice of Histotechnology, 2nd ed. Battelle.

Smit, J. M., Dimopoulou, A., Liss, A. G., Zeebregts, C. J., Kildal, M., Whitaker, I. S., Magnusson, A., Acosta, R. (2009). Preoperative CT angiography reduces surgery time in perforator flap reconstruction. *J. Plast. Reconstr. Aesthet. Surg.* 62: 1112-7.

Song, Y. G., Chen, G. Z., and Song, Y. L. (1984). The free thigh flap: a new free flap concept based on the septocutaneous artery. *Br. J. Plast. Surg.* 37: 149-59.

Spälteholz, W., and Hirsch, C. (1907). Coronararterien und Herzmuskel: Anatomische und experimentelle Untersuchungen. *Dtsch. Med. Wochenschr.* 17: 790.

Spinelli, H. M., Fink, J. A., and Muzaffar, A. R. (1996). The latissimus dorsi perforator-based fasciocutaneous flap. *Ann. Plast. Surg.* 37: 500-6.

Suami, H., Taylor, G. I. and Pan, W. R. (2003). Angiosome territories of the nerves of the lower limbs. *Plast. Reconstr. Surg.* 112: 1790-8.

Tan, B. K., Ng, R. T. H., Tay, N. S., and Tan, B. S. (1999). Tissue microangiography using a simplified barium sulphate cadaver injection technique. *Ann. Acad. Med. Singapore.* 28: 152.

Tansini, I. (1906). Sopra il mio nuovo processo di amputazione della mammella. *Gazetta Medica Italiana.* 57: 141.

Taylor, G. I. (2002). The Twenty-Third Sir Harold Gillies Memorial Lecture. Keeping a head. *Br. J. Plast. Surg.* 55: 543-60.

Taylor, G. I. (2003). The "Gent" consensus on perforator flap terminology: preliminary definitions. *Plast. Reconstr. Surg.* (Discussion). 112: 1384-7.

Taylor, G. I., and Daniel, R. K. (1973). The free flap: composite tissue transfer by vascular anastomosis. *Aust. N. Z. J. Surg.* 43: 1-3.

Taylor, G. I., and Daniel, R. K. (1975). The anatomy of several free flap donor sites. *Plast. Reconstr. Surg.* 56: 243-53.

Taylor, G. I., and Palmer, J. H. (1987). The vascular territories (angiosomes) of the body: Experimental study and clinical applications. *Br. J. Plast. Surg.* 40: 113-41.

Taylor, G. I., and Palmer, J. H. (1992). 'Angiosome theory'. *Br. J. Plast. Surg.* 45: 327-8.

Taylor, G. I., Gianoutsos, M. P., and Morris, S. F. 卌994). The neurovascular territories of the skin and muscles: anatomic study and clinical implications. *Plast. Reconstr. Surg.* 94:1-36.

Taylor, G. I. and Pan, W. R. (1998). Angiosomes of the leg: anatomic study and clinical implications. *Plast. Reconstr. Surg.* 102: 599-616.

Taylor, G. I., Caddy, C. M., Watterson, P. A., and Crock, J. G. (1990). The venous territories (venosomes) of the human body: experimental study and clinical implications. *Plast. Reconstr. Surg.* 86: 185-213.

Thomas, B. P., Geddes, C. R., Tang, M., Williams, J., and Morris, S. F. (2005). The vascular basis of the thoracodorsal artery perforator flap. *Plast. Reconstr. Surg.* 116: 818-22.

Timmons, M. J. (1985). Landmarks in the anatomical study of the blood supply of the skin. *Br. J. Plast. Surg.* 38: 197-207.

Tobin, G. R., Schusterman, M., Peterson, G. H., Nichols, G., and Bland, K. I. (1981a). The intramuscular neurovascular anatomy of the latissimus dorsi muscle: the basis for splitting the flap. *Plast. Reconstr. Surg.* 67: 637–641.

Tobin, G. R., Moberg, A. W., DuBou, R. H., Weiner, L. J., and Bland, K. I. (1981b). The split latissimus dorsi myocutaneous flap. *Ann. Plast. Surg.* 7: 272-80.

Van Landuyt, K. (2006). The Anterolateral Thigh Flap for Lower Extremity Reconstruction. *Semin. Plast. Surg.* 20: 127-132.

Van Landuyt, K., Blondeel, P., Hamdi, M., Tonnard, P., Verpaele, A., and Monstrey, S. (2005). The versatile DIEP flap: its use in lower extremity reconstruction. *Br. J. Plast. Surg.* 58: 2-13.

Van Landuyt, K., Hamdi, M., Blondeel, P., and Monstrey, S. (2005). The compound thoracodorsal perforator flap in the treatment of combined soft-tissue defects of sole and dorsum of the foot. *Br. J. Plast. Surg.* 58: 371-8.

Wang, H. T., Fletcher, J. W., Erdmann, D., and Levin, L. S. (2005). Use of the anterolateral thigh free flap for upper-extremity reconstruction. *J. Hand Surg. [Am].* 30: 859-64.

Waterhouse, N., and Healy, C. (1990). Vastus lateralis myocutaneous flap for reconstruction of defects around the groin and pelvis. *Br J. Surg.* 77: 1275-7.

Wei, F. C., Jain, V., Suominen, S., and Chen, H. C. (2001). Confusion among perforator flaps: what is a true perforator flap? *Plast. Reconstr. Surg.* 107: 874-6.

Wei, F. C., Jain, V., Celik, N., Chen, H. C., Chuang, D. C., and Lin, C. H. (2002). Have we found an ideal soft-tissue flap? An experience with 672 ALT flaps. *Plast. Reconstr. Surg.* 109: 2219-26.

Willmann J. K., Mayer D, Banyai M, Desbiolles, L. M., Verdun, F. R., Seifert, B., Marincek, B., and Weishaupt, D. (2003). Evaluation of peripheral arterial bypass grafts with multi-detector row CT angiography: comparison with duplex US and digital subtraction angiography. *Radiology.* 229: 465-474.

Wolbarst, A. B. (2004). Physics of Radiology, Medical Physics Publishing, Madison, WA 2nd ed.

Wolfram, D., Schoeller, T., Hussl, H., and Wechselberger, G. (2006). The superficial inferior epigastric artery (SIEA) flap: indications for breast reconstruction. *Ann. Plast. Surg.* 57: 593-6.

Woods, A. E., and Ellis, R. C. (1996). Laboratory Histopathology, A Complete Reference; Churchill Livingston.

www.amershamhealth-us.com/shared/pdfs/pi/Omnipaque.pdf. Accessed September 2006.

www.fda.gov/cdrh/ct/risks.html

Wyers, M. C., Fillinger, M. F., Schermerhorn, M. L., Powell, R. J., Rzucidlo, E. M., Walsh, D. B., Zwolak, R. M., and Cronenwett, J. L. (2003). Endovascular repair of abdominal aortic aneurysm without preoperative arteriography. *J. Vasc. Surg.* 38: 730-738.

Xu, D. C., Zhong, S. Z., Kong, J. M., Wang, G. Y., Liu, M. Z., Luo, L. S., and Gao, J. H. (1988). Applied anatomy of the anterolateral femoral flap. *Plast. Reconstr. Surg.* 82: 305-10.

Yang, W. G., Chiang, Y. C., Wei, F. C., Feng, G. M., and Chen, K. T. (2006). Thin anterolateral thigh perforator flap using a modified perforator microdissection technique and its clinical application for foot resurfacing. *Plast. Reconstr. Surg.* 117: 1004-8.

Yap, L. H., Whiten, S. C., Forster, A., and Stevenson, J. H. (2002). The anatomical and

neurophysiological basis of the sensate free TRAM and DIEP flaps. *Br. J. Plast. Surg.* 55: 35-45.

Yildirim, S., Avci, G., and Akoz, T. (2003). Soft-tissue reconstruction using a free anterolateral thigh flap: experience with 28 patients. *Ann. Plast. Surg.* 51: 37–44.

Yildirim, S., Avci, G., Akan, M., Misirlioglu, A., and Akoz, T. (2003). Anterolateral thigh flap in the treatment of postburn flexion contractures of the knee. *Plast. Reconstr. Surg.* 111: 1630-7.

Yildirim, S., Taylan, G., Eker, G., and Akoz, T. (2006). Free flap choice for soft tissue reconstruction of the severely damaged upper extremity. *J. Reconstr. Microsurg.* 22: 599-609.

Yamada, N., Kakibuchi, M., Kitayoshi, H., Matsuda, K., Yano, K., and Hosokawa, K. (2001). A new way of elevating the anterolateral thigh flap. *Plast. Reconstr. Surg.* 108: 1677.

Yu, P. (2004). Characteristics of the anterolateral thigh flap in a Western population and its application in head and neck reconstruction. *Head Neck.* 26: 759-69.

Yu, P., and Youssef, A. (2006). Efficacy of the handheld Doppler in preoperative identification of the cutaneous perforators in the anterolateral thigh flap. *Plast. Reconstr. Surg.* 118: 928-33.